EXPERIMENTAL AND NUMERICAL MODELLING OF THE SPRAY DRYING PROCESS FOR THE PRODUCTION OF THERMALLY STABLE VACCINE POWDERS

EXPERIMENTAL AND NUMERICAL MODELLING OF THE SPRAY DRYING PROCESS FOR THE PRODUCTION OF THERMALLY STABLE VACCINE POWDERS

BLAIR A. MORGAN

A Thesis Submitted to the School of Graduate Studies in Partial Fulfillment of the Requirements for the Degree Doctor of Philosophy

McMaster University

DOCTOR OF PHILOSOPHY (2021) MCMASTER UNIVERSITY

(Chemical Engineering) Hamilton, Ontario

TITLE: EXPERIMENTAL AND NUMERICAL MODELLING OF THE SPRAY DRYING PROCESS FOR THE PRODUCTION OF THERMALLY STABLE VACCINE POWDERS

AUTHOR: Blair A. Morgan
B.Eng.Biosci (McMaster University)

SUPERVISORS: Professor Michael R. Thompson
Professor Emily D. Cranston

NUMBER OF PAGES: xix, 139

Abstract

A major challenge facing the global health community is the production of thermally stable vaccines that eliminate the need for unfavorable cold-chain storage protocols, which often require temperatures as low as -80°C. Spray drying is a promising technique to produce thermally stable vaccine powders that retain their efficacy when stored at ambient conditions. Spray drying is gaining popularity in the pharmaceutical community due to its scalability, low cost and high throughput. Processing by spray drying can rapidly immobilize the active vaccine ingredient, such as a viral vector, in an amorphous glassy matrix of a stabilizing excipient tailored to the biologic being stabilized. This encapsulation and reduction in mobility keeps the biologic isolated from mechanical, thermal or chemical stresses that cause damage and inactivation. However, choosing the best excipient, or excipient blend, and optimizing the formulation are costly and time-consuming processes and furthermore, the effects of spray drying on viral vector activity are not fully understood.

This thesis focuses on modelling the processing environment for preparing such vaccine powders, by both experimental and numerical means, to understand the relevance of mechanical, thermal and chemical stresses on viral vector activity. Specifically, the viral vector studied here was human type 5 adenovirus (AdHu5), with intended use in tuberculosis vaccines. Mechanical stresses associated with the shear inside the nozzle of a spray dryer were experimentally studied. Viral activity losses associated with shear stresses in an atomizing nozzle were attributed to aggregation; aggregation was created by damaging the virus at very high mechanical stresses but most aggregation was attributed to dispersing the virus in the excipient solution. It was concluded that overall, mechanical stresses in the nozzle caused a minimal amount of viral activity loss compared to other processing factors during spray drying, and in fact, could have a positive influence at moderate shear rates since it actually caused the break-up of AdHu5 aggregates.

To investigate thermo-chemical stresses, it was necessary to demonstrate that acoustic levitation of a single drying droplet was an effective screening method to select promising excipients for spray dried vaccines, and could be used to experimentally validate a numerical model of droplet drying. For several different sets of binary carbohydrate blends, levitated particles were found to match property and activity trends seen in spray dried powders when the surrounding temperature of the levitator matched the outlet temperature of the spray dryer. The numerical

droplet drying model could predict drying time, particle size, and component distribution within a final dried particle; the component distribution was used to aid in spatially locating the viral vector which was shown to be related to vaccine thermal stability. The model predictions associated with virus location in a dried particle were confirmed experimentally using coated silica nanoparticles as virus analogues, and several different molecular weight dextrans in the mannitol/dextran blend in order to change the location of the virus.

Overall, this work provides a deeper understanding of how spray drying can be used to produce thermally stable vaccine powders, and the arising guidance can be applied to improve formulation development based on the end targets and applications. Shear stress was found to be a negligible source of viral vector activity loss, and the application of heat to the acoustic levitator was found to create drying conditions that allowed the levitator to create materials that mimicked the properties of spray dried powders. Finally, a numerical model was validated experimentally, with both modelled predictions and confocal laser scanning microscopy confirming that an increase in dextran molecular weight in formulations caused a decrease in viral vector and silica nanoparticles at the air-solid interface. The knowledge gained by using screening methods and mathematical models of the spray drying process can reduce the time and cost inputs of vaccine development by identifying promising excipients with minimal experimentation.

Lay Abstract

To retain their effectiveness, most mass-market vaccines must be stored in refrigerated or frozen conditions but the specialized equipment associated with such storage limits the success of administration programs. Creating dry powder vaccines that can be stored at room temperature is an efficient method to limit liquid vaccine wastage caused by exposure to warmer temperatures. This is achieved by combining the active ingredient with protective stabilizing materials and drying the solution into a powder using spray drying. However, identifying and developing effective dry powder products is costly and time-consuming. This research aims to reduce the costs associated with vaccine development by using other drying methods to identify potential protective sugars without the need for large-scale experiments, as well as by using mathematical models to predict the outcomes of the drying process. The effect of various stresses during the drying process on the active vaccine ingredient are evaluated to improve the effectiveness of the final dry product. Overall, the ability to produce stable dry powder vaccines will allow for more wide-spread vaccination programs and stockpiling of vaccines to better prepare for global pandemics.

Acknowledgements

I would like to start by thanking my supervisors, Dr. Michael R. Thompson and Dr. Emily D. Cranston, for their support and guidance over the past nearly five years. Your excitement and drive for research have been inspirational to me, and I am truly grateful to have been given the opportunity to work on research that excites me in an innovating and promising field.

I would also like to thank Dr. Zhou Xing and his research group in the McMaster Immunology Research Center, including Sam Afkhami, Xueya Feng, Mathy Jeyanathan, and Anna Zganiacz, for their help with all things virus and cell-culture related, as well as our industrial advisors from GSK and Merck. To my summer student, Myla Manser, thank you for all your hard work in the lab at McMaster which made it a smooth transition while I moved to UBC. I look forward to seeing your continued success as you finish up your Master's!

Thank you to all my friends and fellow graduate students that have made the past five years fly by. To the Crannies, past and present, thank you for your willingness to listen and offer advice for my research even though there was not a CNC in sight. To the Modern D&D Crew, thanks for offering a needed respite from the real world every few weekends and always being willing to break-down the newest Marvel news.

Finally, to my family and friends: thank you for your support throughout my PhD. To Alex, Elli, and Joonas, thank you for your encouragement, and the many beers and adventures. To my coach Paula, thank you for your support and flexibility as I tried to balance grad school and running. To Clive, Jody, and Adrienne, thank you for your unwavering love and support throughout grad school and in all aspects of my life. To our PhD kitties Calla, Cleo, and Skittles, you were always there to offer cuddles after a hard day or help sit on the keyboard while I was trying to write. It was always a highlight of every day to come home to your affection. Last, but certainly not least, thank you to my wife Oriana for riding all the highs and lows that grad school has offered by my side. From months apart on exchange, to a week spent in the same car moving to the West Coast, to 12+ months working from home in the same small Vancouver apartment, there is no-one else I would have wanted by my side. Your hard work and dedication inspire me to be my best self in all aspects of my life, in research and beyond. I can't wait to see what adventures await in the next chapter of our lives!

Table of Contents

Table of Figures

Table of Tables

Abbreviations

AdHu5	Human type 5 adenovirus
AFM	Atomic force microscopy
A.U.	Arbitrary units
BSA	Bovine serum albumin
CHRP	Collaborative Health Research Program
CQDM	Quebec Consortium for Drug Discovery
DNA	Deoxyribonucleic acid
DSC	Differential scanning calorimetry
EDC	1-ethyl-3-(3-dimethylaminopropyl) carbodiimide hydrochloride
EDTA	Ethlyenediaminetetraacetic acid
FACS	Flow cytometry
fSiNP	Fluorescent silica nanoparticle
FTIR	Fourier-transform infrared
GFP	Green fluorescent protein
HEPES	4-(2-hydroxyethyl)-1-piperazineethanesulfonic acid
HIV	Human immunodeficiency virus
HSD	Honestly significant difference
LED	Light emitting diode
MEM	Minimum essential medium
MES	2-ethanesulfonic acid
M_r	Molecular weight
OCE	Ontario Centres of Excellence
REA	Reaction engineering approach
RH	Relative humidity
RNA	Ribonucleic acid
PBS	Phosphate buffered saline
PFA	Paraformaldehyde
Pfu	Plaque forming units
pSiNP	Protein-coated silica nanoparticle
SD	Standard deviation

SEM	Scanning electron microscopy
SiNP	Silica nanoparticle
$TCID_{50}$	Median tissue culture infectious dose
TEM	Transmission electron microscopy
T_g	Glass transition temperature
TGA	Thermal gravimetric analysis
USP	United States Pharmacopeia
UV	Ultraviolet
WAXS	Wide angle x-ray scattering
WHO	World Health Organization
XRD	X-ray diffraction

Mathematical Constants and Symbols

α_{v}	Constant based on molecular weight
$\dot{\gamma}$	Characteristic shear rate
ΔP	Difference in vapour pressure at the surface of the droplet and the surrounding atmosphere
δ_{v}	Constant based on molecular weight
ε	Void volume fraction
2θ	Detector angle
λ_{avg}	Average wavelength
σ	Aggregate tensile strength
η	Viscosity
η_0	Pre-exponential viscosity factor at infinite dilution
c	Concentration of dextran
d	Individual particle diameter
D	Aggregate diameter
D_{i}	Diffusion coefficient of *i*
D_{in}	Inner nozzle tip diameter
E_0	Activation energy of viscous flow at infinite dilution
κ	Evaporation rate
k_{B}	Boltzmann constant
$\dot{m}_{\mathrm{gas}}$	Spray gas mass flow rate
$\dot{m}_{\mathrm{liq}}$	Liquid feed mass flow rate
$\dot{M}_{\mathrm{w}}$	Evaporative mass transfer rate of water
MW_w	Molecular weight of water
Pe	Peclet number
r	Radius of the gas layer
R	Universal gas constant
R_{g}	Radius of gyration
R_0	Primary viral particle radius of gyration
R_{H}	Hydrodynamic radius

T	Temperature
v_{av}	Average velocity
v_{gas}	Spray gas velocity
v_{liq}	Liquid feed velocity
x	Number of individual particles in an aggregate
x_{i}	Mass fraction of *i*

Contributions

B. A. Morgan, Z. Xing, E. D. Cranston, M. R. Thompson, **2019**. "Acoustic levitation as a screening method for excipient selection in the development of dry powder vaccines", *International Journal of Pharmaceutics*, **563**, 71-78, DOI: 10.1016/j.ijpharm.2019.03.026.

B. A. Morgan, M. Manser, M. Jeyanathan, Z. Xing, E. D. Cranston, M. R. Thompson, **2020**. "Effect of shear stresses on adenovirus activity and aggregation during atomization to produce thermally stable vaccines by spray drying", *ACS Biomaterials Science & Engineering*, **6**, 7, 4304-4313, DOI: 10.1021/acsbiomaterials.0c00317.

B. A. Morgan, E. Niinivaara, Z. Xing, M. R. Thompson, E. D. Cranston, **2021**. "Validation of a diffusion-based single droplet drying model for encapsulation of a viral-vectored vaccine using an acoustic levitator", Manuscript submitted to *International Journal of Pharmaceutics.*

Chapter 1: Introduction and Objectives

1.1 Introduction

One of the major challenges facing the global health community is the production of thermally stable vaccines that eliminate the need for cold-chain storage requirements. This issue has been identified by global organizations such as the Bill and Melinda Gates Foundation and the World Health Organization (WHO) as a necessary development for fighting diseases with a global impact, such as HIV, malaria, and tuberculosis.[1] Cold chain protocols require storage and transportation at temperatures as low as -80°C to achieve an acceptable shelf life for the product.[2] These low temperatures serve to inhibit molecular movement and hinder aggregation of the active component, therefore avoiding inactivation.[3] However, maintenance of the cold chain storage requirements is very costly and inhibits distribution of vaccines, particularly in poor and developing countries, and any disruption to the cold chain can cause inactivation and loss of product.[4] The WHO has reported higher than 50% vaccine wastage globally, and the government of Ontario has previously estimated that vaccine waste in the province costs upwards of $3 million per year.[5,6] The development of vaccines that have long term thermal stability also allows for the stockpiling of these products for use in times of need, and would aid in the fight against global pandemics such as the current COVID-19 pandemic.

Although storage in various liquid buffer formulations is one option to increase thermal stability, the most widespread method of stabilizing pharmaceuticals containing biologically active agents is by drying them into a powder form.[7,8] Vitrification, or dispersion of the active component within the amorphous phase of a solid matrix in order to limit mobility and interactions, is the stabilizing mechanism behind this.[9] Dry powder vaccines are particularly well-suited to eliminating problems associated with the cold chain, as dry vaccine formulations are less prone to temperature-induced instability, and also allow for stockpiling and alternative administration routes, such as inhalation.[7,10] One of the most common processes to create thermostable dry vaccines is lyophilization, in which the vaccine is frozen, and water is removed by sublimation at low pressures to create a solid, porous cake (also known as freeze drying).[11] However, spray drying has become increasingly more common in the pharmaceutical industry due to low processing costs, easily available equipment, high throughput, and ease of scalability, compared to lyophilization which is more technically complex and time and resource intensive.[12,13] In the spray drying

process, a liquid feed, containing stabilizing excipients and the material to be stabilized, is atomized via pressurized gas into a heated drying chamber. Evaporation of the liquid causes precipitation of the dissolved excipients into solid particles, which are then collected using a cyclone.[14] Many research efforts have focused on particle engineering to optimize parameters impacting the performance of the dried powders, such as particle size and morphology, by controlling the particle formation process.[15] This can include controlling the input parameters to the spray dryer, such as liquid and atomizing gas feed rates, and drying temperature, or by controlling the excipients included in the formulation.

Current formulation development is often based on historic experience, chemical interaction modelling software, and trial and error methods, which has prevented the stabilization of biologics through spray drying from reaching its full potential.[16] These limitations mean that formulation development can rapidly use up large amounts of active vaccine components, and may limit the ability to test the effectiveness of a wide variety of excipients. A high-throughput screening method would allow for rapid, efficient formulation development, however the lack of fundamental knowledge on interactions between various biologics and stabilizing excipients means that any successful screening method will need to evaluate formulations on a case-by-case basis.[10,17] There are many examples of single-droplet drying processes that are comparable to spray drying in the literature, such as levitation by acoustic or aerodynamic forces, suspension of a droplet on a thin filament, or large single-droplet drying columns.[18] However, there exist no examples in the literature comparing single droplet drying techniques to spray drying for the purpose of stabilizing biologic materials.

The other challenge in developing thermally stable dry powder vaccine products are the multiple stresses inherent to the spray drying process that can damage the sensitive material being stabilized. During spray drying, materials are exposed to thermal, shear, and desiccation stresses, as well as a large air-liquid or air-solid interfacial area.[14] The structural integrity of human type 5 adenovirus (AdHu5) when exposed to thermal stresses has previously been reported in the literature, however for the other stresses we must rely on experience gained from studying other biologic materials such as proteins and enzymes.[19–21] In order to reduce adenoviral activity loss caused by the spray drying process, we first must understand the mechanisms that determine AdHu5 instability when exposed to the various processing stresses. Adenoviruses are commonly

used to deliver vaccines against infectious diseases such as tuberculosis, and are the focus of all the research done in this thesis.[22]

1.2 Thesis Objectives

Although thermally stable, spray dried powder vaccines are a promising development, identifying and optimizing excipient formulations is a costly and time-consuming task. The impact of the various processing stresses of spray drying, both individually and in combination, are also not well-understood when applied to viral vectors. In order for spray dried vaccine products to become industrially viable, it is essential to understand where process inactivation is occurring so it can be minimized, as well as to reduce the time and financial costs of formulation development. This thesis aims to provide a deeper understanding of how the spray drying process can be used to create thermally stable vaccine powders, and how the processing parameters can be controlled to prevent damage to viral vectors. The tools created and used for this work, including the acoustic levitator and the droplet drying model, will assist both the research community and the vaccine industry in designing, developing, and bringing viral-vector based dry powder vaccines to market. The main objectives of this thesis are as follows:

1. **Investigate the effect of shear stresses on a human type 5 adenovirus (AdHu5).** Compared to thermal and dehydration stresses, which are both integral to the spray drying process and widely reported on in the literature, the impact of shear stresses on biologic materials is less clear. The goal of this work is to determine how much consideration should be given to shear stresses when developing AdHu5-based spray dried vaccines. Understanding the mechanisms governing viral vector inactivation during spray drying is important to reduce development times by identifying the steps of the spray drying process that are most damaging and focusing optimization efforts on those steps.
2. **Develop a screening method and a mathematical model that can accurately mimic or model spray drying.** Identification of a suitable screening method can limit the amount of material necessary to develop new stabilizing excipient formulations, and therefore reduce the cost of development. The development of a mathematical model that can predicted the performance of spray dried powders will also reduce formulation development times and costs by identifying potential stabilizing excipients without the need for experimental studies. The main contribution of this model will be the ability to predict the distribution

of components within the final dried particle, and more specifically the distribution of AdHu5, which plays a large role in determining viral vector activity loss.

1.3 Thesis Outline

This thesis is comprised of two peer-reviewed manuscripts, and one manuscript in preparation for submission, and a total of six chapters.

Chapter 1: Introduction and Objectives

This chapter introduces the main themes and motivation of this work, as well as the overall objectives and outline of this thesis.

Chapter 2: Literature Review

This chapter presents an overview of the relevant academic literature and concepts involved in the work done in this thesis.

Chapter 3: Effect of Shear Stresses on Adenovirus Activity and Aggregation During Atomization to Produce Thermally Stable Vaccines by Spray Drying

This chapter presents the first study of the effect of shear stresses from spray drying on an adenoviral vector. Shear stresses are an unavoidable stress produced by spray drying, and can lead to deactivation and aggregation of viral vectors. This work found that shear stresses during spray drying reversed adenovirus aggregation that was present in the liquid formulation, and could slightly improved formulation activity, although the activity gains or losses from shear stresses are minimal compared to the overall spray drying process losses. This chapter has been published in *ACS Biomaterials Science & Engineering*.[23]

Chapter 4: Acoustic Levitation as a Screening Method for Excipient Selection in the Development of Dry Powder Vaccines

This chapter examines feasibility of using an acoustic levitator drying system as a screening method for spray drying by comparing the dry powders created through each processing method. Three different binary excipient blends were evaluated for similarities in morphology, crystallinity, water content, glass transition temperature, and viral activity. This work concluded that acoustic levitation could create materials with characteristics that follow the trends seen in materials

produced via spray drying, and therefore is a suitable screening method. This chapter has been published in the *International Journal of Pharmaceutics.*[24]

Chapter 5: Validation of a Diffusion-Based Single Droplet Drying Model for Encapsulation of a Viral-Vectored Vaccine Using an Acoustic Levitator

This chapter describes the development and validation of a mathematical drying model based on diffusion of components. The predictions made by the model were compared to experimental results from the acoustic levitator for various excipient blends at various drying conditions. It was concluded that the model could accurately predict particle characteristics such as drying time, particle size, and component distribution, and is an important step towards reducing formulation development time and cost by using modelling as a starting point. This has been submitted for publication in the *International Journal of Pharmaceutics*.

Chapter 6: Conclusions and Future Outlook

This chapter summarizes the major contributions from this work and discusses potential directions for future work in the development of thermally stable dry powder vaccines through spray drying.

References

1. Ford, A. Q., Touchette, N., Hall, B. F., Hwang, A. & Hombach, J. Global Vaccine and Immunization Research Forum: Opportunities and challenges in vaccine discovery, development, and delivery. *Vaccine* **34**, 1489–1495 (2016).

2. Wang, W. Instability, stabilization, and formulation of liquid protein pharmaceuticals. *Int. J. Pharm.* **185**, 129–188 (1999).

3. Kumru, O. S. *et al.* Vaccine instability in the cold chain: Mechanisms, analysis and formulation strategies. *Biologicals* **42**, 237–259 (2014).

4. Hasija, M., Li, L., Rahman, N. & Ausar, S. F. Forced degradation studies: an essential tool for the formulation development of vaccines. *Vaccine Dev. Ther.* **3**, 11–33 (2013).

5. Weir, E. & Hatch, K. Preventing cold chain failure: Vaccine storage and handling. *Can. Med. Assoc. J.* **171**, 1050 (2004).

6. World Health Organisation. *Monitoring vaccine wastage at country level*. (2005).

7. Amorij, J. P., Huckriede, A., Wilschut, J., Frijlink, H. W. & Hinrichs, W. L. J. Development of stable influenza vaccine powder formulations: Challenges and possibilities. *Pharm. Res.* **25**, 1256–1273 (2008).

8. Croyle, M. A., Cheng, X. & Wilson, J. M. Development of formulations that enhance physical stability of viral vectors for gene therapy. *Gene Ther.* **8**, 1281–1290 (2001).

9. Crowe, J. H., Carpenter, J. F. & Crowe, L. M. The Role of Vitrification in Anhydrobiosis. *Annu. Rev. Physiol.* **60**, 73–103 (1998).

10. Chen, D. & Kristensen, D. Opportunities and challenges of developing thermostable vaccines. *Expert Rev. Vaccines* **8**, 547–557 (2009).

11. McAdams, D., Chen, D. & Kristensen, D. Spray drying and vaccine stabilization. *Expert Rev. Vaccines* **11**, 1211–1219 (2012).

12. Ré, M. I. Microencapsulation By Spray Drying. *Drying Technol.* **16**, 1195–1236 (1998).

13. Franks, F. Freeze-drying of bioproducts: Putting principles into practice. *Eur. J. Pharm.*

Biopharm. **45**, 221–229 (1998).

14. Saluja, V. *et al.* A comparison between spray drying and spray freeze drying to produce an influenza subunit vaccine powder for inhalation. *J. Controlled Release* **144**, 127–133 (2010).

15. Vehring, R. Pharmaceutical particle engineering via spray drying. *Pharm. Res.* **25**, 999–1022 (2008).

16. Ameri, M. & Maa, Y. F. Spray drying of biopharmaceuticals: Stability and process considerations. *Drying Technol.* **24**, 763–768 (2006).

17. Toniolo, S. P. *et al.* Excipient selection for thermally stable enveloped and non-enveloped viral vaccine platforms in dry powders. *Int. J. Pharm.* **561**, 66–73 (2019).

18. Schutyser, M. A. I., Perdana, J. & Boom, R. M. Single droplet drying for optimal spray drying of enzymes and probiotics. *Trends Food Sci. Technol.* **27**, 73–82 (2012).

19. Rexroad, J. *et al.* Structural stability of adenovirus type 5. *J. Pharm. Sci.* **92**, 665–678 (2003).

20. Maa, Y. F. & Hsu, C. C. Protein denaturation by combined effect of shear and air-liquid interface. *Biotechnol. Bioeng.* **54**, 503–512 (1997).

21. Xu, Y. *et al.* Protein quantity on the air-solid interface determines degradation rates of human growth hormone in lyophilized samples. *J. Pharm. Sci.* **103**, 1356–1366 (2014).

22. Afkhami, S. *et al.* Spray dried human and chimpanzee adenoviral-vectored vaccines are thermally stable and immunogenic in vivo. *Vaccine* **35**, 2916–2924 (2017).

23. Morgan, B. A. *et al.* Effect of Shear Stresses on Adenovirus Activity and Aggregation during Atomization To Produce Thermally Stable Vaccines by Spray Drying. *ACS Biomater. Sci. Eng.* **6**, 4304–4313 (2020).

24. Morgan, B. A., Xing, Z., Cranston, E. D. & Thompson, M. R. Acoustic levitation as a screening method for excipient selection in the development of dry powder vaccines. *Int. J. Pharm.* **563**, 71–78 (2019).

Chapter 2: Background and Literature Review

2.1 Stabilization of Viruses and Viral-Vector Based Products

Viral vectors have been shown to have several advantages compared to traditional vaccine products.[1] These advantages include highly efficient transduction of DNA, inducing high levels of antibody responses, and high immunogenicity, which reduces the need for adjuvants and increases the safety of the final vaccine.[1–3] In addition to the antibody response, viral-vector based vaccines can induce a cytolytic T cell response that can target regions of genetic material conserved between different strains of the same virus, which is an important step towards a universal influenza vaccine and an effective HIV vaccine.[4] Specifically, compared to retroviral and lentiviral vectors, adenoviral vectors of the type used in this work show a better safety response (although studies have shown that anywhere between 30% to 100% of humans may have developed an immunity to adenoviruses caused by high amounts of exposure).[1,5]

The stabilization of viral vector based vaccine products can significantly reduce costs and increase the effectiveness of vaccination programs by eliminating cold-chain protocols.[6] However, compared to inactive or protein-based vaccines, thermostabilization of live viral vectors represents a significant challenge as there is a much greater chance of inactivation.[7] The viral vector used for all of the work in this thesis was a recombinant replication-deficient human type 5 adenoviral vector (AdHu5). Adenoviruses are categorized as non-enveloped viruses, consisting of a protein capsid surrounding a nucleoprotein core, and have a diameter of 70 to 100 nm, as seen in Figure 2.1.[3]

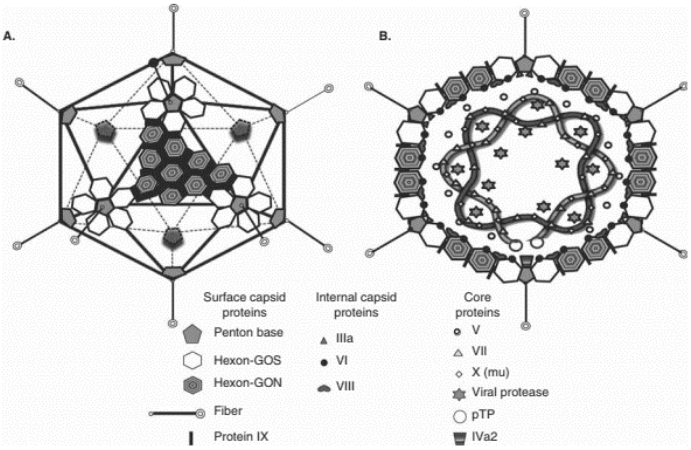

Figure 2.1: (A) Outer structure of an adenovirus particle showing surface proteins; (B) Cross-sectional view of an adenovirus particle showing DNA, and surface and core proteins. Figure reproduced from reference 3.

The ability of an adenovirus particle to infect a host is dependent on maintaining the structure shown in Figure 2.1, as well as the integrity of the genetic material.[8] This opens up many pathways for inactivation throughout the various processing techniques used to stabilize these viral vectors. The most obvious route for viral deactivation is through damage to the fragile fiber proteins on the capsid, which are responsible for initiating the infection process by attaching to host cells.[9] These fiber proteins can be damaged by exposure to physical forces such as shear, as well as denatured or unfolded by exposure to heat or interfaces, as can the penton and hexon proteins shown in Figure 2.1.[10] Unfolding of the capsid proteins can also allow access to previously hidden chemical groups, causing further loss of infectivity via aggregation.[11] Aggregation can also occur when the virus is exposed to very acidic or low ionic strength conditions.[12] The genetic material contained within the capsid can also be damaged by exposure to UV light; however, adenoviruses (in particular) are one of the most resistant viruses to UV damage and can still infect cells with damaged DNA.[13] Many of these degradation pathways are exacerbated at air-liquid or air-solid interfaces, which increase exposure to UV and oxidative stresses as well as provides a driving force for protein unfolding based on hydrophobic amino acid groups.[14–16] Although there have been many efforts made to understand the inactivation processes that occur during virus or viral vector stabilization, the complexity and multicomponent nature of these biologics still presents a challenge for the industry.[17]

2.2 Vitrification to Create Thermally Stable Products

One solution to preventing changes to the protein structure and chemical reactions with biologic materials from occurring is to immobilize the biologic in a matrix through vitrification.[18] Vitrification is a widely used strategy to stabilize sensitive materials, which are encapsulated in a matrix of an amorphous, brittle glass to reduce both the mobility of a biologic and remove its interactions at interfaces and with other particles.[6] In this case, an amorphous, brittle glass refers to a material that has been cooled such that the molecules are in an unordered state (amorphous), and the molecular mobility of the material is low enough that chemical reactions and motion within the matrix are effectively stopped (brittle glass).[19]

The most common and effective method of vitrification for stabilization is storing biologic materials in a water-based solution at temperatures ranging from -20°C to -80°C, where the biologic is entrapped within the frozen solution.[20] To increase the long-term stability, and raise storage temperature requirements to between -20°C to 4°C, buffers and cryoprotectants such as glycerol or sucrose are often added to liquid storage formulations.[21] However, this method requires constant maintenance of sub-zero or refrigerated temperatures and is very costly to maintain throughout production, distribution, storage, and eventual usage.[22] To reduce costs and limit vaccine waste due to temperature fluctuations during storage, the encapsulating matrix can also consist of dry, solid state excipients. This is achieved by the water replacement hypothesis, which posits that as water is removed from the system during the drying process, the matrix excipients protect proteins in the biologic by hydrogen bonding to charged and polar groups where water was previously bound to prevent structural changes and denaturation when in the dry state, as shown in Figure 2.2.[18] Various single and blended excipients have been shown to successfully stabilize biologic materials in the dry state, including carbohydrates, amino acids, and polymers.[23]

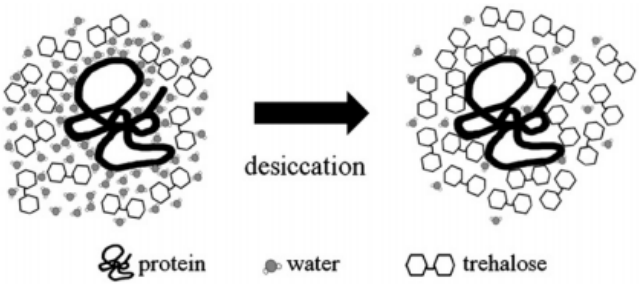

Figure 2.2: A depiction of the water replacement hypothesis, shown for trehalose molecules replacing water molecules to stabilize a folded protein. Figure reproduced from reference 24.

The other mechanism behind stabilization is the vitrification hypothesis, which theorizes that the dry state excipient locks the material being stabilized in place, limiting mobility and aggregation, as well as offering protection from reactants and exposure at interfaces.[18] Although these are separate stabilization hypotheses, it is widely believed that these mechanisms act in tandem in order to achieve stabilization of a material.[18]

2.2.1 Processing Methods

There are many techniques to dehydrate excipient and biologic solutions that are widely accepted in the pharmaceutical industry, including air drying, freeze drying, spray-freeze drying, spray drying, supercritical drying, and vacuum drying, all of which have their own potential benefits and drawbacks.[6] Freeze drying (or lyophilization) is the most widely used of these methods, and several lyophilized products can be found on the market.[24] In this process, the sample is frozen, creating a solid matrix of ice and excipients, and the ice is removed via sublimation under vacuum.[25] This method reduces the exposure of sensitive materials to heat, however the final material can only be administered via reconstitution and injection, unless further processing is done to create particles of an acceptable size for inhalation, introducing more stresses to the biologic.[26] Other alternatives, such as spray drying and spray-freeze drying, can create particles again to be administered via reconstitution but are also within an acceptable size range and distribution for inhalation, which has been shown to induce a better immune response than intramuscular injection for certain influenza-based products.[27] Pulmonary delivery allows for these products to be administered without the use of needles, which can increase patient compliance and comfort, and reduce the risk of blood-based disease transmission.[28] These powders can also be reconstituted and injected, offering several delivery methods that can be tailored to the product

and situation. Figure 2.3 shows a comparison of spray-freeze dried and spray dried inulin powders used for inhalation. The spray-freeze dried particles are significantly more porous and larger than the spray dried powders, which are smaller and more solid in appearance.

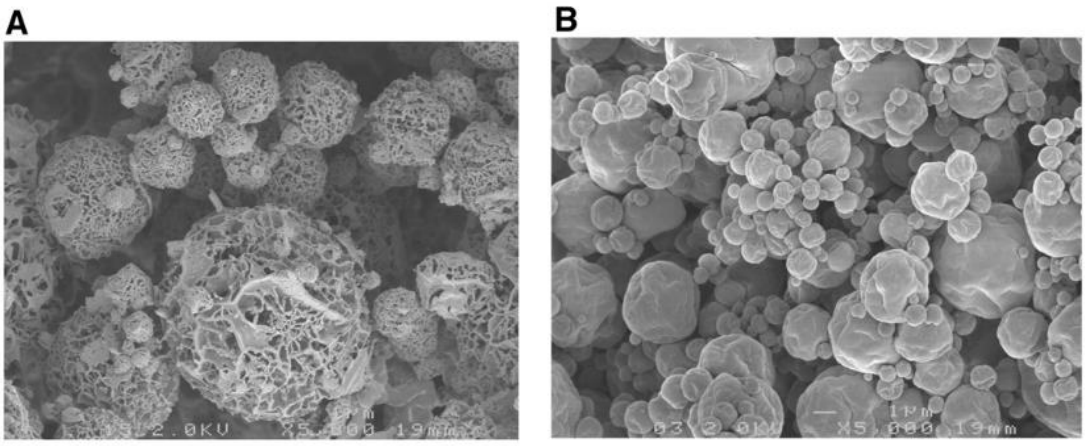

Figure 2.3: An SEM comparison of spray-freeze dried (A) and spray dried (B) powders of inulin containing an influenza subunit vaccine. Figure reproduced from reference 27.

2.2.2 Long-Term Stability

When designing thermally stable dry powder vaccines products, it is important to consider both the immediate losses in activity caused by processing stresses, as well as the losses caused by physical instabilities over longer periods of time.[29] The long-term (weeks to months) stability of thermostable products must be suitably high to administer the distribution of vaccines within rural or under-developed regions that may lack the infrastructure to maintain cold chain protocols.[7] Two of the more important material properties that can impact long-term stability are the glass transition temperature (T_g; the temperature at which a brittle glass transforms into a rubbery glass), and the moisture content or the ability of the encapsulating material to uptake water. These two material characteristics are inherently linked, as water is a plasticizing agent that will depress the glass transition temperature and can also induce changes in the crystal structure (if present), leading to instability in the prodyct.[30–32]

Both the chemical and physical stability of the material are dependent on the T_g, as storage at or above the T_g will greatly increase the mobility of the entrapped biologic and increase the chance of its degradation.[33,34] The ideal storage temperature is at the so-called Kauzmann temperature, approximately 50°C below the T_g.[35] At this temperature, molecular movement is

considered equivalent to that of the crystalline state (i.e. insignificant).[36] Amorphous materials are more likely to fully encapsulate and stabilize biologics compared to crystalline materials, as it is more favorable to have a homogeneous crystal structure and thus will exclude the biologic from areas of such long-range order. Studies in the literature have reported that proteins and peptides have greater stability in amorphous materials.[28] In this case, crystalline refers to a material where the molecules form a highly ordered structure. Shifts from crystalline to amorphous, and amorphous to crystalline, have both been observed in the literature for spray dried powders, with a loss in biologic stability seen in each case due to increased motion as the excipient matrix shifts.[30,37,38]Although amorphous materials generally make for more stable products, they also tend to take up more water than crystalline counterparts, meaning that there may need to be a balance of glassy amorphous material to stabilize the biologic and crystalline material to limit moisture uptake.[39]

2.2.3 Selection of Excipients

A wide variety of stabilizing excipients have been reported in the literature. Of these, the most common are sugars and polysaccharides. This is attributed to sugars and polysaccharides contributing to biologic stabilization through both the vitrification and water replacements mechanisms.[40] Many of the carbohydrates commonly reported also have high T_g values and tend to be amorphous when spray dried, both of which are important factors when determining long-term stability.[28,41] Less frequently, proteins and amino acids such as albumin and leucine have also been reported as excipients, although these are more usually included as additives to carbohydrate-based formulations.[38,42] Proteins and amino acids that are surface active and larger than the material being stabilized will compete for space at air-liquid and air-solid interfaces, forcing the biologic into the center of the particles and limiting damaging interactions.[43] There are also reports in the literature of additives such as surfactants, divalent ions, and polymers being included in formulations to increase stability. Surfactants such as Pluronic F68 have been used in spray dried vaccine formulations, and act similarly to proteins as stabilizers by competing for space at the interface, as well as reducing aggregation.[44,45] Divalent ions have been reported to stabilize the viral capsids of rotavirus and adenovirus, as well as a spray dried live attenuated measles vaccine, by preserving the conformation of proteins and lipids at the surface of viral capsids and envelopes.[42,46–48] Finally, polymers such as Eudragit L30 and L100 have been used to protect spray dried vaccines from the enteric environment and allow for oral delivery.[49,50]

Of all the carbohydrate excipients that have been reported to successfully stabilize biologics in the literature, the most common are trehalose, sugar alcohols like mannitol and sorbitol, and sucrose. Dextran and dextrin have also been used successfully. Trehalose in particular has been studied with almost all spray dried vaccine products reported in the literature, and in nature can be found in large quantities in organisms that can survive anhydrobiosis.[51] Similarly, sucrose is widely studied and also found in these organisms.[51] The success of these materials is attributed to the water replacement hypothesis by successfully hydrogen bonding with the biologic in the place of water, which has been shown to be particularly true for enveloped viruses with lipid membranes.[35] Trehalose also has a T_g of approximately 121°C, well above the storage temperature of spray dried powders which is necessary to maintain a glassy matrix.[40] Finally, trehalose is also a relatively small molecule compared to many other polysaccharides used for stabilization, which minimizes steric hindrance between trehalose and the biologic, to allow for tighter packing that limits molecular movement.[35] In contrast, large molecules such as dextran, have been shown in several instances to be ineffective in hydrogen bonding with biologics because of steric hindrance, although dextran is still able to from a glassy matrix with limited molecular mobility and has a suitable T_g of 83°C for room temperature storage.[39,52] Both trehalose and dextran however are hygroscopic, and can take up moisture leading to decreased stability.[53] Mannitol, in contrast, takes up very little water and has a reported T_g of 13°C.[54,55] There is a cost though, as spray dried mannitol is usually crystalline and will not stabilize biologics alone as well as an amorphous material.[54]

The success of blends composed of two or more excipients for stabilizing biologics in the literature suggests that combining excipients with complementary properties is advantageous for optimizing viral activity retention. Other excipients, such as the amino acids, proteins, and surfactants discussed above, are usually added to carbohydrate formulations to enhance properties such as flowability and moisture resistance, though they have been shown to be ineffective at stabilizing viruses and viral vectors on their own.[38,56] Looking at the wide array of excipients that can be considered for stabilization highlights the importance of establishing guidance in the criteria for excipient selection and the optimization of formulations based on the biologic being stabilized. Integrating stabilization optimization (both short term and long term) into the development process early is anticipated to reduce costly needs to re-formulate farther down the development pathway.[57]

2.3 Spray Drying

Currently, the standard (low risk) method to improve the shelf life of a liquid vaccine formulation is through lyophilization.[58] One major limitation for lyophilized products is that they require reconstitution in a liquid medium before administration since the dry solids require subsequent milling to be delivered by other methods. A promising alternative drying technique for flowable particulate solids is spray drying, which has been used in the food industry since 1901 when the technology was first patented.[59] Spray drying has since become popular in the pharmaceutical industry due to its scalability, customization, high throughput, and relatively low operational costs.[60] Examples of pharmaceutical products stabilized through spray drying include drugs, vitamins, bacteria and bacteriophage, proteins, and enzymes.[61–64] Spray drying for vaccine development was first reported in the literature as early as 2001, when Bot et al. reported spray drying lipid-based microparticles containing an inactivated influenza virus.[65]

Briefly, spray drying is a continuous drying process where a liquid feed containing a solvent, stabilizing excipients, and sensitive materials to be stabilized, are dispersed from a nozzle as an aerosol using atomizing gas. The spray enters a heated drying chamber, where the solvent begins to evaporate from the surface of the droplets, eventually causing precipitation of the solutes at the surface and further drying to produce a dried particle. The dried particles are then separated out from the evaporated solvent and drying gas using a cyclone. A schematic of the spray drying process is shown in Figure 2.4.

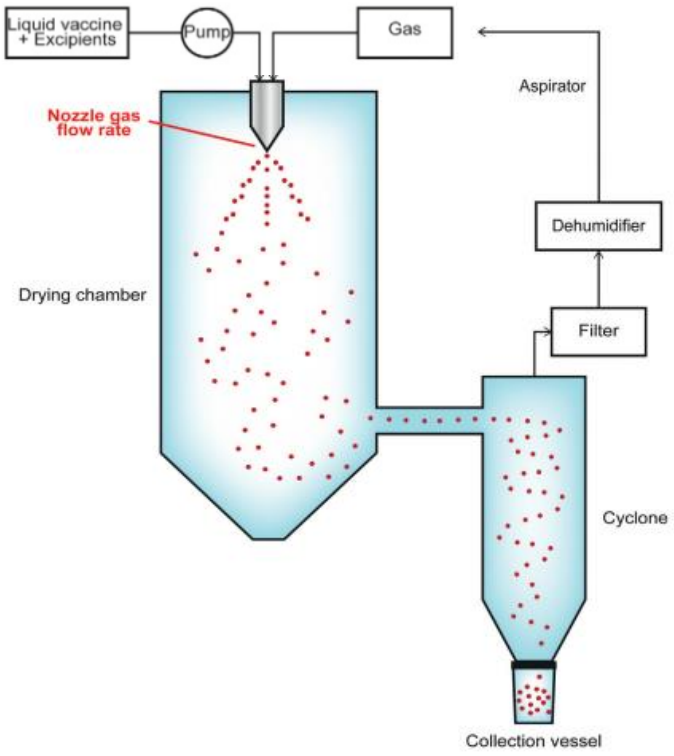

Figure 2.4: A schematic of the spray drying process. The formulation is pumped through a nozzle along with atomizing gas, and enters the heating drying chamber. Evaporation of the solvent causes the formation of solid particles which are then collected using a cyclone. Figure adapted from references 49 and 67.

2.3.1 Spray Drying to Stabilize Vaccine Products

Spray drying is particularly well suited to the stabilization of heat sensitive products, as rapid evaporation of the solvent reduces thermal damage to the biologic.[60] Thermally stable vaccine powders based on viral vectors have successfully been produced for a variety of viruses and viral vectors, including adenovirus, herpes simplex virus, influenza, and measles virus.[26,38,42,66] To date, no spray dried vaccine products are available on the market. One of the only successfully marketed spray dried product containing biologically active material was Exubera, an inhalable insulin produced by Pfizer, which was removed from markets in 2007 for non-spray drying related concerns.[58] However, research continues to be done into spray dried vaccines and there are several products in the clinical trial stage of development.[48] In order to successfully create a thermally stable product, careful consideration needs to be made for both the selection of the encapsulating agent (Sec 2.2.3 above), as well as the spray dryer processing parameters.[38,61,67,68]

Stabilization of many different viruses, viral vectors, bacteria, and bacteriophage has been reported in the literature, using many of the excipients discussed in Section 2.2.3. One of the earliest reports of stabilizing a vaccine product through spray drying in the literature is from 2006, when Wong et al. reported stabilization of *Mycobacterium smegmatis*, a model bacterium for tuberculosis vaccines, by spray drying with L-leucine.[69] Since then, stabilization of bacterium for tuberculosis vaccines through spray drying has been improved to 12 months of storage at room temperature without any loss in viability using blended leucine, bovine serum albumin, polyvinylpyrrolidone, mannitol, and trehalose.[70] Other reports of spray dried tuberculosis vaccines in the literature include stabilization of adenovirus 35 with mannitol, cyclodextrin, trehalose, and dextran; stabilization of several tuberculosis antigen proteins and the adjuvant Lipokel with mannitol; and stabilization of tuberculosis antigen 85B with poly(lactic-*co*-glycolic acid).[53,71,72] Gomez et al. also successfully stabilized a tuberculosis subunit vaccine through spray drying with trehalose and trileucine, and showed that it remained stable after storage at 40°C for one month and up to 26 months at a storage temperature of 25°C.[73,74] Our own research group has successfully stabilized human type 5 adenovirus at room temperature through spray drying with a blend of mannitol and dextran with the end goal of creating a thermally stable spray dried tuberculosis vaccine.[38,67,75] The yearly recurrence of an influenza season means that there are also many studies being done on stabilizing both live attenuated and whole inactivated influenza antigen vaccines based on need.[48] Sou et al. used trehalose with leucine to stabilize whole inactivated influenza antigen; Kanojia et al. spray dried a whole inactivated PR8 influenza virus with trehalose; and Lovalenti et al. used either trehalose or sucrose, along with a variety of proteins, amino acids, surfactants, and ions, to stabilize live attenuated influenza vaccines (Type-A H1N1 and B-strain influenza).[45,76,77] Trehalose and a blend of trehalose and dextran have also been successfully used by our research group to stabilize PR8 influenza.[35] Compared to other spray dried vaccine products where a wide variety of stabilizing excipients can be found in the literature, the best stability reported for influenza is nearly universally with trehalose, or with trehalose as the dominant component in a blend.

2.3.2 Potential Routes for Viral Inactivation During Spray Drying

The overall spray drying process consists of several unit processes performed in series, including pumping, atomization, droplet drying, and powder collection.[58] Each of these steps

subject the virus or viral vector to stresses that can cause activity loss, such as shear stresses during the atomization step or thermal stresses during the drying step.[78]

Shear stresses during atomization are the first potentially significant processing stress to which the virus or viral vector is exposed. Although there are shear stresses caused by pumping the liquid formulation, the shear stresses produced by atomization are much higher.[79] There is a lack of direct measurement concerning the effect of shear stresses on viral vectors in the literature; however, studies on proteins and bacteria have reported varied results, from finding shear insignificant to attributing 93% of bacterial death during spray drying to shear.[80–82] Investigations of the impact of various nebulizers on bacteriophage also concluded that the combination of pressure and shear stresses within the nebulizers was relatively unharmful.[83,84] The mechanism for viral damage caused by shear stresses is mechanical, with proteins and viral capsid components undergoing conformational changes, as well as mechanical damage to DNA and RNA structures.[85,86] With an increase in shear stress, there is also an increase in the air-liquid interfacial area during the atomization step. Any increase in the air-liquid interfacial area has been linked to an increase in protein aggregation, and can induce unfolding of proteins causing a loss of function.[43,87] Similar to shear stresses, there is also a lack of research on the specific effects of increased air-liquid interfaces on viruses and viral vectors.

Thermal stresses arise as the liquid feed is heated in the nozzle but have a more prolonged effect as an aerosolized solution comes into contact with the heated air in the drying chamber, causing the solvent to evaporate. Although the temperature is high during drying, the likelihood of thermal degradation is low due to evaporative self-cooling of the droplets.[88,89] The relatively short drying time, in the range of milliseconds, also limits the amount of damage caused by the thermal stresses associated with drying.[90] Exposure to high temperatures for short periods of time may actually be beneficial to the stabilization of the viral vector, as there is less time for migration to interfaces to occur, and the increase in droplet viscosity as water evaporates can limit protein unfolding and mobility.[90] The most damaging stressor during this step is dehydration, which is a significant factor in the rate of biologic inactivation or death.[91,92] To minimize damage caused by dehydration, stabilizing excipients that are specific to the viral vector must be carefully selected to fulfill the stabilizing mechanisms described by the vitrification and water replacement hypotheses.[93]

The final step in the spray drying process, powder collection, also exposes the viral vector being stabilized to thermal stresses.[43] Thermal disruption of the capsid proteins on the vertices of AdHu5 has been reported in the literature to occur at temperatures as low as 45°C, which is lower than the spray dryer outlet temperature for many spray dried vaccine formulations reported in the literature.[17,48] Figure 2.5 shows the thermal disruption of AdHu5 capsids at 50°C. The RH within the collection chamber also influences the final moisture content of the dried powder, with an increase in moisture being linked to higher activity losses as outlined in section 2.2.2.[88]

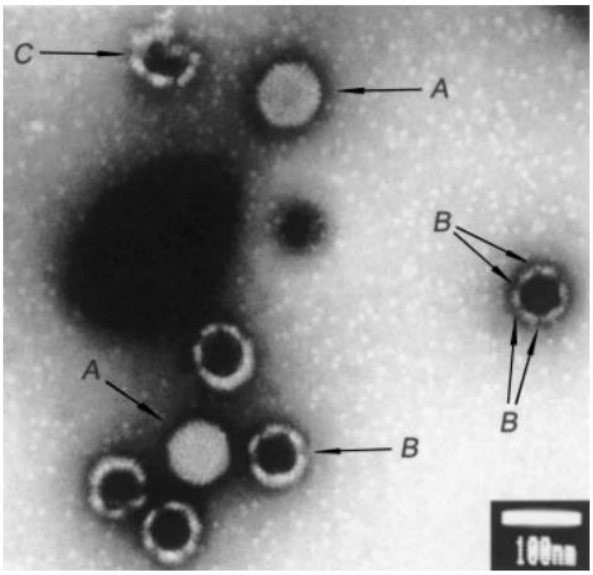

Figure 2.5: A TEM image of AdHu5 at 50°C, showing undisrupted viral capsids (designated A), individually disrupted vertices (designated B) and a completely disrupted capsid (designated C). Figure reproduced from reference 17.

2.3.3 Spray Drying Process Parameters that Determine Particle Characteristics

Many of the processing parameters selected for spray drying have a direct impact on droplet size and evaporation rate, and therefore on particle formation, as well as viral activity. Optimization studies have shown that the most important process parameter to consider is dependant on the application (for example, particle size is a major consideration for spray drying inhalable powders, whereas viral activity is paramount for a powder vaccine that is reconstituted).[67] The evaporation rate is one of two values that determines the Peclet number (Pe), a dimensionless number that can be used to predict which particle morphologies will arise during

formation. The Peclet number is described by the ratio of the evaporation rate to the diffusion rate of each component:[94]

$$Pe = \frac{\kappa}{8D_i} \tag{2.1}$$

where κ is the evaporation rate of the solvent and D_i is the diffusion coefficient of component *i*. If the droplet drying, and therefore the evaporation rate, is slow, then Pe will be less than 1 and the resulting particle will be solid throughout since solutes diffuse away from the surface faster than the solvent evaporates; if the drying and evaporation rate is fast and Pe is greater than 1, then the particles will tend to be hollow as the solutes cannot diffuse away from the surface as the interface recedes, and precipitate earlier.[95] These particles may remain spherical and solid, or may collapse to form a variety of bowl or donut-like morphologies.[96] The spray drying parameters that have the largest impact on particle formation include concentration of the solution being spray dried, liquid feed flow rate, spray gas flow rate, and drying temperature.[97] Studies have also noted changes in particle properties depending on the type of nozzle used for the spray drying process.[98,99]

Increasing the concentration of the feed solution will increase the size of the final dried particles, as well as particle density.[67,99] As the particle dries, there is less disparity between the solute concentration at the surface and at the interior, lowering the driving force for diffusion away from the surface.[100] This causes dissolved excipients to precipitate earlier than they would in a droplet with a lower solute concentration, and it can also increase the thickness of a particle shell as there is more solute in the droplet interior when the shell first forms therefore increasing the density. An increase in solute concentration can also hinder solute diffusion by increasing the overall viscosity of the solution.[101] Slowing solute diffusion can change the surface composition and morphology of the particles by causing an increase in solute concentration at the droplet surface and earlier precipitation of solutes. Additionally, an increase in viscosity will decrease the droplet breakup rate as the liquid feed is sprayed, leading to an increase in the final droplet size.[102]

Changes in both the liquid feed and spray gas flow rates has a direct impact on the size of droplets formed during aerosolization. Decreasing the liquid feed rate reduces the amount of liquid dispersed by atomization and exponentially reduces the droplet size formed.[67,102,103] Similarly, increasing the spray gas flow rate increases the amount of energy used to atomize the liquid feed and leads to a decrease in droplet size.[67,99]

Of all the spray drying parameters, drying temperature has the largest impact on particle formation. An increase or decrease in drying temperature has a corresponding effect on the evaporation rate of the solvent and therefore the Peclet number of the system, with higher temperatures leading to higher Peclet numbers and particles that are more likely to be larger and more hollow than those formed at lower temperatures.[94] Higher drying temperatures can also exceed the glass transition temperatures of the excipients, causing particle coalescence via bridging after shell formation and leading to an overall larger particle size for the product powder.[104] Conversely, lower drying temperatures reduce the Peclet number and tend to produce smaller, more dense particles, however more water is retained which can depress the glass transition temperature and also lead to particle cohesion.[34] Changes in crystallization kinetics of excipients have also been linked to changes in solvent evaporation rate and temperature, with increasing temperature causing an increase in percent crystallinity of materials.[96,105]

Although all the discussed parameters have individual impacts on particle formation, they also interact with each other to form a complex system. Increasing the viscosity of the feed solution can decrease the liquid feed flow rate at a given setpoint, increasing the liquid feed rate can decrease the drying temperature at a given setpoint as there is an increase in material at a lower temperature in the drying chamber, and increasing the spray gas flow rate has a similar impact on drying temperature at a given set point.[67,96,106] This interplay between parameters means that optimizing the processing parameters for spray drying must be done on a per-formulation basis, a time and resource consuming task, although general guidelines have been published such as the one shown in Figure 2.6.[67,107,108] This also highlights the need for accurate particle engineering guidelines and models of the spray drying process that can be used before experimentation to reduce the resources necessary for optimization.[109]

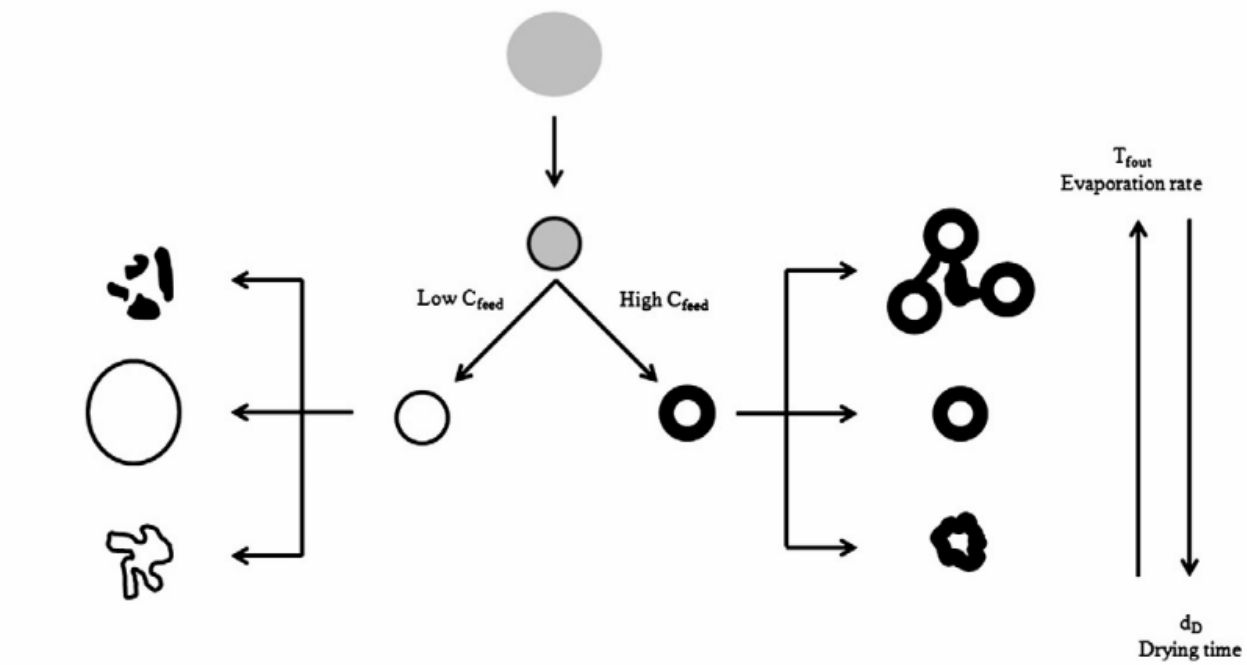

Figure 2.6: A guideline for how liquid feed concentration, drying temperature, and drying time impact the morphology of spray dried powders. Figure reproduced from reference 105.

2.4 Experimentally Modelling the Spray Drying Environment

The development process for spray dried vaccine formulations (process and formulation optimization followed by *in vitro* and potentially *in vivo* testing) means that large amounts of valuable virus or viral vector are consumed every development cycle. The ability to use an experimental technique to model spray drying while eliminating or reducing the amount of virus or viral vector necessary would aid in reducing development costs and expedite formulation discovery and optimization. At its most basic level, spray drying depends on the evaporation of a solvent from a droplet containing dissolved solids.[110] Many techniques exist to study single droplet drying, which date back to the earlier 1950's when Ranz and Marshall used capillary suspension as a spray drying model.[111] Superhydrophobic surfaces have also been used as another intrusive or contact drying method.[112] Examples of less-intrusive techniques such free-falling monodisperse droplet chains and levitation techniques are also examined in the literature, and have the additional benefit of being contactless, eliminating differences in heat and mass transfer that can occur with contact methods.[113–115] Levitation techniques allow for measurements to be made on the same droplet throughout the drying process, as the droplet is held steady in one position with an increased size and drying time compared to spray drying. This is also beneficial for validation of

mathematical single droplet drying models with experimental data.[116] The general disadvantages to levitation techniques are long drying times (approximately 15 to 20 minutes per particle), manual particle deposition and collection, and the limitation of only producing one particle at a time, leading to long preparation times to create enough mass for characterization.

Ultrasonic acoustic levitation is frequently being used nowadays to model single droplet drying since it is less experimentally complex and intrusive than other levitation methods such as electrodynamic and aerodynamic levitation, and small scale acoustic levitators are now readily available in the market.[114] By this technique, a sonotrode is used to create an ultrasonic wave that is reflected off either a flat or a concave acoustic reflector to create a standing wave. Within this standing wave, there are a number of equally spaced sound pressure nodes and anti-nodes. Samples can then be levitated in these acoustic nodes, with the upwards acoustic force from the standing wave counteracting the downwards force of gravity to hold the sample in place.[117] Figure 2.7 shows a commercially available acoustic levitator, as well as a schematic of the working principle of the technique.

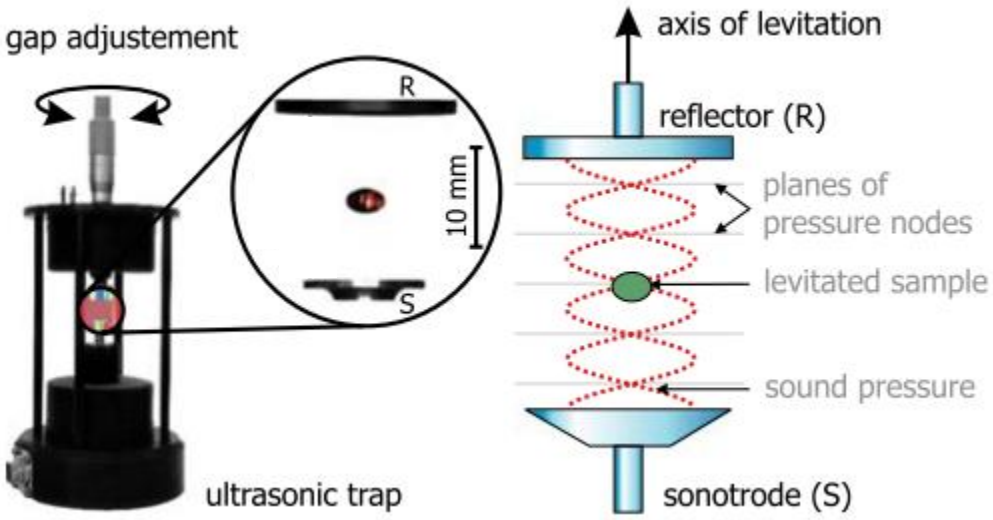

Figure 2.7: (Left) Experimental set-up of a commercially available acoustic levitator showing a sample levitated between the sonotrode (S) and the reflector (R). (Right) A schematic of the working principle of acoustic levitation. Figure adapted from reference 115.

2.4.1 Acoustic Levitation as a Model Spray Drying Environment

The usefulness of a single droplet drying model for spray drying has been identified in the literature, and the ability to slow down the drying process to make accurate observations has many benefits when spray drying pharmaceutical products.[113,118] Acoustic levitation is well suited to that task, as it is contactless, allows for easy control over drying conditions to ensure they are similar to spray drying, and significantly slows down the drying process for easy observation.[119] The biggest downside when comparing acoustic levitation to spray drying is that the particles created in the levitator are several orders of magnitude larger than spray dried particles. There are several examples in the literature that have compared the drying of both pure solvent droplets and droplets containing dissolved solids in acoustic levitation and spray drying.[113,120] Schiffter and Lee reported one of the first comprehensive comparisons between acoustic levitation and spray drying in a two-part publication, involving both pure water droplets, and aqueous solutions of mannitol, trehalose, and catalase.[113,120] They found that despite the differences in droplet sizes between the two techniques, acoustic levitation could be used as a tool to study spray drying. Sherwood and Reynolds numbers measured in the levitator were of the same order of magnitude as those numbers for spray drying, and when solutes were included in the acoustically levitated samples, there was a strong similarity in particle morphology between the two techniques.[113,120] Finally, they also investigated the impact of acoustic streaming on the drying process. Acoustic streaming causes an increase in heat and mass transfer at the surface of acoustically levitated droplets, due to movement of air from the ultrasonic wave, and has been suggested as a potential downside when using acoustic levitation as a spray drying model.[121] However, Schiffter and Lee reported that the acoustic streaming effect actually created forced-convection conditions similar to those found in the spray dryer when the droplets are in free-fall in the drying chamber.[120] Wulsten et al. also reported acoustic levitation as an effective technique to investigate the impact of the solvent system on the morphology of spray dried powders, although a thorough comparison between the two techniques was not undertaken.[122] Figure 2.8 shows a comparison between levitated and spray dried catalase powders.

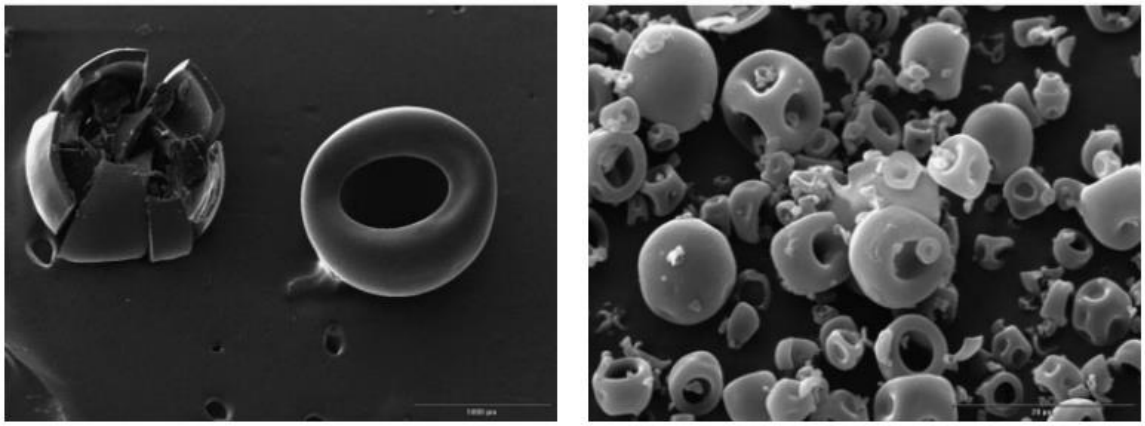

Figure 2.8: An SEM image comparison of levitated (left) and spray dried (right) catalase, processed at the same temperature and displaying a similar collapsed bowl or donut morphology despite the difference in particle size. Figure adapted from reference 117.

The contactless and container-less nature of acoustic levitation allows for real time measurements to be made on the same particle throughout the drying process, and the portability of commercially available levitators allows for the equipment to be set up within other analytical environments.[123] This has been done using wide and small angle x-ray scattering to study crystallization kinetics in real time and follow the developing structure and aggregation of material in the drying droplet.[124,125] Acoustic levitation is particularly advantageous for studying crystallization kinetics, as the lack of contact between the sample and levitator removes extrinsic heterogenous nucleation that is unavoidable in other intrusive processing methods.[126] The small sample size used in acoustic levitation is also beneficial for reducing costs when studying rare or expensive materials. Leiterer et al. set up an acoustic levitator within a synchrotron in order to study the crystallization behaviour of the pharmaceutically-relevant materials aspirin and vitamin C.[124] Using this set-up, they were able to observe the natural crystallization kinetics of these materials from aqueous solutions. This group also reported the use of the same experimental set-up to study the aggregation behaviour of apoferritin and gold nanoparticles in an aqueous droplet.[123,124] They were able to fit the x-ray scattering data to core-shell and spherical models in order to determine the structure of aggregated proteins and nanoparticles.[123,124] In contrast, Benmore and Weber were able to use a similar experimental set-up to create amorphous levitated materials by quenching levitated samples in liquid nitrogen before the materials were able to crystallize.[126] The ability to create both amorphous and crystalline materials is advantageous in the

pharmaceutical industry, as crystallinity can increase long-term stability, while amorphous materials are more soluble and increase short-term stability.[39,126]

The ability to sample droplets from various timepoints throughout the drying process is a key advantage of acoustic levitation as a tool for studying the drying of biologic materials.[127] Lorenzen and Lee used acoustic levitation to study the deactivation kinetics of L-glutamate dehydrogenase by removing droplets of enzyme solution at various points throughout the drying process and measuring residual enzyme activity.[127] They also examined the impact of drying conditions, formulation concentration, and formulation composition on the deactivation kinetics, and found that the residual moisture in the particles had the largest impact.[127] These techniques can be applied to a variety of biologic materials to give a better understanding of the timing and mechanisms of degradation throughout the drying process, which can then be used to improve activity retention.

2.5 Numerically Modelling the Spray Drying Environment

Like environmental modelling of spray drying, accurate numerical modelling can also expedite formulation development while reducing costs by eliminating the need for initial experiments. Unlike environmental modelling, though, numerical modelling can predict the particle formation process and model how components (i.e., excipients, viral vectors, and water) diffuse and segregate as a droplet dries. The ability to predict the distribution of viral vector in a dry particle could then be linked to activity based on the amount present at or near the air-solid interface.[15,16,38] Carrigy et al. demonstrated this for bacteriophage and recommended the use of a shell former that precipitates at the surface early in order to limit access to the air-solid interface.[128] Understanding how particles form during the spray drying process is a critical factor in successfully tailoring powder properties, including particle size, morphology, crystallinity, density, and the component distribution (for blends), for the end product.[129] Between formulation considerations and spray drying process parameters, that are a wide range of variables that can be manipulated to control these properties during the drying process.[108] Figure 2.9 shows a typical drying curve during the formation of a particle, indicating morphological and temperature changes throughout the drying process.[100]

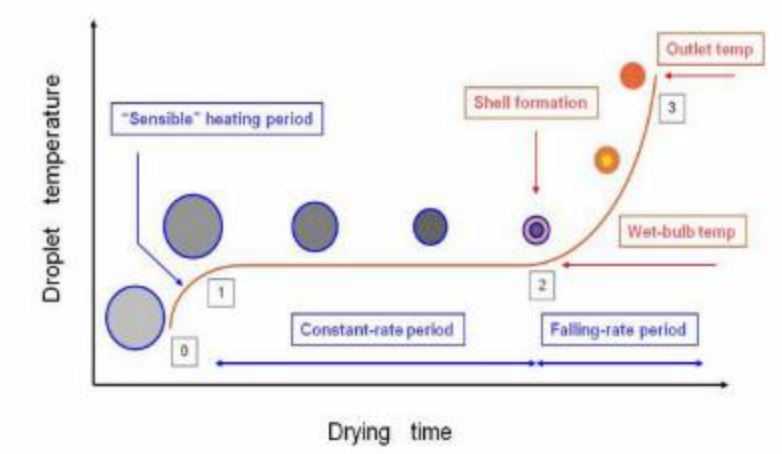

Figure 2.9: A characteristic drying curve for a spray dried droplet, indicating changes in droplet temperature, morphology, and drying stages. Figure reproduced from reference 96.

The droplet drying process can be broken down into two different stages, indicated in Figure 2.9: the constant rate stage, where solvent evaporates from the surface of the droplet at a constant rate; and the falling rate period, where the formation and thickening of a solid shell or crust begins to hinder solvent diffusion and the evaporation rate slows as the solvent must now diffuse through the shell to depart to the surroundings.[116]

2.5.1 Material Properties that Determine Particle Characteristics

There are many material properties that will affect the particle formation process during spray drying. These include excipient size, solubility, crystallization kinetics, and hydrophilicity or hydrophobicity.[94] As seen in Equation (2.1) for the Peclet number, solute diffusion coefficients play a large role in determining when a solid shell will form and the final distribution of components in the particle, and all that is related to the molecular size of the dissolved material by the Stokes-Einstein equation:[68]

$$D_i = \frac{k_B T}{6\pi\eta R_{Hi}} \tag{2.2}$$

where k_B is the Boltzmann constant (J/K), T is the droplet temperature (K), η is the viscosity of the solvent (Pa*s), and R_{Hi} is the hydrodynamic radius of component *i* (m). Using Equation 2.2, it can be seen that the diffusion coefficient of a component will decrease as the size of the excipient molecule increases, leading to slower diffusion and as a result of evaporation, leading to rapid shell formation and the increased probability of a hollow or collapsed particle.[68]

The solubility and hydrophilicity or hydrophobicity of a component can also determine if it will concentrate on the droplet surface, independent of the material diffusion coefficient.[94,130] Materials with higher solubilities will tend to produce smaller, solid particles as it takes longer for the excipient to reach saturation at the surface of the droplet, compared to excipients with lower solubilities.[130] In a similar manner, hydrophobic materials will produce larger particles than hydrophilic ones, as the more hydrophobic excipients will tend to concentrate at the droplet surface and precipitate earlier. Crystallization of components during the drying process will also impact the morphology and size of the final dried particles. Crystal growth on the surface of droplets will create powders with a rougher morphology, whereas their formation in the interior can provide structural support to the hollow regions, preventing particle collapse and leading to larger particle sizes.[96,131]

These material properties can also be taken advantage to control the distribution of components within a particle, and to create particles with specific core-shell morphologies. When developing dry powders for the purpose of stabilizing biologics, one critical factor in determining deactivation is the amount of biologic material at the surface of the particle.[15,16] It is equally likely, though unresearched, that any air interface, even those internal of a particle, will result in deactivation. Excipients that are large molecules, hydrophobic, surface active, or poorly soluble will tend to concentrate at the surface of the droplet, competing with the virus or viral vector for space at the surface and pushing them to the interior of a particle; viruses should be viewed as particulate matter in these circumstances, with no solubility in the droplet solvent. The segregation of components arising within a drying droplet can be used to change the surface morphology of the final dried particles by creating a surface coating of materials such as amino acids or chitosan, increasing the flowability and dispersibility of the powders.[132,133] To visualize the effect of component segregation on a particle, Figure 2.10 shows the change in surface morphology of immunoglobin particles spray dried with and without the amino acid leucine as an additive.[68] Although there are benefits to controlling component segregation, it can also negatively impact viral activity, as segregation of the virus at the surface of spray dried leucine particles has been hypothesized as the main downside to using pure leucine as a stabilizing excipient.[38]

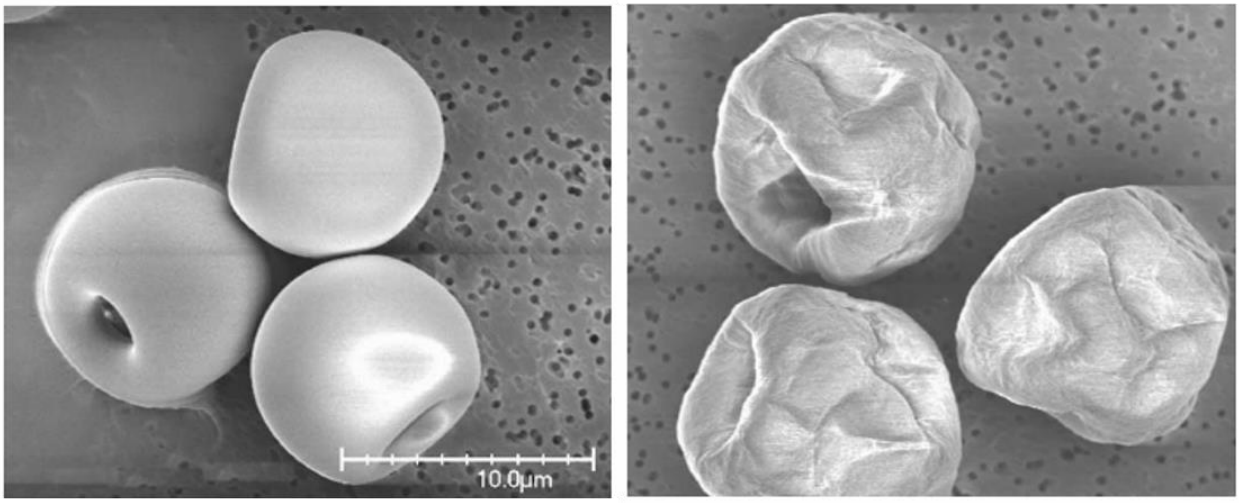

Figure 2.10: Spray dried immunoglobin without leucine (left) and with leucine (right), showing the change in surface morphology with the addition of a surface-active component. Figure adapted from reference 68.

2.5.2 Droplet Drying Models

Modelling the spray drying process is a useful tool that can be used to optimize and design experiments, as well as reduce product development time and cost by reducing the amount of testing necessary.[134] Many different droplet drying models exist in the literature, as the complexity of the single droplet drying process involving mass transfer, heat transfer, phase changes, and fluid dynamics means that there are many potential approaches for model development.[135] Most common in the literature are continuous or two-stage models, although models with up to five discrete drying stages have been developed.[118,136]

Published droplet drying models can be broken down into several categories: semi-empirical, deterministic drying models, and reaction engineering approach (REA) models, each of which have their own benefits and drawbacks.[110] Semi-empirical models for spray drying use data from a characteristic drying curve obtained under controlled drying conditions, which can then be used to model different operating conditions.[137,138] These models use simplified equations that can be solved quickly, and work well for small particles; however they are sometimes overly simplified and may not work well when drying conditions are significantly different from the control.[139] Deterministic models are more complex as they use a set of differential equations, along with corresponding initial and boundary conditions, to describe the droplet drying process.[140] Although

these deterministic models do not usually require experimental droplet drying data as inputs, the moving boundary makes the computational complexity high and often requires extensive computational time and power.[110] They also require knowledge of properties such as diffusion coefficients and thermal conductivities, which limits the model to materials where these properties are already measured or requires additional experimentation.[136] REA models operate under the assumption that evaporation is an activation process with an energy barrier that must be overcome.[140,141] These model computations are relatively fast, however, similar to the semi-empirical models, also require experimental data to relate the activation energy for evaporation to the liquid content of the droplet.[142,143] REA models have been compared to experimental results for many different solute materials, including mannitol, dextrin, and food products, with accurate predictions under a variety of drying conditions.[110,142–145]

As discussed in Section 2.2.2, the crystalline or amorphous nature of spray dried products is important for the long term stability of encapsulated biologics and the ability to predict the crystal structure of excipients should be a goal for any comprehensive spray drying model used to develop thermally stable vaccines. There are a few examples in the literature of crystallinity predictions, however they are often not validated or not valid for non-crystallizing systems.[97,115] One of the most comprehensive model for predicting component crystallinity comes from Hoe et al., who used calculations of the Peclet number, surface enrichment, drying time, and surface saturation to predict the crystallization window of each component, with a longer crystallization window being correlated to increased crystallinity.[97] Abdullahi et al. also calculated component supersaturation at the droplet surface to determine crystallinity, however they also calculated the rate constants of crystal nucleation and growth and related them to the droplet viscosity and interfacial tension to get a very accurate prediction for crystal formation at the droplet surface of multicomponent systems, in agreement with their experimental results.[146] The downside to this model is that it must be adapted to work for amorphous systems, and the authors state that the drying process after shell formation must be described in more detail for the model to be complete.[146]

Similarly, the component distribution in the final particle is important for determining long term stability of thermally stable vaccines, but models in the literature are not validated or are limited to binary mixtures or surface compositions only.[115,147] Being able to accurately model the

distribution of components throughout a final dry particle, along with the surface composition of the particle, will reduce formulation development costs and time by enabling initial screening for excipients to be done without in-lab experimentation. Porowska et al. developed a continuous diffusion-based droplet drying model to predict the surface composition for a system of two excipients dissolved in water.[148] Rather than modelling specific excipients, they used a general small excipient 'A' and a general large excipient 'B' and used a ratio of diffusion coefficients to make predictions of surface composition.[148] Grasmeijer et al. also developed a continuous diffusion-based model of droplet drying, using previously published data to determine diffusion coefficients for trehalose, bovine serum albumin, and water.[147,149] They were able to use this model to predict a wide variety of droplet properties, including temperature history throughout the drying process, component distribution, and the glassy or rubbery state of the particle based on the T_g.[147] Ordoubadi et al. were able to develop and validate experimentally a droplet drying model that could predict the drying kinetics of multi-solvent systems containing solutes, using a time-dependant Peclet number to predict the behaviour of the solutes within the droplet.[150] The work done in Chapter 5 of this thesis aims to improve on the existing models by predicting and validating the distribution of adenovirus within a dry particle without the need for experimental data for diffusion coefficients. Future work in this area should focus on combining crystallinity and component distribution predictions into one continuous model that is valid for a wide variety of excipients and drying conditions that does not require experimental data as an input to the model.

References

1. Rollier, C. S., Reyes-Sandoval, A., Cottingham, M. G., Ewer, K. & Hill, A. V. S. Viral vectors as vaccine platforms: Deployment in sight. *Curr. Opin. Immunol.* **23**, 377–382 (2011).

2. Aucouturier, J., Dupuis, L. & Ganne, V. Adjuvants designed for veterinary and human vaccines. *Vaccine* **19**, 2666–2672 (2001).

3. Appaiahgari, M. B. & Vrati, S. Adenoviruses as gene/vaccine delivery vectors: promises and pitfalls. *Expert Opin. Biol. Ther.* **15**, 337–351 (2015).

4. Liu, M. A. Immunologic basis of vaccine vectors. *Immunity* **33**, 504–515 (2010).

5. Bauer, G. *et al.* In vivo biosafety model to assess the risk of adverse events from retroviral and lentiviral vectors. *Mol. Ther.* **16**, 1308–1315 (2008).

6. Amorij, J. P., Huckriede, A., Wilschut, J., Frijlink, H. W. & Hinrichs, W. L. J. Development of stable influenza vaccine powder formulations: Challenges and

possibilities. *Pharm. Res.* **25**, 1256–1273 (2008).

7. Alcock, R. *et al.* Long-term thermostabilization of live poxviral and adenoviral vaccine vectors at supraphysiological temperatures in carbohydrate glass. *Sci. Transl. Med.* **2**, 1–9 (2010).

8. Tatsis, N. & Ertl, H. C. J. Adenoviruses as vaccine vectors. *Mol. Ther.* **10**, 616–629 (2004).

9. Lasaro, M. O. & Ertl, H. C. J. New insights on adenovirus as vaccine vectors. *Mol. Ther.* **17**, 1333–1339 (2009).

10. Russell, W. C., Valentine, R. C. & Pereira, H. G. The effect of heat on the anatomy of the adenovirus. *J. Gen. Virol.* **1**, 509–522 (1967).

11. Evans, R. K. *et al.* Development of Stable Liquid Formulations for Adenovirus-Based Vaccines. *J. Pharm. Sci.* **93**, 2458–2475 (2004).

12. Rexroad, J., Evans, R. K. & Middaugh, C. R. Effect of pH and ionic strength on the physical stability of adenovirus type 5. *J. Pharm. Sci.* **95**, 237–247 (2006).

13. Eischeid, A. C., Meyer, J. N. & Linden, K. G. UV disinfection of adenoviruses: Molecular indications of DNA damage efficiency. *Appl. Environ. Microbiol.* **75**, 23–28 (2009).

14. Drusch, S. & Diekmann, S. Microencapsulation by Spray Drying. *Handb. Encapsulation Control. Release* **3937**, 35–46 (2015).

15. Devineni, D. *et al.* Storage stability of keratinocyte growth factor-2 in lyophilized formulations: Effects of formulation physical properties and protein fraction at the solid-air interface. *Eur. J. Pharm. Biopharm.* **88**, 332–341 (2014).

16. Xu, Y. *et al.* Protein quantity on the air-solid interface determines degradation rates of human growth hormone in lyophilized samples. *J. Pharm. Sci.* **103**, 1356–1366 (2014).

17. Rexroad, J. *et al.* Structural stability of adenovirus type 5. *J. Pharm. Sci.* **92**, 665–678 (2003).

18. Crowe, J. H., Carpenter, J. F. & Crowe, L. M. The Role of Vitrification in Anhydrobiosis. *Annu. Rev. Physiol.* **60**, 73–103 (1998).

19. Franks, F. *Biophysics and biochemistry at low temperatures*. (Cambridge University Press, 1985).

20. Cruz, P. E. *et al.* Screening of novel excipients for improving the stability of retroviral and adenoviral vectors. *Biotechnol. Prog.* **22**, 568–576 (2006).

21. Croyle, M. A., Cheng, X. & Wilson, J. M. Development of formulations that enhance physical stability of viral vectors for gene therapy. *Gene Ther.* **8**, 1281–1290 (2001).

22. Nyberg-Hoffman, C. & Aguilar-Cordova, E. Instability of adenoviral vectors during transport and its implication for clinical studies. *Nat. Med.* **5**, 955–957 (1999).

23. Costantino, H. R., Langer, R. & Klibanov, A. M. Aggregation of a lyophilized pharmaceutical protein, recombinant human albumin: Effect of moisture and stabilization

by excipients. *Bio/Technology* **13**, 493–496 (1995).

24. Langford, A., Bhatnagar, B., Walters, R., Tchessalov, S. & Ohtake, S. Drying technologies for biopharmaceutical applications: Recent developments and future direction. *Drying Technol.* **36**, 677–684 (2018).

25. Adams, G. The principles of freeze-drying. in *Cryopreservation and Freeze-Drying Protocols* (eds. Day, J. G. & Stacey, G. N.) (Humana Press, 2007). doi:https://doi.org/10.1007/978-1-59745-362-2_2

26. Saluja, V. *et al.* A comparison between spray drying and spray freeze drying to produce an influenza subunit vaccine powder for inhalation. *J. Controlled Release* **144**, 127–133 (2010).

27. Amorij, J. P. *et al.* Pulmonary delivery of an inulin-stabilized influenza subunit vaccine prepared by spray-freeze drying induces systemic, mucosal humoral as well as cell-mediated immune responses in BALB/c mice. *Vaccine* **25**, 8707–8717 (2007).

28. Weers, J. G., Tarara, T. E. & Clark, A. R. Design of fine particles for pulmonary drug delivery. *Expert Opin. Drug Deliv.* **4**, 297–313 (2007).

29. Brandau, D. T., Jones, L. S., Wiethoff, C. M., Rexroad, J. & Middaugh, C. R. Thermal Stability of Vaccines. *J. Pharm. Sci.* **92**, 218–231 (2003).

30. Tong, P. & Zografi, G. Effects of water vapor absorption on the physical and chemical stability of amorphous sodium indomethacin. *AAPS PharmSciTech* **5**, e26 (2004).

31. Yu, L. Amorphous pharmaceutical solids: Preparation, characterization and stabilization. *Adv. Drug Deliv. Rev.* **48**, 27–42 (2001).

32. Ahlneck, C. & Zografi, G. The molecular basis of moisture effects on the physical and chemical stability of drugs in the solid state. *Int. J. Pharm.* **62**, 87–95 (1990).

33. Duddu, S. & Dal Monte, P. Effect of glass transition temperature on the stability of lyophilized formulations containing a chimeric therapeutic monoclonal antibody. *Pharm. Res.* **14**, 591–595 (1997).

34. Hancock, B. C. & Zografi, G. The Relationship Between the Glass Transition Temperature and the Water Content of Amorphous Pharmaceutical Solids. *Pharmaceutical Research* **11**, 471–477 (1994).

35. Toniolo, S. P. *et al.* Excipient selection for thermally stable enveloped and non-enveloped viral vaccine platforms in dry powders. *Int. J. Pharm.* **561**, 66–73 (2019).

36. Shamblin, S. & Tang, X. Characterization of the time scales of molecular motion in pharmaceutically important glasses. *J. …* **103**, 4113–4121 (1999).

37. Vandenheuvel, D., Meeus, J., Lavigne, R. & Van den Mooter, G. Instability of bacteriophages in spray-dried trehalose powders is caused by crystallization of the matrix. *Int. J. Pharm.* **472**, 202–205 (2014).

38. LeClair, D. A., Cranston, E. D., Xing, Z. & Thompson, M. R. Evaluation of excipients for enhanced thermal stabilization of a human type 5 adenoviral vector through spray drying.

Int. J. Pharm. **506**, 289–301 (2016).

39. Hatley, R. H. M. & Blair, J. A. Stabilisation and delivery of labile materials by amorphous carbohydrates and their derivatives. *J. Mol. Catal. B Enzym.* **7**, 11–19 (1999).

40. Grasmeijer, N., Stankovic, M., de Waard, H., Frijlink, H. W. & Hinrichs, W. L. J. Unraveling protein stabilization mechanisms: Vitrification and water replacement in a glass transition temperature controlled system. *Biochim. Biophys. Acta - Proteins Proteomics* **1834**, 763–769 (2013).

41. Hancock, B. C., Shamblin, S. L. & Zografi, G. Molecular Mobility of Amorphous Pharmaceutical Solids Below Their Glass Transition Temperatures. *Pharmaceutical Research* **12**, 799–806 (1995).

42. Ohtake, S. *et al.* Heat-stable measles vaccine produced by spray drying. *Vaccine* **28**, 1275–1284 (2010).

43. Walters, R. H. *et al.* Next generation drying technologies for pharmaceutical applications. *J. Pharm. Sci.* **103**, 2673–2695 (2014).

44. Kreilgaard, L., Frokjaer, S., Flink, J. M., Randolph, T. W. & Carpenter, J. F. Effects of additives on the stability of recombinant human factor XIII during freeze-drying and storage in the dried solid. *Arch. Biochem. Biophys.* **360**, 121–134 (1998).

45. Lovalenti, P. M. *et al.* Stabilization of live attenuated influenza vaccines by freeze drying, spray drying, and foam drying. *Pharm. Res.* **33**, 1144–1160 (2016).

46. Turnbull, A. E., Skulimowski, A., Smythe, J. A. & Alexander, I. E. Adeno-associated virus vectors show variable dependence on divalent cations for thermostability: implications for purification and handling. *Hum. Gene Ther.* **11**, 629–635 (2004).

47. Erk, I. *et al.* A Zinc Ion Controls Assembly and Stability of the Major Capsid Protein of Rotavirus. *J. Virol.* **77**, 3595–3601 (2003).

48. Kanojia, G. *et al.* Developments in the formulation and delivery of spray dried vaccines. *Hum. Vaccines Immunother.* **13**, 2364–2378 (2017).

49. Leclair, D. A., Cranston, E. D., Lichty, B. D., Xing, Z. & Thompson, M. R. Consecutive Spray Drying to Produce Coated Dry Powder Vaccines Suitable for Oral Administration. *ACS Biomater. Sci. Eng.* **4**, 1669–1678 (2018).

50. Año, G. *et al.* A new oral vaccine candidate based on the microencapsulation by spray-drying of inactivated Vibrio cholerae. *Vaccine* **29**, 5758–5764 (2011).

51. Crowe, L. M., Reid, D. S. & Crowe, J. H. Is trehalose special for preserving dry biomaterials? *Biophys. J.* **71**, 2087–2093 (1996).

52. Allison, S. D., Chang, B., Randolph, T. W. & Carpenter, J. F. Hydrogen bonding between sugar and protein is responsible for inhibition of dehydration-induced protein unfolding. *Arch. Biochem. Biophys.* **365**, 289–298 (1999).

53. Jin, T. H., Tsao, E., Goudsmit, J., Dheenadhayalan, V. & Sadoff, J. Stabilizing formulations for inhalable powders of an adenovirus 35-vectored tuberculosis (TB)

vaccine (AERAS-402). *Vaccine* **28**, 4369–4375 (2010).

54. Corbanie, E. A. *et al.* Spray drying of an attenuated live Newcastle disease vaccine virus intended for respiratory mass vaccination of poultry. *Vaccine* **25**, 8306–8317 (2007).

55. Im, A. L. I. K., Kers, M. I. J. A. & Ail, S. T. L. N. The Physical State of Mannitol after Freeze-Drying : Effects of Mannitol Concentration , Freezing Rate , and a Noncrystallizing Cosolute. *J. Pharm. Sci.* **87**, 931–935 (1998).

56. Feng, A. L. *et al.* Mechanistic models facilitate efficient development of leucine containing microparticles for pulmonary drug delivery. *Int. J. Pharm.* **409**, 156–163 (2011).

57. Kristensen, D. & Chen, D. Stabilization of vaccines: Lessons learned. *Hum. Vaccin.* **6**, 227–231 (2010).

58. McAdams, D., Chen, D. & Kristensen, D. Spray drying and vaccine stabilization. *Expert Rev. Vaccines* **11**, 1211–1219 (2012).

59. Fleming, R. S. The Spray Process of Drying. *J. Ind. Eng. Chem.* **13**, 447–449 (1921).

60. Ré, M. I. Microencapsulation By Spray Drying. *Drying Technol.* **16**, 1195–1236 (1998).

61. Bharate, S. S., Bharate, S. B. & Bajaj, A. N. Interactions and incompatibilities of pharmaceutical excipients with active pharmaceutical ingredients : a comprehensive review. *J. excipients food Chem.* **1**, 3–26 (2010).

62. Grasmeijer, N. Improving protein stabilization by spray drying: formulation and process development. (University of Groningen, 2016).

63. Vandenheuvel, D. *et al.* Feasibility of spray drying bacteriophages into respirable powders to combat pulmonary bacterial infections. *Eur. J. Pharm. Biopharm.* **84**, 578–582 (2013).

64. Ghandi, A., Powell, I. B., Howes, T., Chen, X. D. & Adhikari, B. Effect of shear rate and oxygen stresses on the survival of Lactococcus lactis during the atomization and drying stages of spray drying: A laboratory and pilot scale study. *J. Food Eng.* **113**, 194–200 (2012).

65. Bot, A. I. *et al.* Receptor-mediated targeting of spray-dried lipid particles coformulated with immunoglobulin and loaded with a prototype vaccine. *Pharm. Res.* **18**, 971–979 (2001).

66. LeClair, D. A., Li, L., Rahman, N., Cranston, E. D. & Thompson, M. R. Stabilization of HSV-2 viral vaccine candidate by spray drying. *Int. J. Pharm.* **569**, 118615 (2019).

67. LeClair, D. A., Cranston, E. D., Xing, Z. & Thompson, M. R. Optimization of Spray Drying Conditions for Yield, Particle Size and Biological Activity of Thermally Stable Viral Vectors. *Pharm. Res.* **33**, 2763–2776 (2016).

68. Vehring, R. Pharmaceutical particle engineering via spray drying. *Pharm. Res.* **25**, 999–1022 (2008).

69. Wong, Y. L. *et al.* Drying a tuberculosis vaccine without freezing. *Proc. Natl. Acad. Sci.*

U. S. A. **104**, 2591–2595 (2007).

70. Price, D. N., Kunda, N. K., Ellis, R. & Muttil, P. Design and Optimization of a Temperature-Stable Dry Powder BCG Vaccine. *Pharm. Res.* **37**, (2020).

71. Lu, D. *et al.* Pulmonary immunization using antigen 85-b polymeric microparticles to boost tuberculosis immunity. *AAPS J.* **12**, 338–347 (2010).

72. Tyne, A. S. *et al.* TLR2-targeted secreted proteins from Mycobacterium tuberculosis are protective as powdered pulmonary vaccines. *Vaccine* **31**, 4322–4329 (2013).

73. Gomez, M. *et al.* Development of a formulation platform for a spray-dried, inhalable tuberculosis vaccine candidate. *Int. J. Pharm.* **593**, 120121 (2021).

74. Gomez, M. *et al.* Microparticle encapsulation of a tuberculosis subunit vaccine candidate containing a nanoemulsion adjuvant via spray drying. *Eur. J. Pharm. Biopharm.* **163**, 23–37 (2021).

75. Afkhami, S. *et al.* Spray dried human and chimpanzee adenoviral-vectored vaccines are thermally stable and immunogenic in vivo. *Vaccine* **35**, 2916–2924 (2017).

76. Sou, T., Morton, D. A. V., Williamson, M. & Meeusen, E. N. Spray-dried influenza antigen with trehalose and leucine produces an aerosolizable powder vaccine formulation that induces strong systemic and mucosal immunity after pulmonary administration. *J. Aerosol Med. Pulm. Drug Deliv.* **28**, 361–371 (2015).

77. Kanojia, G. *et al.* A Design of Experiment approach to predict product and process parameters for a spray dried influenza vaccine. *Int. J. Pharm.* **511**, 1098–1111 (2016).

78. Saluja, V. *et al.* A comparison between spray drying and spray freeze drying to produce an in fl uenza subunit vaccine powder for inhalation. *J. Controlled Release* **144**, 127–133 (2010).

79. Hasija, M., Li, L., Rahman, N. & Ausar, S. F. Forced degradation studies: an essential tool for the formulation development of vaccines. *Vaccine Dev. Ther.* **3**, 11–33 (2013).

80. Ghandi, A., Powell, I., Chen, X. D. & Adhikari, B. Drying kinetics and survival studies of dairy fermentation bacteria in convective air drying environment using single droplet drying. *J. Food Eng.* **110**, 405–417 (2012).

81. To, B. C. S. & Etzel, M. R. Survival of Brevibacterium linens (ATCC 9174) after Spray Drying , Freeze Drying , or Freezing. *J. Food Sci.* **62**, 167–170 (1997).

82. Gong, P. *et al.* Injury Mechanisms of Lactic Acid Bacteria Starter Cultures During Spray Drying : A Review. *Drying Technol.* **32**, 793–800 (2014).

83. Carrigy, N. B. *et al.* Anti-Tuberculosis Bacteriophage D29 Delivery with a Vibrating Mesh Nebulizer, Jet Nebulizer, and Soft Mist Inhaler. *Pharm. Res.* **34**, 2084–2096 (2017).

84. Carrigy, N. B. *et al.* Prophylaxis of mycobacterium tuberculosis H37Rv infection in a preclinical mouse model via inhalation of nebulized bacteriophage D29. *Antimicrob. Agents Chemother.* **63**, 1–13 (2019).

85. Levy, M. S. *et al.* Effect of shear on plasmid DNA in solution. *Bioprocess Eng.* **20**, 7–13 (1999).

86. Maa, Y.-F. & Hsu, C. C. Effect of high shear on proteins. *Biotechnol. Bioeng.* **51**, 458–465 (1996).

87. Maa, Y. F. & Hsu, C. C. Protein denaturation by combined effect of shear and air-liquid interface. *Biotechnol. Bioeng.* **54**, 503–512 (1997).

88. Ameri, M. & Maa, Y. F. Spray drying of biopharmaceuticals: Stability and process considerations. *Drying Technol.* **24**, 763–768 (2006).

89. Cal, K. & Sollohub, K. Spray drying technique. I: Hardware and process parameters. *J. Pharm. Sci.* **99**, 575–586 (2010).

90. Schmid, K. Spray drying of protein precipitates and evaluation of the nano spray dryer B-90. *PhD Thesis, Ludwig-Maximilians-University, Munich* (2011).

91. Magazù, S., Maisano, G., Migliardo, P. & Villari, V. Experimental simulation of macromolecules in trehalose aqueous solutions: A photon correlation spectroscopy study. *J. Chem. Phys.* **111**, 9086–9092 (1999).

92. Grasmeijer, N., Tiraboschi, V., Woerdenbag, H. J. & Frijlink, H. W. Identifying critical process steps to protein stability during spray drying using a vibrating mesh or a two- fluid nozzle. *Eur. J. Pharm. Sci.* **128**, 152–157 (2019).

93. Maltesen, M. J. & van de Weert, M. Drying methods for protein pharmaceuticals. *Drug Discov. Today Technol.* **5**, 81–88 (2008).

94. Vehring, R., Foss, W. R. & Lechuga-Ballesteros, D. Particle formation in spray drying. *J. Aerosol Sci.* **38**, 728–746 (2007).

95. Tsapis, N., Bennett, D., Jackson, B., Weitz, D. A. & Edwards, D. A. Trojan particles: large porous carriers of nanoparticles for drug delivery. *Proc. Natl. Acad. Sci. U. S. A.* **99**, 12001–12005 (2002).

96. Maa, Y. F., Costantino, H. R., Nguyen, P. A. & Hsu, C. C. The effect of operating and formulation variables on the morphology of spray-dried protein particles. *Pharm. Dev. Technol.* **2**, 213–223 (1997).

97. Hoe, S. *et al.* Use of a Fundamental Approach to Spray-Drying Formulation Design to Facilitate the Development of Multi-Component Dry Powder Aerosols for Respiratory Drug Delivery. *Pharm. Res.* 449–465 (2014). doi:10.1007/s11095-013-1174-5

98. Verhey, J. G. P. Vacuole formation in spray powder particles II: Location and prevention of air incorporation. *Netherlands Milk Dairy J.* **26**, 186–202 (1972).

99. Elversson, J., Millqvist-Fureby, A., Alderborn, G. & Elofsson, U. Droplet and particle size relationship and shell thickness of inhalable lactose particles during spray drying. *J. Pharm. Sci.* **92**, 900–910 (2003).

100. Huang, D. Modeling of Particle Formation during Spray Drying. *Eur. Dry. Conf. - EuroDrying'2011* 26–28 (2011).

101. Carrasco, F., Chornet, E., Overend, R. P. & Costa, J. A generalized correlation for the viscosity of dextrans in aqueous solutions as a function of temperature, concentration, and molecular weight at low shear rates. *J. Appl. Polym. Sci.* **37**, 2087–2098 (1989).

102. Lin, S. P. & Reitz, R. D. Drop and spray formation from a liquid jet. *Annu. Rev. Fluid Mech.* **30**, 85–105 (1998).

103. Hede, P. D., Bach, P. & Jensen, A. D. Two-fluid spray atomisation and pneumatic nozzles for fluid bed coating / agglomeration purposes : A review. *Chem. Eng. Sci.* **63**, 3821–3842 (2008).

104. Roos, Y. H. Importance of glass transition and water activity to spray drying and stability of dairy powders. *Lait* **82**, 475 (2002).

105. Chiou, D., Langrish, T. A. G. & Braham, R. The effect of temperature on the crystallinity of lactose powders produced by spray drying. *J. Food Eng.* **86**, 288–293 (2008).

106. Büchi Labortechnik. Training Papers: Spray Drying. 1–19 (2002).

107. Maury, M., Murphy, K., Kumar, S., Shi, L. & Lee, G. Effects of process variables on the powder yield of spray-dried trehalose on a laboratory spray-dryer. *Eur. J. Pharm. Biopharm.* **59**, 565–573 (2005).

108. Vicente, J., Pinto, J., Menezes, J. & Gaspar, F. Fundamental analysis of particle formation in spray drying. *Powder Technol.* **247**, 1–7 (2013).

109. Baldelli, A., Boraey, M. A., Nobes, D. S. & Vehring, R. Analysis of the Particle Formation Process of Structured Microparticles. *Mol. Pharm.* **12**, 2562–2573 (2015).

110. Mezhericher, M., Levy, A. & Borde, I. Theoretical models of single droplet drying kinetics: A review. *Drying Technol.* **28**, 278–293 (2010).

111. Ranz, W. E. & Marshall, W. R. Evaporation from drops. *Chem. Eng. Prog.* **48**, (1952).

112. Perdana, J., Fox, M. B., Schutyser, M. A. I. & Boom, R. M. Mimicking spray drying by drying of single droplets deposited on a flat surface. *Food Bioprocess Technol.* **6**, 964–977 (2013).

113. Schiffter, H. & Lee, G. Single-droplet evaporation kinetics and particle formation in an acoustic levitator. Part 1: Evaporation of water microdroplets assessed using boundary-layer and acoustic levitation theories. *J. Pharm. Sci.* **96**, 2274–2283 (2006).

114. Mondragon, R. *et al.* Study of the drying behavior of high load multiphase droplets in an acoustic levitator at high temperature conditions. *Chem. Eng. Sci.* **66**, 2734–2744 (2011).

115. Baldelli, A. & Vehring, R. Control of the radial distribution of chemical components in spray-dried crystalline microparticles. *Aerosol Sci. Technol.* **50**, 1130–1142 (2016).

116. Sloth, J. *et al.* Model based analysis of the drying of a single solution droplet in an ultrasonic levitator. *Chem. Eng. Sci.* **61**, 2701–2709 (2006).

117. tec5 AG. Ultrasonic levitator user manual. 1–30 (2004).

118. Nešić, S. & Vodnik, J. Kinetics of droplet evaporation. *Chem. Eng. Sci.* **46**, 527–537

(1991).

119. Schutyser, M. A. I., Perdana, J. & Boom, R. M. Single droplet drying for optimal spray drying of enzymes and probiotics. *Trends Food Sci. Technol.* **27**, 73–82 (2012).

120. Schiffter, H. & Lee, G. Single-droplet evaporation kinetics and particle formation in an acoustic levitator. Part 2: Drying kinetics and particle formation from microdroplets of aqueous mannitol, trehalose, or catalase. *J. Pharm. Sci.* **96**, 2284–2295 (2006).

121. Yarin, A. L., Brenn, G., Kastner, O., Rensink, D. & Tropea, C. Evaporation of acoustically levitated droplets. **399**, 151–204 (1999).

122. Wulsten, E., Kiekens, F., van Dycke, F., Voorspoels, J. & Lee, G. Levitated single-droplet drying: Case study with itraconazole dried in binary organic solvent mixtures. *Int. J. Pharm.* **378**, 116–121 (2009).

123. Delißen, F., Leiterer, J., Bienert, R., Emmerling, F. & Thünemann, A. F. Agglomeration of proteins in acoustically levitated droplets. *Anal. Bioanal. Chem.* **392**, 161–165 (2008).

124. Leiterer, J., Delißen, F. & Emmerling, F. Structure analysis using acoustically levitated droplets. *Anal. Bioanal. Chem.* **391**, 1221–1228 (2008).

125. Klimakow, M. *et al.* Combined Synchrotron XRD / Raman Measurements : In Situ Identification of Polymorphic Transitions during Crystallization Processes. *Langmuir* **26**, 11233–11237 (2010).

126. Benmore, C. J. & Weber, J. K. R. Amorphization of molecular liquids of pharmaceutical drugs by acousticlevitation. *Phys. Rev. X* **1**, 1–7 (2011).

127. Lorenzen, E. & Lee, G. Slow motion picture of protein inactivation during single-droplet drying: a study of inactivation kinetics of L-glutamate dehydrogenase dried in an acoustic levitator. *J. Pharm. Sci.* **101**, 2239–2249 (2012).

128. Carrigy, N. B. *et al.* Trileucine and Pullulan Improve Anti-Campylobacter Bacteriophage Stability in Engineered Spray-Dried Microparticles. *Ann. Biomed. Eng.* **48**, 1169–1180 (2020).

129. Nandiyanto, A. B. D. & Okuyama, K. Progress in developing spray-drying methods for the production of controlled morphology particles: From the nanometer to submicrometer size ranges. *Adv. Powder Technol.* **22**, 1–19 (2011).

130. Elversson, J. & Millqvist-Fureby, A. Particle size and density in spray drying - Effects of carbohydrate properties. *J. Pharm. Sci.* **94**, 2049–2060 (2005).

131. Mönckedieck, M. *et al.* Spray drying of mannitol carrier particles with defined morphology and flow characteristics for dry powder inhalation. *Drying Technol.* **35**, 1843–1857 (2017).

132. Yang, J., Sliva, A., Banerjee, A., Dave, R. N. & Pfeffer, R. Dry particle coating for improving the flowability of cohesive powders. *Powder Technol.* **158**, 21–33 (2005).

133. Li, H. Y. & Birchall, J. Chitosan-modified dry powder formulations for pulmonary gene delivery. *Pharm. Res.* **23**, 941–950 (2006).

134. Huang, L. & Mujumdar, A. S. Development of a new innovative conceptual design for horizontal spray dryer via mathematical modeling. *Drying Technol.* **23**, 1169–1187 (2005).

135. Langrish, T. A. G. Multi-scale mathematical modelling of spray dryers. *J. Food Eng.* **93**, 218–228 (2009).

136. Mezhericher, M., Levy, A. & Borde, I. Theoretical drying model of single droplets containing insoluble or dissolved solids. *Drying Technol.* **25**, 1025–1032 (2007).

137. Fyhr, C. & Kemp, I. C. Comparison of different drying kinetics models for single particles. *Drying Technol.* **16**, 1339–1369 (1998).

138. Langrish, T. A. G. & Kockel, T. K. The assessment of a characteristic drying curve for milk powder for use in computational fluid dynamics modelling. *Chem. Eng. J.* **84**, 69–74 (2001).

139. Keey, R. B. *Drying of Losse and Particulate Materials*. (Hemisphere Publishing, 1992).

140. Boel, E. *et al.* Unraveling particle formation: From single droplet drying to spray drying and electrospraying. *Pharmaceutics* **12**, 1–58 (2020).

141. Chen, X. D. & Xie, G. Z. Fingerprints of the drying behaviour of particulate or thin layer food materials established using a reaction engineering model. *Food Bioprod. Process. Trans. Inst. Chem. Eng. Part C* **75**, 213–222 (1997).

142. Lin, S. X. Q. & Chen, X. D. Prediction of air-drying of milk droplet under relatively high humidity using the reaction engineering approach. *Drying Technol.* **23**, 1395–1406 (2005).

143. Chen, X. D. The basics of a reaction engineering approach to modeling air-drying of small droplets or thin-layer materials. *Drying Technol.* **26**, 627–639 (2008).

144. Al Zaitone, B., Al-Zahrani, A., Al-Shahrani, S. & Lamprecht, A. Drying of a single droplet of dextrin: Drying kinetics modeling and particle formation. *Int. J. Pharm.* **574**, 118888 (2020).

145. Har, C. L., Fu, N., Chan, E. S., Tey, B. T. & Chen, X. D. Unraveling the droplet drying characteristics of crystallization-prone mannitol - experiments and modeling. *AIChE J.* **63**, 1839–1852 (2017).

146. Abdullahi, H., Burcham, C. L. & Vetter, T. A mechanistic model to predict droplet drying history and particle shell formation in multicomponent systems. *Chem. Eng. Sci.* **224**, 115713 (2020).

147. Grasmeijer, N., Frijlink, H. W. & Hinrichs, W. L. J. Model to predict inhomogeneous protein–sugar distribution in powders prepared by spray drying. *J. Aerosol Sci.* **101**, 22–33 (2016).

148. Porowska, A. *et al.* Predicting the surface composition of a spray-dried particle by modelling component reorganization in a drying droplet. *Chem. Eng. Res. Des.* **110**, 131–140 (2016).

149. Ekdawi-Sever, N., De Pablo, J. J., Feick, E. & Von Meerwall, E. Diffusion of sucrose and

α,α-trehalose in aqueous solutions. *J. Phys. Chem. A* **107**, 936–943 (2003).

150. Ordoubadi, M. *et al.* Multi-Solvent Microdroplet Evaporation: Modeling and Measurement of Spray-Drying Kinetics with Inhalable Pharmaceutics. *Pharm. Res.* **36**, (2019).

Chapter 3: Effect of shear stresses on adenovirus activity and aggregation during atomization to produce thermally stable vaccines by spray drying

Throughout the spray drying process, there are many causes of damage to sensitive biologic components, including shear stress, increased air-liquid interfacial area, high temperatures, and dehydration. This work investigates the effects of the shear stresses inherent to spray drying on activity and aggregation of a model viral vector. A spray dryer nozzle was used to shear mannitol/dextran solutions, which were then quantified for viral activity losses and viral aggregation. Even at the highest shear rates tested, activity losses were significantly less than losses caused by the overall heated spray drying process, indicating that shear does not need to be a major consideration. This report is the first quantifying the effect of shear on viral vectors, and can be used as a guide when optimizing activity retention in spray dried formulations.

In this chapter, I was responsible for the design of experiments, and all aggregate sizing experiments. Atomization and viral activity experiments were performed by both myself and an undergraduate researcher, Myla Manser, under my direction. Myla also performed viscosity measurements. Author Mangalakumari Jeyanathan assisted with development and training on the flow cytometry method of quantifying viral activity used in this work. The manuscript was drafted by myself, with editorial assistance from supervisors Dr. Michael Thompson and Dr. Emily Cranston, as well as author Dr. Zhou Xing, and was approved by all authors before submission.

B. A. Morgan, M. Manser, M. Jeyanathan, Z. Xing, E. D. Cranston, M. R. Thompson, **2020**. "Effect of shear stresses on adenovirus activity and aggregation during atomization to produce thermally stable vaccines by spray drying", *ACS Biomaterials Science & Engineering*, **6**, 7, 4304-4313, DOI: 10.1021/acsbiomaterials.0c00317.

Abstract

Considering the substantive potential benefits of thermally stable dry powder vaccines to public health, causes for inactivation of their sensitive viral vectors during preparation require intensive study. The focus of this work was atomization of suspensions containing encapsulating excipients and a human type 5 adenovirus, involving a detailed investigation of shear stresses in the nozzle of a spray dryer. Samples were sprayed at 25 °C into falcon tubes and immediately evaluated for viral activity by *in vitro* testing, minimizing the confounding of thermal effects on the deactivation of the virus, although interfacial stresses could not be decoupled from shear stresses. Despite expectations of only virus deactivation with ever-increasing shear stresses in the spray nozzle, some conditions were found to show better activity than the positive control, leading to investigations of viral aggregation. It was found that the adenovirus experienced minor aggregation when mixed with the excipient solutions, which was reversed by subjecting samples to moderate shear conditions in the spray nozzle. At very high shear rates, activity diminished again due to damage to the viral capsid fibers, which also led to the production of new aggregates after atomization. Despite these findings, activity losses caused by shear were small compared to the overall spray drying process loss. However, formulation composition, solution viscosity and process conditions should be considered carefully for optimization due to their impact on aggregation. This is the first known report comparing shear, aggregation, and biologic activity loss during the atomization step of spray drying viral vaccines.

Keywords

Shear stress, aggregation, spray drying, particle sizing, process stresses, deactivation

3.1 Introduction

The immobilization of viruses and viral vectors such as adenovirus, herpes simplex virus, measles virus, and Newcastle disease virus in excipients like mono-, di- and poly-saccharides by spray drying has proven to be promising in preparing vaccines with high thermal stability, minimizing the necessity for adhering to cold chain protocols in maintaining long term efficacy.[1–4] Risk mitigation in spray drying for vaccine manufacture requires an analysis of its unit operations including pumping, atomization, drying, and collection, and evaluating their detrimental effects on the viral vector being stabilized.[5] These unit operations expose any viral vector to thermophysical stresses, growth of the air-liquid interface, and desiccation, all of which are potentially damaging to these sensitive biologics.[5,6] There are many studies in the literature on damage to enzymes, proteins, and bacteria during spray drying but no guidance on the harmful impact to viruses or viral vectors, which are more sensitive functionally to structural changes.[7–9]

The disclosed research is part of a series of studies examining the elementary factors of spray drying influencing the potency of thermally stable vaccines based on adenoviral vectors. Through optimization studies, viral activity was recognized to be dependent on system temperature and spray gas flow rate (and therefore shear) during spray drying, though the scope of prior work did not analyze the factors in detail or attempt to decouple interacting parameters.[3,10] Subsequently, thermal stresses were examined with the same adenovirus in studies of droplet drying with an acoustic levitator, finding that moderately heated air (30 - 55°C) could actually decrease activity losses by causing faster immobilization of the viral vector in a solidified matrix of mixed saccharides.[11]

One major difference between spray drying and acoustic levitation is atomization prior to droplet drying in the former case. Common to pharmaceutical spray drying, atomization involves two impinging fluids, compressed gas and a liquid suspension (containing the stabilizing excipients and the viral vector in our case) to produce a fine dispersion of droplets.[12] This subjects the liquid to large shear stresses that are proportional to the feed rates of these two fluid streams and the design of the nozzle.[9] However, looking for specific atomization examples within the spray drying literature shows that little is known about the damaging effects of shear on biologics, with only two relatable cases in which both found the effect to be insignificant.[13,14] In fact, no examples exist for viruses other than what can be indirectly implied from spray drying optimization

studies.[3,10] The most comprehensive previous study on shear damage of a biologic related to spray drying, found that up to 93% of bacterial death occurring during spray drying of *Lactococcus lactis* and the damage was attributed to shear stresses during atomization by the spray nozzle.[9] Considering bacteria are commonly an order of magnitude larger than adenoviruses making them more prone to high shear stresses based on contact area, and the differences in structure and mechanical properties of gram-positive bacteria versus viruses, these results have little applicability to the present work and their study provided limited information by only investigating three shear rates.[15,16]

The recognized effects of shear on biologics are conformational changes to enzymes, proteins, and components of the viral capsid, as well as disrupting the RNA/DNA structure of biologics such as viruses and bacteria.[7,17] Maa and Hsu investigated the effects of shear, or shear combined with increased interfacial area, on the activity of two model proteins using either a concentric-cylinder shear device or a rotor/stator homogenizer in the presence of air.[7,18] They concluded that denaturation resulted from shear damage and changes to the protein conformation increased due to growth of the air-liquid interface. More specifically for viruses, virus-like particles, and viral surrogates, a small number of studies on shear damage are found in the literature (though not directed to spray drying). Michalsky et al. considered the effect of shear stresses attributed to stirring and pumping but did not observe any change in infectivity of a recombinant baculovirus of *Autographa californica* M nucleopolyhedrovirus.[19] The shear rates in that case were far too low to be comparable to the two-fluid nozzle of a spray dryer, making it difficult to interpret its relevance to the current work. D'Souza et al. used high-pressure homogenization to investigate pressure, shear stresses, and temperature as parameters affecting human enteric virus surrogates, and found up to 3 log loss was obtained, although the effects were not differentiated in their analysis of causes.[20]

The objective of the current work was to conduct a detailed investigation on the effects of shear stresses (under 15 different shear conditions) in a spray dryer nozzle on a frequently utilized vaccine platform, the human type 5 adenovirus, dispersed in a solution of sugar alcohols and polysaccharides. Since spray drying inherently produces an increase in the air-liquid interface, the effect of shear will be confounded with this contributing effect in the study. *In vitro* activity testing

was done before and after shearing. We also investigated the effect that shearing has on adenovirus aggregation, and how that may be related to changes in activity due to shear stress.

3.2 Materials and Methods

3.2.1 Chemicals and adenoviral vector

Excipients D-mannitol and dextran (M_r 40,000 kDa) were purchased as USP grades from Millipore-Sigma (Ontario, Canada). Purified water was produced using a Barnstead GenPure Pro water purification system from ThermoFisher Scientific (Waltham, MA) with a resistivity of 18.2 MΩ cm. Life Technologies protocols were used to prepare cell media in-house from α-minimum essential medium (α-MEM) supplemented with 10% fetal bovine serum and 1% streptomycin/penicillin (Invitrogen, Ontario, Canada). A recombinant replication deficient human serotype 5 adenovirus expressing green fluorescent protein (AdHu5GFP) was produced in-house at the vector facility of the McMaster University Immunology Research Center as described previously.[21,22] The stock viral vector suspension consisted of phosphate buffered saline (PBS) with 10% by volume glycerol. Each milliliter of viral stock contains 4.3×10^{12} viral particles, and 5.1×10^{10} plaque forming units (pfu), as determined via plaque assay dilutions done with PBS++ (1X PBS with 1% $CaCl_2$ and 1% $MgCl_2$). A deactivated AdHu5GFP sample was prepared by exposing 20 µL of stock adenovirus suspension to UV light for 45 minutes in a biosafety cabinet. *In vivo* activity via flow cytometry (as described in Section 2.5) was used to confirm that the virus was deactivated by comparing the GFP expression of the deactivated virus sample to a negative control with no virus.

3.2.2 Atomization experiments

Trial solutions for the study contained 4% or 8% by weight of an excipient blend at a ratio of 3:1 mannitol:dextran, which was previously found to be highly effective for thermal stabilization of the (non-enveloped) AdHu5GFP viral vector.[23,24] The viral vector stock suspension (10 µL) was added to 10 mL of excipient solution, yielding a viral concentration of 5.1×10^7 pfu. To ensure homogeneity of the tested mixtures, the stock virus suspension was gently mixed in its vial by repeated inversion by hand before being added to the excipient solution. Once combined, the total excipient and virus suspension was taken up into the pipette tip (10 µL) and re-ejected into the vial and this gentle mixing by pipette was repeated five times combined with inverting the

viral five times. Sources of added shear stress, such as vortex mixing, were avoided during preparation of the test suspensions. In order to control the shear stresses of atomization under investigation, a B-290 Mini Spray Dryer (Büchi, Switzerland) was used.[4,10,11] The spray nozzle (0.7 mm diameter) was operated at room temperature to minimize thermal stresses on the viral vector, and atomized samples were collected directly into 50 mL Falcon tubes while still in liquid form. The characteristic shear rate at the nozzle tip was controlled by adjusting the spray gas feed rate between 282 and 1373 L/h, and setting the liquid feed rate to 188, 290, or 440 mL/h.

For all experiments that did not require viral activity testing, AdHu5GFP was not included in the formulation to minimize vector usage and meet biosafety requirements (the active virus is classified as biosafety level II); since the compositional fraction of the viral was very small (approximately 0.1 wt%) in the formulation, there would be no observable rheological difference in the solution by its absence. The reported data were collected from 3-4 repeated trials, conducted separately by two researchers over a span of several months. Positive controls constituted either a 10 mL 4% or 8% excipient solution with 10 µL viral vector stock suspension added, without any shear applied, hereafter referred to as the "zero shear" samples. The test suspensions used for the "zero shear" samples were prepared in the same manner as those for the sheared samples.

3.2.3 Excipient solution viscosity

Dynamic viscosities of the excipient blend solutions, at 4% and 8%, were measured using a Discovery Hybrid Rheometer (TA Instruments; New Castle, DE) with a Peltier plate using a 40 mm cone geometry. Testing was done at a controlled temperature of 25°C by a frequency sweep from 0.1 to 5000 rad/s using approximately 0.5 mL of solution.

3.2.4 Viral aggregation measurements

Viral aggregation was measured using a qViro-X nanoparticle counter (Izon Science; Christchurch, New Zealand) with a NP150 thermoplastic polyurethane membrane with a single nanopore. The analysis range of the NP150 covers particle sizes in the range of 70 to 420 nm (Izon Science; Christchurch, New Zealand). Sheared samples composed of virus and excipient, as well as the "zero shear" samples, were diluted by a factor of five in electrolyte buffer (10 mM HEPES, 150 mM NaCl and 4% by weight sucrose) to increase conductivity within the range required for the qViro-X instrument before testing. An adenovirus control was composed of 10 µL of the viral

vector stock suspension diluted by adding 990 µL of electrolyte buffer, without excipients, in order to measure the aggregation of the stock virus suspension. It was necessary to dilute the stock virus suspension further than other samples in order to meet the recommended particle concentration for the qViro-X instrument (1×10^{10} particles/mL). All experiments were run with a voltage of 0.46 V applied across the pore. A pressure of 0.6 kPa was applied to the fluid cell using the instrument's variable pressure module to increase the rate of particles passing through the pore. Samples were measured until either 500 events had been recorded or 10 min had elapsed, limited by the qViro-X control software. The relationship between blockade event magnitude and particle size was calibrated using CPC100 qNano carboxylated polystyrene calibration beads (Izon Science; Christchurch, New Zealand) with a mean particle size of 115 nm.

3.2.5 *In vitro* activity testing

In order to minimize potential adenovirus activity loss during storage at room temperature, sheared samples were stored on ice and tested on the same day they were produced. 100 µL of a collected sheared sample (excipient and virus) was mixed with 900 µL of culture media. A549 lung epithelial cells were cultured for five to seven days, until 80 – 90% confluent, then plated into a 96 well flat bottom plate at a concentration of approximately 4×10^4 cells per well. Each well was then incubated with 100 µL of the sample/media mixture overnight, after which point the cells were prepared for flow cytometry. Media was aspirated from the wells and each well was rinsed with 100 µL of PBS. Cells were then trypsinized, and each well was pipetted into a plastic 5 mL round-bottom flow cytometry tube (Corning; Corning, NY) before being centrifuged at 1400 rpm for 5 minutes. The supernatant was discarded and 1 mL of PBS containing 2 mM ethylenediaminetetraacetic acid (EDTA) was added to prevent clumping. The cells were again centrifuged at 1400 rpm for five minutes, the supernatant was discarded, and 1 mL of 1% paraformaldehyde (PFA) was added to each tube to fix the cells. Finally, the cells were centrifuged at 1800 rpm for five minutes, the supernatant discarded, and 200 µL of FACS buffer (0.5% w/v BSA in PBS) was added.

The prepared cells were processed according the Miltenyi Biotec instructions for flow cytometry and run on a MACSQuant Analyzer 10 (Miltenyi Biotec; Bergisch Gladbach, Germany). After method optimization, it was identified that a minimum of 10,000 cells (25%) were necessary for accurate data (between 25% and 50% of the plated cells were analyzed per run

for reported results). Data were analyzed using FlowJo software (Tree Star; Ashland, OR): briefly, the autogate function was used to identify the live cell population on of graph of forward scatter versus side scatter in order to reduce variability between experiments. The singlet live cell population was then separated from non-singlet live cells by a user-defined gate on a graph of forward scatter height versus forward scatter area. Finally, the data from a negative control consisting of uninfected A549 cells was gated on a fluorescence histogram graph to remove false GFP positives and split the live, singlet cell population into GFP-positive and GFP-negative. An example of the three gates applied to samples can be seen in Appendix 3, Figure A3.1. This gate was then applied to all other samples to identify the percentage of the population that was GFP-positive. The percentage of cells expressing GFP was compared against a standard curve using GraphPad Prism (GraphPad Software; La Jolla, CA) to generate a titre value. The standard curve was generated using modality of infection (MOI) values ranging from 0.1 to 100 and can be found in Appendix 3, Figure A3.2.

3.2.6 Calculation of characteristic shear rates

The nozzle operates with the excipient solution fed down a central channel by a peristaltic pump with the spray gas fed through a concentric channel around the liquid channel. The mixing zone occurs outside of the nozzle, as shown in Figure 3.1. External mixing nozzles allow for more control over atomization since both the liquid and spray gas flow rates can be controlled independently.[25]

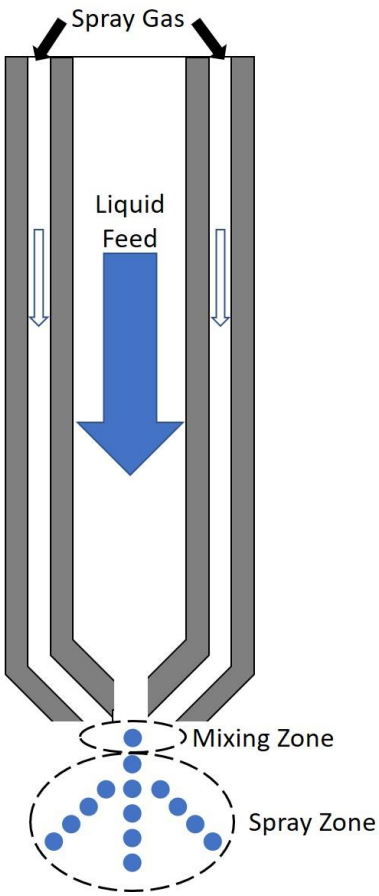

Figure 3.1: Schematic cross-section of a two-fluid external mixing nozzle such as the one used in this work.

The shear rate in the external mixing nozzle can be estimated as long as only the momentum transfer between the spray gas and liquid feed is considered. If the mass flow rate of liquid in the nozzle is in the same order of magnitude as the mass flow rate of air in the nozzle, as is the case for our experiments using a lab-scale spray dryer, then the average velocity v_{av} (m/s) at the mixing point can be estimated by Equation 3.1:[25]

$$v_{av} = \frac{v_{gas}}{1 + \frac{\dot{m}_{liq}}{\dot{m}_{gas}}} \tag{3.1}$$

where v_{gas} is the velocity of the spray gas at the point of atomization given in units of m/s, and $\dot{m}_{liq}$ and $\dot{m}_{gas}$ are the mass flow rates of the liquid feed and spray gas, respectively, in units of

kg/s. For this calculation, the diameter of the inner nozzle tip was 0.7 mm, while the inner nozzle cap diameter was 1 mm and the outer nozzle cap diameter was 1.5 mm. The mass flow rates are calculated by converting the known volumetric flow rates in units of L/h using the density of either air (the spray gas) or the measured density of the excipient solution. A density of 1.225 kg/m^3 was used for air and a density of 1060 kg/m^3 was used as the average of the excipient solution samples. The average density was used to allow for direct comparisons between 4% and 8% solutions, causing a variation in the shear rate calculation of $\pm 3 \times 10^3$ s^{-1}. Finally, an estimate for the characteristic shear rate $\dot{\gamma}$ in the spray dryer nozzle was made using Equation 3.2:[9,25]

$$\dot{\gamma} = \frac{2\left(v_{av} - v_{liq}\right)}{D_{in}} \tag{3.2}$$

where D_{in} is the inner diameter of the nozzle tip (0.7 mm) and v_{liq} is the velocity of the liquid at the point of atomization given in units of m/s.

3.2.6 Calculation of aggregate tensile strength

Equation 3.3 can be used to calculate the force necessary to break up particle aggregates:[26]

$$\sigma = \frac{1.1\left(\frac{1-\varepsilon}{\varepsilon}\right)H}{d^2} \tag{3.3}$$

where σ is the tensile strength of the aggregate (N/m^2), ε is the void volume fraction of the aggregate (unitless), H is the force required to break the bond between individual particles [in Newtons], and d is the individual particle diameter [in meters]. In order to calculate the void volume fraction for each, Equation 3.4 can be used:

$$\varepsilon = \frac{4}{3}\pi\left(\frac{D}{2}\right)^2 - x\left(\frac{4}{3}\pi\left(\frac{d}{2}\right)^2\right) \tag{3.4}$$

where D is the diameter of the aggregate given in m, and x is the number of individual particles that make up that aggregate (between two and four in this work).

3.2.7 Statistical analysis

All sheared samples were used to infect three wells of cells every time activity was evaluated, to assess the variability of the flow cytometry measurements. Quoted uncertainty in the measurements represented the standard deviation of triplicate well infections. Results were statistically analyzed using Microsoft Excel (Microsoft; Redmon, WA) and the Real Statistics Resource Pack plug-in, where applicable.[27] Viral activity results were considered statistically significantly different for $p \leq 0.05$ as determined using a one-way analysis of variance with a Tukey-Kramer Honestly Significant Difference (HSD) post hoc test. For aggregation tests, results were considered statistically significantly different for $p \leq 0.05$ as determined using a two-sided t-test.

It should be noted that characteristic shear rates of 97×10^3 s^{-1}, 225×10^3 s^{-1}, and 258×10^3 s^{-1} for the 4% formulation were tested separately from other shear rates due to a defect in the stock viral vector suspension used, and that the shear rate of 433×10^3 s^{-1} has been omitted due to high variability in the activity (the standard deviation was greater than 60% of the mean, which should not be the case for flow cytometry data).

3.3 Results and Discussion

3.3.1 Effect of shear rate on viral vector activity

The viral vector AdHu5GFP in a 4% excipient solution of mannitol:dextran (3:1 weight ratio) was atomized through a spray dryer nozzle (without heat) at 15 different characteristic shear rates calculated using Equation 3.2, and listed in Table 3.1 along with the spray gas and liquid feed rate settings used for these experiments. Viral activity of the sheared fluid was reported as titre loss versus shear rate in Figure 3.2; throughout these discussions it was a matter of choice to reflect on viral efficacy based on ‘activity loss’ rather than ‘activity’. The spray gas rate, liquid feed rate and excipient concentration were selected based on previous spray drying experiments with the same viral vector.[4,11] Figure 3.2 does not show the anticipated monotonic increase in viral titre loss with shear rate demonstrated previously in other works for bacteria but rather, at moderate shear conditions there was a decrease in activity loss.[9] More specifically, the titre loss decreased from 3.72×10^6 pfu for the “zero shear” sample to a minimum value of 1.55×10^6 pfu ($p < 0.046$) at a shear rate of 391×10^3 s^{-1}, above which the titre loss increased until it levelled off around

2.3×10^6 pfu at higher shear rates. Notably, all shear rates tested had lower activity losses than the "zero shear" sample, implying that shear (within the range tested) had an unexpectedly positive impact on viral activity.

Table 3.1. Characteristic shear rates in the spray dryer nozzle as determined by the spray dryer pump setting and the flow rate of the atomizing spray gas.

		Liquid feed rate (mL/h) [Spray dryer pump setting (%)]		
		188 [13]	290 [20]	440 [30]
Spray gas flow rate (L/h) [Spray dryer setting]	282 [20]	145×10^3 s^{-1}	121×10^3 s^{-1}	97×10^3 s^{-1}
	439 [30]	258×10^3 s^{-1}	225×10^3 s^{-1}	189×10^3 s^{-1}
	666 [40]	433×10^3 s^{-1}*	391×10^3 s^{-1}	342×10^3 s^{-1}
	1051 [50]	736×10^3 s^{-1}	686×10^3 s^{-1}	623×10^3 s^{-1}
	1373 [55]	992×10^3 s^{-1}	938×10^3 s^{-1}	868×10^3 s^{-1}

* The shear rate of 433×10^3 s^{-1} has been removed from activity results due to unusual variability.

Statistical analysis of data in Figure 3.2 showed that the titre loss at a shear rate of 391×10^3 s^{-1} was significantly different from the titer losses at 0, 97×10^3, 121×10^3, 225×10^3, 258×10^3, and 686×10^3 s^{-1} (indicated with asterisks over the plotted bars that were statistically different from the minimum which was itself denoted by a # in Figure 3.2). Statistical analysis increased our confidence in labelling this point a minimum, with at least one shear rate causing a statistically significant increase in titre losses on either side of 391×10^3 s^{-1}. Each shear rate condition was repeated 3 to 4 times, and the *in vitro* activity testing was repeated in triplicate for each sample to assess the reproducibility of the methods; the precision is represented by the error bars in Figure 3.2 and is not identical for all data points but is small compared to the standard deviation values typically shown on log loss plots for activity loss after spray drying.[4,11] Overall, small variability in the measured titre losses allow us to draw statistically relevant conclusions from the data set and recognize relevant fluctuations that suggest that there are optimal shear conditions that lead to smaller viral activity losses. This variability also accounts for the lack of pattern in the activity losses seen at the various non-significant shear rates, although the same statistically significant minima and overall trends appeared in repeated preliminary experiments (data not shown).

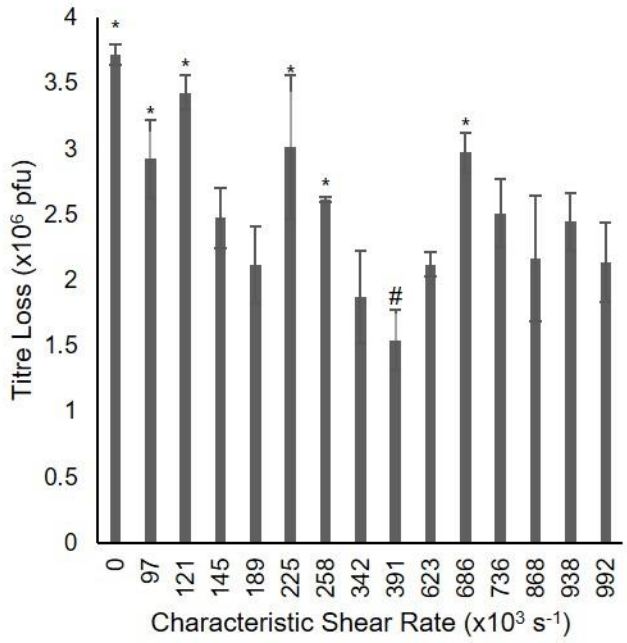

Figure 3.2: Titre loss of AdHu5GFP after shearing of a 4% mannitol/dextran and virus suspension at characteristic shear rates ranging from 97×10^3 to 992×10^3 s^{-1}. Error bars represent standard deviation of triplicate infections from each shear rate. Data points marked with a (*) are statistically significantly different from the data point marked with a (#).

To support the phenomenon seen for AdHu5GFP in the 4% formulation, a more concentrated 8% excipient and virus suspension was subjected to the same range of discrete characteristic shear rates. Titre loss as a function of shear rate for the 8% samples is shown in Figure 3.3. Similar to the results with the 4% suspension, viral activity was improved at moderate shear rates compared to the "zero shear" sample. A significant minimum was seen at 258×10^3 s^{-1} ($p < 0.036$), which was lower than the shear rate that corresponded to the smallest activity loss for the 4% formulation. This minimum in titre loss (1.73×10^6 pfu) was statistically different from the losses at tested shear rates of 342×10^3, 391×10^3, 623×10^3, 686×10^3, 736×10^3, and 938×10^3 s^{-1}. With the more concentrated 8% suspension, two additional minima were detected at 433×10^3 s^{-1} ($p < 0.044$) and 992×10^3 s^{-1} ($p < 0.050$), that could not be deemed statistically insignificant. While almost all titre loss values remained lower than the "zero shear"

sample (except at 736×10^3 s^{-1}) the activity losses were higher for 8% formulations compared to 4%.

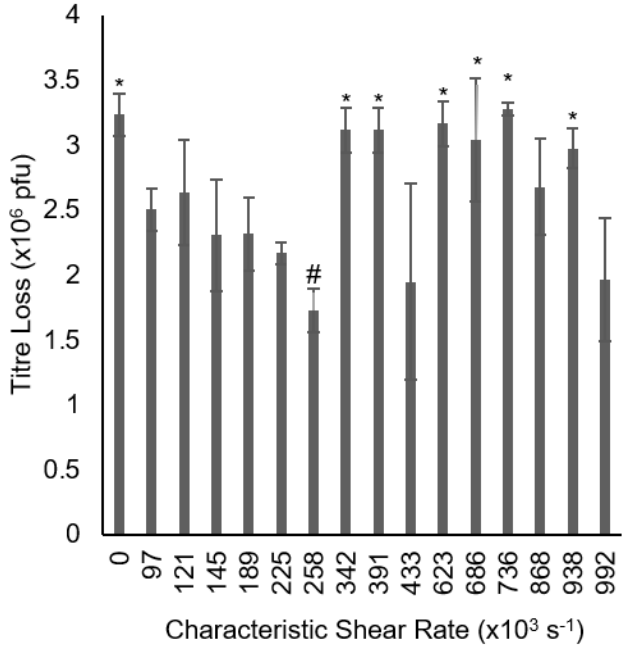

Figure 3.3: Titre loss of AdHu5GFP after shearing of an 8% mannitol/dextran and virus suspension at characteristic shear rates ranging from $97 \times 10^3 s^{-1}$ to $992 \times 10^3 s^{-1}$. Error bars represent standard deviation of triplicate infections from each shear rate. Data points marked with a (*) are statistically significantly different from the data point marked with a (#).

Importantly, the shear stresses applied in these experiments led to relatively small activity losses compared to normal spray drying losses, and under normal operating conditions, shear was deemed to not significantly impact viral efficacy. We note that the activity results in Figure 3.2 and Figure 3.3 are presented on a linear scale, not the more conventional *log* loss scale, to emphasize the differences between the various shear rates. If converted to log loss, the values for the sheared 4% formulations ranged from 0.16 to 0.49 log and from 0.18 to 0.45 log for 8%, which are generally acceptable losses for manufacturing thermally stable vaccines. Compared to the losses expected in fully spray dried samples (with shear, atomization, heat and drying that are ca. 0.5 to 4 log loss) these values are small. Only in highly optimized systems have we achieved losses

of less than 0.5 log after spray drying with this formulation.[10] As such, even at the highest shear rates tested, viral activity was relatively well-maintained in this study.

From the fluctuations in titre loss measured over the large range of shear rates (and shear stresses) we infer that several physical mechanisms were affecting viral activity. We hypothesized that viral aggregates were present in the "zero shear" and lower shear rate samples, causing the increased activity loss due to a decrease in free non-aggregated viruses available to infect cells. If this aggregation is produced by diluting viral vectors in solutions of mixed saccharides, it would be a new concern for the field of thermally stable vaccines. Following this hypothesis, the single minimum in viral activity loss measured with the 4% suspension and the three minima associated with the 8% suspension were assumed to be caused by the break up of different aggregates once a critical shear stress was applied, where the specific critical shear stress was related to the size of the aggregate.

Superimposed on this aggregation phenomenon, increasing shear stresses had a detrimental effect on the structural integrity of the viral vector, albeit minor, causing activity losses to increase after the minima, though only up to a plateau in titre loss. It is reasonable to believe that this damage occurs in the mixing zone of the nozzle where shear stresses are magnitudes higher than before or afterwards in the process (Figure 3.1). Adenoviruses, such as AdHu5GFP used here, are composed of an non-enveloped icosahedral capsid containing genetic information, with elongated fiber-like proteins extending from each of the 12 vertices of the capsid.[28] These fibers are responsible for binding to cellular receptors for initiation of the infection process, however are considered very fragile and are the most probable candidates for shear damage in the virus structure.[29] The next section examines the hypothesis of viral aggregation and the effects of shear on de-aggregation.

3.3.2 Effect of shear rate on viral vector aggregation

Viral particle size was measured using the qViro-X technique for control samples and samples that had been subjected to shear rates of 0, 121×10^3, 391×10^3, and 686×10^3 s^{-1} for 4% formulations, and 0, 121×10^3, 258×10^3, and 686×10^3 s^{-1} for 8% formulations. These samples were chosen so that there would be aggregation data from zero shear up to shear rates encompassing one activity loss minima for each formulation. The cut-off particle size for the measurements was set at 420 nm by the nanopore size of the qViro-X membrane used. Figure

3.4(a) shows the particle size distributions for the controls: (1) a viral vector stock suspension and (2) a UV-deactivated sample of the same viral vector stock suspension – neither sample included excipients nor were they sheared. The distributions are overlaid to highlight the difference between an unaggregated and highly aggregated sample. UV deactivation of adenoviruses has been shown to primarily occur due to viral DNA damage; aggregation of the deactivated sample is a likely side effect of the deactivation process caused by adenoviral protein damage.[30,31]

The control stock suspension was found to contain particles with a monomodal size distribution, including few aggregates (with sizes larger than 129 nm), giving a mean particle diameter of 99 ± 17 nm. This is consistent with the range of 70 – 100 nm cited in the literature for primary adenovirus particles, as well as values measured by the same technique.[32,33] Defining 129 nm as the "cut-off" above which particles are considered aggregated is explained below with Table 3.2. The near-absence of aggregates in the stock suspension matches with previous findings using disc centrifugation.[34] The size distribution of the other control, the UV-deactivated sample, had a similar monomodal distribution with a broader right-sided shoulder (with a mean of 113 ± 28 nm) and had many more particles larger than 129 nm, i.e., aggregates, than present in the stock suspension. These results were primarily used to assess the effectiveness of the qViro-X technique to measure both aggregated and non-aggregated adenovirus particles. Figure 3.4(b) and 3.4(c) show the size distribution of the 4% and 8% formulation "zero shear" samples for comparison. The distributions more closely resemble the stock viral suspension than the UV-deactivated sample, but include more aggregates than the former case. The size distributions for the other six samples can be found in Appendix 3, Figures A3.3 – A3.8.

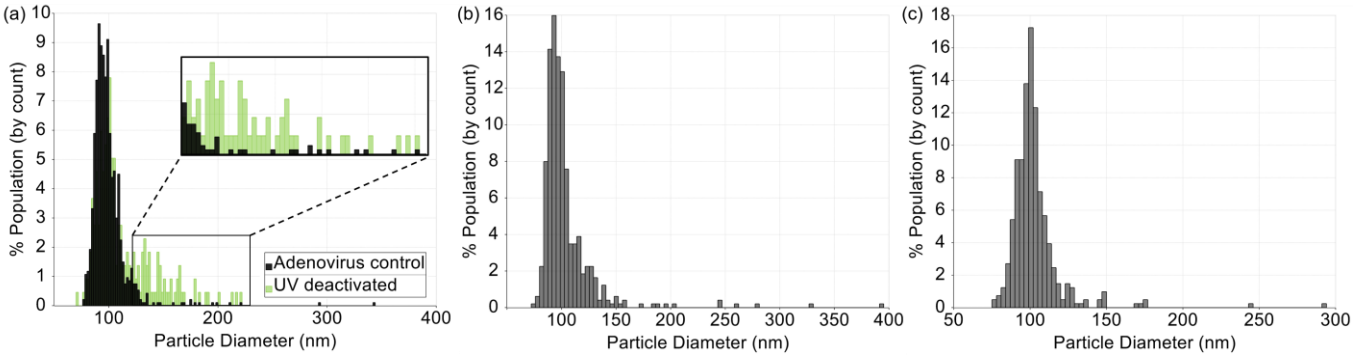

Figure 3.4: (a) Comparison of the size distributions for the stock adenovirus control (particle count of 933) and a UV-deactivated virus control (particle count of 218). The stock sample has a main peak of single virus particles with a few larger aggregates; the deactivated sample has a main peak that is centered around a larger diameter, has a large right-sided shoulder, and many more large aggregates. (b) Size distribution of the 4% formulation "zero shear" sample (particle count of 488). (c) Size distribution of the 8% formulation "zero shear" sample (particle count of 406).

To understand the de-aggregation mechanics and assess whether the changes in number/size of aggregates could explain the decrease in titer loss at certain shear rates during atomization, the possible geometric make-up of viral aggregates first needed to be estimated. The icosahedral shape of the adenovirus can be well approximated by a sphere.[35] Based on this assumption, a radius of gyration (R_g) could be assigned to aggregates composed of two, three, and four primary viral particles (with radius R_0) following the work of McEvoy et al., who predicted the size of influenza virus aggregates.[36] Aggregate geometry allows the calculation of the void volume fraction, which in turn may be used to estimate the bond strength between cohesively attached particles. Although changes in the geometry of an individual viral particle would affect the void volume, studies on the mechanical strength of adenovirus capsids suggests that forces higher than those used in this study are necessary for deformation.[16,37] The various aggregates, equations, and calculated diameters were derived using a primary particle diameter of 99 nm and are summarized in Table 3.2, along with the estimated void volume fraction for each aggregate (Equation 3.4). It should be noted that these geometries are intended only as an estimate in order

to interpret aggregation results, and that the actual aggregates will vary somewhat due to the variability of size and shape naturally present in the viral particles. The volume-based diameters calculated in Table 3.2 for suggested available geometries are compared to measured aggregates above 129 nm in Figure 3.5 for both the 4% and 8% formulation samples; the diameter of 129 nm was selected as the "cut-off" by taking the smallest measured adenovirus diameter (72 nm) and using the dimer formula in Table 3.2 to calculate the smallest potential aggregate size. Since a primary viral particle may vary between 72-105 nm (Figure 3.4), the calculated sizes shown in the figure are merely representative of a geometry, we do not believe that the geometries used in this analysis describe all possible aggregate geometries present in the suspension. It was simply needed that the measured aggregates and predicted geometries were similar in size in order to later estimate the tensile strength of these aggregates.

Table 3.2: Equations and calculated volume-based diameters to estimate the size of four different configurations of adenovirus aggregates, as well as void volume fractions (for calculating adenovirus bond strength) calculated using Equation 3.4. The dotted circles denote the hydrodynamic volumes represented by these geometries.

Aggregate Geometry	Equation*	Calculated Diameter (nm)	Void Volume Fraction
Monomer 	$R_g = R_0$	99	-
Dimer 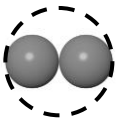	$R_g^2 = \frac{16}{5}R_0^2$	177	0.65
Triangular trimer 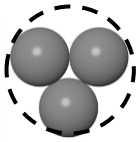	$R_g^2 = \frac{29}{5}R_0^2$	238	0.78
Linear trimer 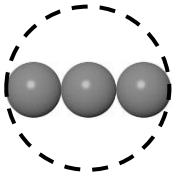	$R_g^2 = \frac{49}{5}R_0^2$	310	0.90
Pyramidal tetramer 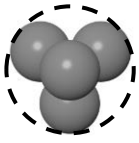	$R_g^2 = \frac{37}{5}R_0^2$	270	0.80

* from reference 36

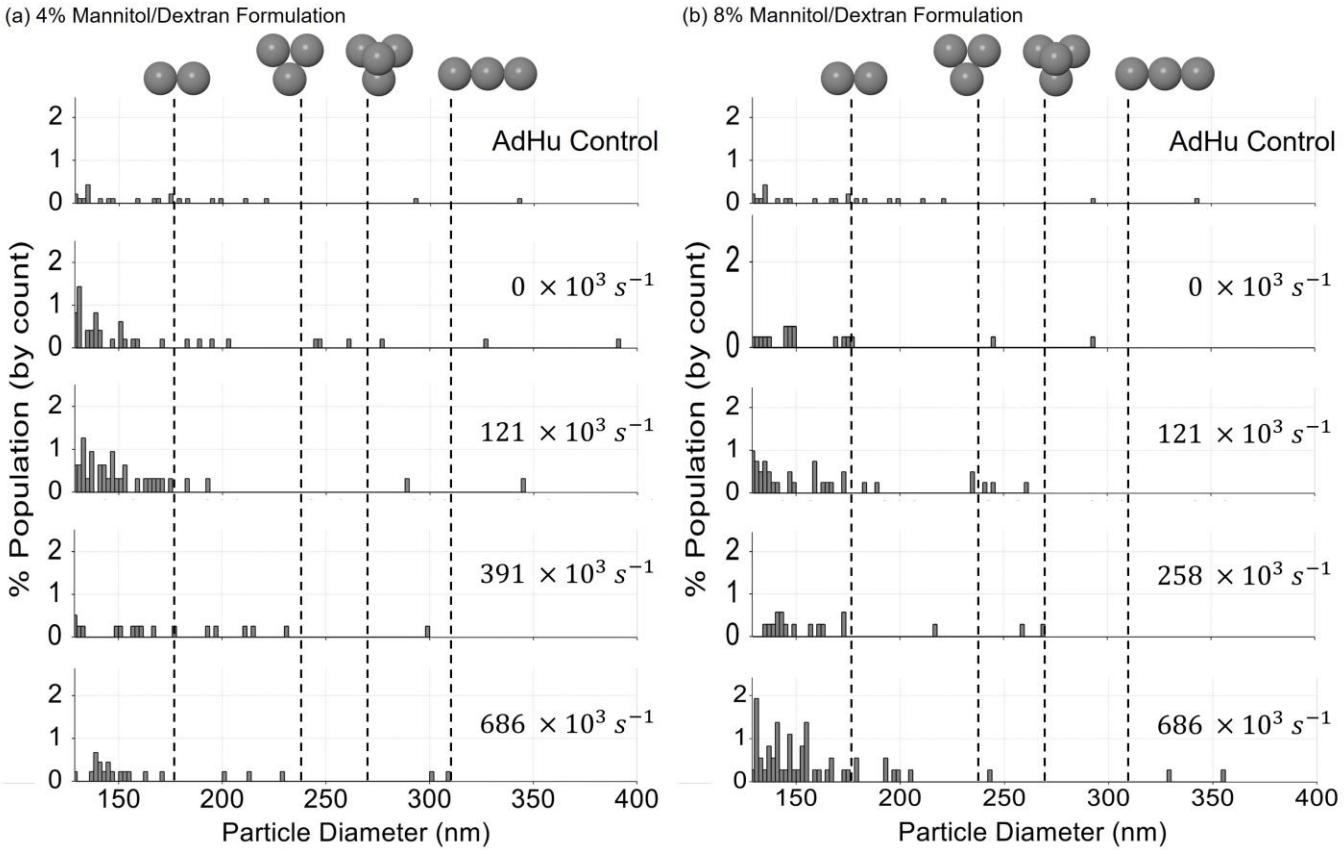

Figure 3.5: Comparison of predicted aggregate diameters with measured adenovirus particle diameters above 129 nm for (a) 4% formulations with no applied shear ("zero shear" sample), an applied shear rate of 121×10^3, 391×10^3, and 686×10^3 s^{-1} (from top to bottom); and (b) 8% formulations with no applied shear ("zero shear" sample), an applied shear rate of 121×10^3, 258×10^3, and 686×10^3 s^{-1} (from top to bottom).

For trials with the 4% formulation, the "zero shear" sample had the highest frequency of large aggregates relative to the stock suspension among the sheared samples, as seen in Figure 3.5(a). These aggregates were a result of the stock suspension being added to the solution with excipients. Observed aggregates were largely dimers yet included larger masses consisting of at least three to four adenoviruses like the pyramidal tetramer or linear trimer. As the shear rate was increased from 0, the largest aggregates (close to 400 nm) no longer appeared in the analysis, possibly fractured since they would be the weakest of the particles shown in the figure; at each shear rate, only a critical aggregate size will persist whereas larger particles will break apart

according to Rumpf's theory for the fracture strength of agglomerated solids.[26] After shearing at 121×10^3 s^{-1}, newer particle sizes around 340 nm appear that may be related to fracturing of those larger aggregates or simply other geometric configurations not capable of being broken up at this shear rate. At a shear rate of 391×10^3 s^{-1}, the particle size distribution most closely resembled the control stock viral suspension supporting that the minimum in activity loss at this shear rate for the 4% formulation is linked to the state of viral aggregation.

However, when the shear rate was increased further to 686×10^3 s^{-1}, the amount of dimer aggregates present in the 4% formulation increased relative to the sample collected at 391×10^3 s^{-1} though the maximum aggregate size remained similar; both the 391×10^3 s^{-1} and the 686×10^3 s^{-1} shear rates had aggregate sizes that suggested both the triangular and linear trimers, but not the pyramidal tetramer. The production of new (but relatively small) aggregates at 686×10^3 s^{-1} is thought to be due to removal of the fiber-like proteins on the viral capsid under these shear forces, allowing for stronger cohesive bridging between viral particles. Although the shoulder on the distribution at approximately 125 nm is at a diameter smaller than that predicted in Table 3.2 for dimer aggregates, it is thought to be composed of dimers of viral particles with primary diameters smaller than 99 nm, or dimers of shear-damaged viral particles without fiber proteins, causing them to appear smaller than predicted.

For trials with the 8% formulation, all sheared samples and the 'zero shear' sample showed more aggregation than the control stock suspension, as seen in Figure 3.5(b). Though difficult to make definitive conclusions from the data, it did not appear that there were more or larger aggregates at this higher excipient concentration in the 'zero shear' sample. This indicates that the concentration of the excipients at 4% was sufficient to affect the virus population in suspension and the higher concentration produced no new interactions that would lead to further aggregation. As observed with the 4% formulation, the largest aggregate size decreased in samples by increasing shear from 0 to 121×10^3 s^{-1} while the amount of overall aggregation remained similar between the two operating states. The sample sheared at 258×10^3 s^{-1} (the first minimum in Figure 3.3) showed the least amount of total aggregation, and had a similar maximum aggregate size to the 121×10^3 s^{-1} sheared sample; the particle size distribution was not as close to the control stock suspension as seen for the 4% formulation at the shear rate corresponding to minimum activity loss but the sample did contain considerably fewer aggregates than at other shear condition. The

sample subjected to 686×10^3 s^{-1} displayed the most aggregates as well as the largest aggregates for the 8% formulation. Based on the higher shear stresses afforded by its higher suspension viscosity, a higher frequency of viruses in this sample were expected to experience damaged capsid fibers, giving the greatest degree of aggregation and deactivation observed.

With only two formulation concentrations studied, we cannot fully model the trend between concentration and the shear rate at which titre loss minima are seen, however, the two-fold increase in concentration from 4% to 8% caused a 1.5-fold decrease in the shear rate that minimized activity loss, suggesting an inverse linear relationship between concentration and minimal shear rate. As the concentration, and therefore viscosity, of the suspension increases, it is more likely that damage to the viral structure, and further aggregation, will occur at high shear rates. Therefore, it is recommended to err on the lower end of the applied shear rates during processing, particularly when using more concentrated excipient formulations.

Comparing the particle size distributions in Figure 3.5 to the titre loss data in Figures 3.2 and 3.3, the degree to which viruses were bound in aggregates correlated with higher activity losses. At low or zero shear conditions, the occurring aggregation was attributed to the stock virus suspension being mixed with the excipient saccharides. The mean particle diameters (Appendix 3, Table A3.1) support this finding, showing the samples from both 4% and 8% formulations at "zero shear" had mean particle diameters (104 ± 27 and 103 ± 18 nm, respectively) that were statistically higher than that of the viral stock suspension (99 ± 17 nm) ($p < 0.05$). From this we infer that excipient concentration does not appear to significantly affect aggregation and although the cause of 'aggregation due to mixing' is unknown, changes in local ionic strength or pH as the virus and mixed saccharides are brought together may be contributing factors.[38] For both 4% and 8% formulations, the samples showing the least aggregation in Figure 3.5 (391×10^3 s^{-1} and 258×10^3 s^{-1}, respectively) correspond to an activity loss minima; the lower shear rate for the minima in the 8% suspension can be attributed to its higher viscosity, indicating the phenomenon was shear stress dependent which would be consistent with an aggregate's fracture strength. Motion through the velocity gradients in the nozzle and mixing zone as the liquid formulation is compressed can increase particle-particle collisions leading to further aggregation and therefore differing aggregate sizes in the sheared samples.[39,40] The detailed fluid dynamics of the spray dryer nozzle and mixing zone are outside the scope of this work; however, Hede et al. noted that turbulent flow is necessary

to break up the liquid flow into droplets.[25] The secondary mechanism for aggregation was attributed to damaged capsid fibers that occurred at higher shear rates. Removal of the viral capsid fiber proteins would allow for closer packing of virus particles, leading to new interparticle bonds and therefore aggregates to be created. These damage-induced aggregates may contribute to the second and third activity minima seen in the 8% formulation as they are broken up.

3.3.3 Strength of a viral aggregate

Accepting the proposed aggregate geometries above, and the evidence that the minima for titer loss seen with the 4% and 8% formulations corresponded to one or more of these aggregate geometries breaking up, it is possible to estimate the (tensile) fracture strength of these aggregates based on the corresponding shear stress when break up occurred. Equation 3.3 can be rearranged to calculate H, the interparticle bond strength between two adenovirus particles, giving researchers a valuable parameter for predicting process conditions that favor de-aggregation. To the best of our knowledge, this H value has not been reported in the literature previously for adenoviruses. The estimated value will be limited to adenoviral suspensions of comparable viscosity to our formulations, namely 1.1×10^{-3} Pa · s and 1.3×10^{-3} Pa · s, for 4% and 8%, respectively, and displaying Newtonian behaviour across the range of shear conditions under consideration. This Newtonian behaviour, as expected for aqueous dextran solutions, means that there will be a linear relationship between the shear rate and the shear stress in the nozzle.[41] The shear rates at activity loss minima were equated to the break up of aggregate sizes based on their calculated void volume fractions, with the highest void volume fraction aggregate being considered to fracture at the lowest shear rate minima and the lowest void volume fraction aggregate fracturing at the highest shear rate minima per formulation.

Table 3.3 gives the tensile fracture strengths of each aggregate, ordered from lowest to highest in terms of volume fraction, calculated using the given suspension viscosities and shear rates. The calculated values for the viral interparticle bond strength are all of similar magnitude, between 10 and 33 pN, leading us to conclude that the assumptions above were reasonable. These calculated H values are similar to those reported by Dobrowsky et al. for the strength of adhesion between HIV surface proteins and cellular receptors, which ranged between 18 and 33 pN.[42] The difference in calculated bond strength for the linear trimer in the 4% and 8% formulations is small and within the error of the calculation based on the error in shear rate calculations. As a result of

this analysis, we conclude that 25 pN is a reasonable estimate of the viral bond strength, which should allow researchers to predict the shear rates that correspond to activity loss minima based on the viscosity of their suspensions being spray dried.

Table 3.3: The tensile strength required to break up each viral aggregate geometry at the various activity loss minima in the 4% and 8% formulations. The tensile strength values were then used to calculate the viral interparticle bond strengths with Equation 3.3.

Aggregate Geometry (Concentration used in calculation)	Shear rate @ minima (x 10^3 s^{-1})	Tensile strength (N/m^2)	Bond strength (pN)
Linear trimer (8%)	258	347	28
Linear trimer (4%)	391	417	33
Pyramidal tetramer (8%)	433	583	21
Triangular trimer (8%)	433	583	18
Dimer (8%)	992	1335	10

3.4 Conclusion

Overall, these data show that there are several mechanisms acting on the virus during the atomization step (including both shear and interfacial stresses) of thermally stable dry powder vaccine production, impacting both viral activity and aggregation. Initial mild aggregation occurs when the stock adenovirus suspension is mixed with excipients, and similarly increased aggregation is seen at higher shear rates caused by damage to the viral capsid fibers, along with increased activity losses. Some of the initial minor aggregation can be reversed by applying moderate shear stresses to the sample, leading to minima in measured activity losses. The exact shear rate at which the most de-aggregation and activity recovery occurs, varies depending on the formulation viscosity, with higher viscosity suspension s requiring a lower shear rate to minimize activity loss. While the highest shear rates used in this work caused damage to the viral capsid fibers and an increase in activity loss, the overall effect of shear on adenovirus activity is low compared to conventional spray drying losses and in line with other findings in the literature that shear has little to no effect on the biologic and even at the highest shear rate, viral activity was

maintained. If optimization during formulation development is possible, the spray gas and liquid feed rates can be tuned based on suspension viscosity and viral aggregate tensile strength to minimize viral vector activity loss.

3.5 Supporting Information

Example for the live cell population, singlet cell population, and GFP positive/negative population gates applied to flow cytometry samples; the standard curve used to analyze flow cytometry data; particle size distributions for the six samples not shown in main text; table of mean and mode particle diameters for both 4% and 8% formulations.

3.6 Acknowledgements

The authors thank Prof. K. Mossman for equipment use; Sam Afkhami, Xueya Feng and Anna Zganiacz for cell culture training and assistance; and Susan Collins, Heera Marway and Zoya Tabunshchyk for equipment training and troubleshooting help. This study is supported by funds from the Canadian Institutes of Health Research, the Natural Sciences and Engineering Research Council of Canada, and Ontario Centres of Excellence (OCE) (Collaborative Health Research Program CHRP523837-18).

3.7 References

1. Ohtake, S. *et al.* Heat-stable measles vaccine produced by spray drying. *Vaccine* **28**, 1275–1284 (2010).

2. Corbanie, E. A. *et al.* Spray drying of an attenuated live Newcastle disease vaccine virus intended for respiratory mass vaccination of poultry. *Vaccine* **25**, 8306–8317 (2007).

3. LeClair, D. A., Li, L., Rahman, N., Cranston, E. D. & Thompson, M. R. Stabilization of HSV-2 viral vaccine candidate by spray drying. *Int. J. Pharm.* **569**, 118615 (2019).

4. LeClair, D. A., Cranston, E. D., Xing, Z. & Thompson, M. R. Evaluation of excipients for enhanced thermal stabilization of a human type 5 adenoviral vector through spray drying. *Int. J. Pharm.* **506**, 289–301 (2016).

5. Grasmeijer, N. Improving protein stabilization by spray drying: formulation and process development. (University of Groningen, 2016).

6. Saluja, V. *et al.* A comparison between spray drying and spray freeze drying to produce an influenza subunit vaccine powder for inhalation. *J. Controlled Release* **144**, 127–133 (2010).

7. Maa, Y.-F. & Hsu, C. C. Effect of high shear on proteins. *Biotechnol. Bioeng.* **51**, 458–465 (1996).

8. Perdana, J., Fox, M. B., Schutyser, M. A. I. & Boom, R. M. Enzyme inactivation kinetics: Coupled effects of temperature and moisture content. *Food Chem.* **133**, 116–123 (2012).

9. Ghandi, A., Powell, I. B., Howes, T., Chen, X. D. & Adhikari, B. Effect of shear rate and oxygen stresses on the survival of Lactococcus lactis during the atomization and drying stages of spray drying: A laboratory and pilot scale study. *J. Food Eng.* **113**, 194–200 (2012).

10. LeClair, D. A., Cranston, E. D., Xing, Z. & Thompson, M. R. Optimization of Spray Drying Conditions for Yield, Particle Size and Biological Activity of Thermally Stable Viral Vectors. *Pharm. Res.* **33**, 2763–2776 (2016).

11. Morgan, B. A., Xing, Z., Cranston, E. D. & Thompson, M. R. Acoustic levitation as a screening method for excipient selection in the development of dry powder vaccines. *Int. J. Pharm.* **563**, 71–78 (2019).

12. He, P., Davis, S. S. & Illum, L. Chitosan microspheres prepared by spray drying. *Int. J. Pharm.* **187**, 53–65 (1999).

13. Gong, P. *et al.* Injury Mechanisms of Lactic Acid Bacteria Starter Cultures During Spray Drying : A Review. *Drying Technol.* **32**, 793–800 (2014).

14. To, B. C. S. & Etzel, M. R. Survival of Brevibacterium linens (ATCC 9174) after Spray Drying , Freeze Drying , or Freezing. *J. Food Sci.* **62**, 167–170 (1997).

15. Shiu, C., Zhang, Z. & Thomas, C. A comparison of the mechanical properties of different bacterial species. in *Focus on Biotechnology, vol. 2* 155–162 (Springer, Dordrecht, 2001). doi:10.1007/0-306-46888-3_11

16. Snijder, J. *et al.* Integrin and Defensin Modulate the Mechanical Properties of Adenovirus.

J. Virol. **87**, 2756–2766 (2013).

17. Levy, M. S. *et al.* Effect of shear on plasmid DNA in solution. *Bioprocess Eng.* **20**, 7–13 (1999).

18. Maa, Y. F. & Hsu, C. C. Protein denaturation by combined effect of shear and air-liquid interface. *Biotechnol. Bioeng.* **54**, 503–512 (1997).

19. Michalsky, R., Pfromm, P. H., Czermak, P., Sorensen, C. M. & Passarelli, A. L. Effects of temperature and shear force on infectivity of the baculovirus Autographa californica M nucleopolyhedrovirus. *J. Virol. Methods* **153**, 90–96 (2008).

20. D'Souza, D. H., Su, X., Roach, A. & Harte, F. High-Pressure Homogenization for the Inactivation of Human Enteric Virus Surrogates. *J. Food Prot.* **72**, 2418–2422 (2009).

21. Wang, J. *et al.* Single Mucosal, but Not Parenteral, Immunization with Recombinant Adenoviral-Based Vaccine Provides Potent Protection from Pulmonary Tuberculosis. *J. Immunol.* **173**, 6357–6365 (2004).

22. Roediger, E. K., Kugathasan, K., Zhang, X. Z., Lichty, B. D. & Xing, Z. Heterologous boosting of recombinant adenoviral prime immunization with a novel vesicular stomatitis virus-vectored tuberculosis vaccine. *Mol. Ther.* **16**, 1161–1169 (2008).

23. Toniolo, S. P. *et al.* Excipient selection for thermally stable enveloped and non-enveloped viral vaccine platforms in dry powders. *Int. J. Pharm.* **561**, 66–73 (2019).

24. Thompson, M. R., Xing, Z., LeClair, D. A. & Cranston, E. D. Enhanced thermal stability for adenoviral vectors through spray drying. (2019).

25. Hede, P. D., Bach, P. & Jensen, A. D. Two-fluid spray atomisation and pneumatic nozzles for fluid bed coating / agglomeration purposes : A review. *Chem. Eng. Sci.* **63**, 3821–3842 (2008).

26. Rumpf, H. The strength of granules and agglomerates. *Agglom. First Int. Symp. Agglom. Philadelphia, 1962* 379–418 (1962).

27. Zaiontz, C. Real Statistics Resource Pack (Release 6.2). (2019).

28. Appaiahgari, M. B. & Vrati, S. Adenoviruses as gene/vaccine delivery vectors: promises

and pitfalls. *Expert Opin. Biol. Ther.* **15**, 337–351 (2015).

29. Lasaro, M. O. & Ertl, H. C. J. New insights on adenovirus as vaccine vectors. *Mol. Ther.* **17**, 1333–1339 (2009).

30. Eischeid, A. C., Meyer, J. N. & Linden, K. G. UV disinfection of adenoviruses: Molecular indications of DNA damage efficiency. *Appl. Environ. Microbiol.* **75**, 23–28 (2009).

31. Beck, S. E., Hull, N. M., Poepping, C. & Linden, K. G. Wavelength-dependent damage to adenoviral proteins across the germicidal UV spectrum. *Environ. Sci. Technol.* **52**, 223–229 (2018).

32. Vogel, R. *et al.* Quantitative Sizing of Nano/Microparticles with a Tunable Elastomeric Pore Sensor. *Anal. Chem.* **83**, 3499–3506 (2011).

33. Kennedy, M. A. & Parks, R. J. Adenovirus virion stability and the viral genome: Size matters. *Mol. Ther.* **17**, 1664–1666 (2009).

34. Bondoc Jr., L. L. & Fitzpatrick, S. Size distribution analysis of recombinant adenovirus using disc centrifugation. *J. Ind. Microbiol. Biotechnol.* **20**, 317–322 (1998).

35. Berkowitz, S. A. & Philo, J. S. Monitoring the homogeneity of adenovirus preparations (a gene therapy delivery system) using analytical ultracentrifugation. *Anal. Biochem.* **362**, 16–37 (2007).

36. McEvoy, M. *et al.* Improved Particle Counting and Size Distribution Determination of Aggregated Virus Populations by Asymmetric Flow Field-Flow Fractionation and Multiangle Light Scattering Techniques. *Biotechnol. Prog.* **27**, 547–554 (2011).

37. Ortega-Esteban, A. *et al.* Minimizing tip-sample forces in jumping mode atomic force microscopy in liquid. *Ultramicroscopy* **114**, 56–61 (2012).

38. Rexroad, J., Evans, R. K. & Middaugh, C. R. Effect of pH and ionic strength on the physical stability of adenovirus type 5. *J. Pharm. Sci.* **95**, 237–247 (2006).

39. Flesch, J. C., Spicer, P. T. & Pratsinis, S. E. Laminar and turbulent shear-induced flocculation of fractal aggregates. *AIChE J.* **45**, 1114–1124 (1999).

40. Meakin, P. Fractal aggregates. *Adv. Colloid Interface Sci.* **28**, 249–331 (1987).

41. Carrasco, F., Chornet, E., Overend, R. P. & Costa, J. A generalized correlation for the viscosity of dextrans in aqueous solutions as a function of temperature, concentration, and molecular weight at low shear rates. *J. Appl. Polym. Sci.* **37**, 2087–2098 (1989).

42. Dobrowsky, T. M. *et al.* Adhesion and fusion efficiencies of human immunodeficiency virus type 1 (HIV-1) surface proteins. *Sci. Rep.* **3**, 1–9 (2013).

Appendix 3: Chapter 3 Supporting Information

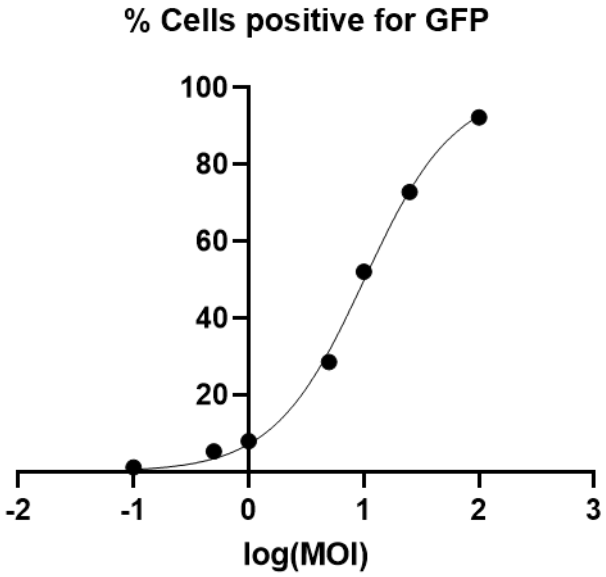

Figure A3.1: Calibration curve for converting the percentage of cells positive for green fluorescent protein (GFP) as determined by flow cytometry to a modality of infection (MOI) value. The curve was generated by determining the percentage GFP expression in samples infected with MOI values of 0.1, 0.5, 1, 5, 10, 25, and 100.

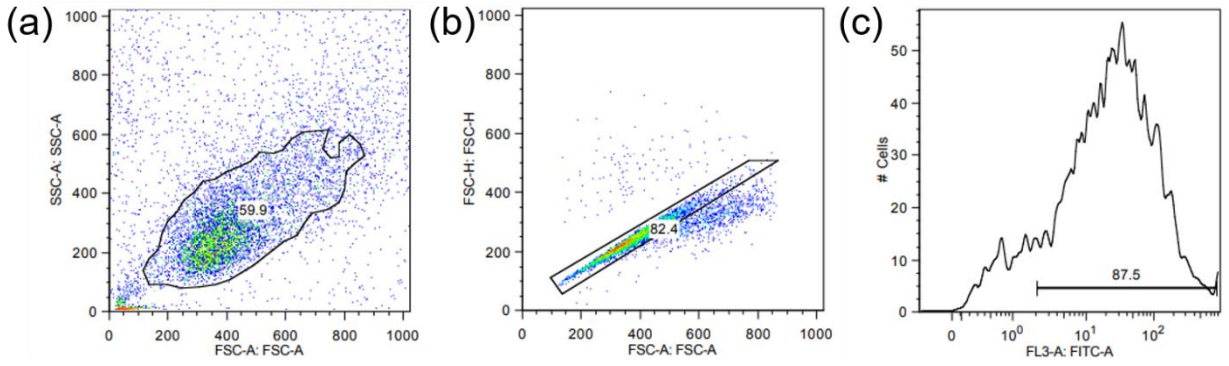

Figure A3.2: Gates applied to flow cytometry data from samples at a shear rate of 121×10^3 s^{-1} using FlowJo software: (a) the autogate applied to raw data to identify the live cell population; (b) the user-defined gate applied to separate the singlet live cell population from non-singlet live cells;

(c) the user-defined gate applied to separate GFP-positive cells from GFP-negative cells. Gate (c) was set on a negative control that was run once for every well plate and applied to all samples from that plate.

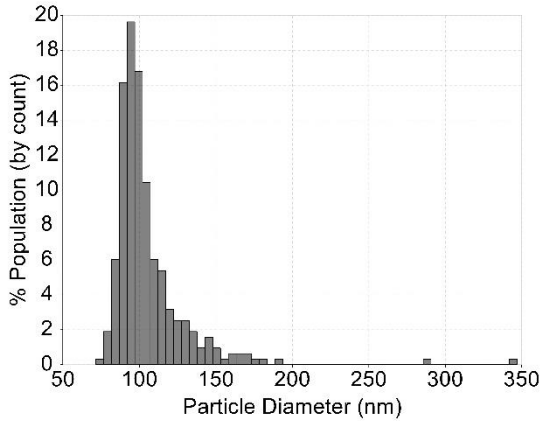

Figure A3.3: Size distribution histogram for the 4% sample at a shear rate of 121×10^3 s^{-1}. The particle count for this sample was 316.

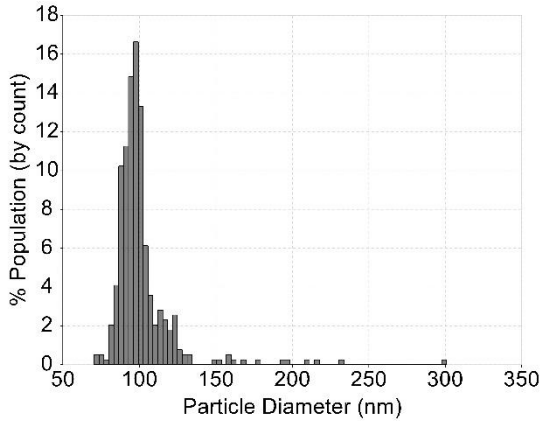

Figure A3.4: Size distribution histogram for the 4% sample at a shear rate of 391×10^3 s^{-1}. The particle count for this sample was 391.

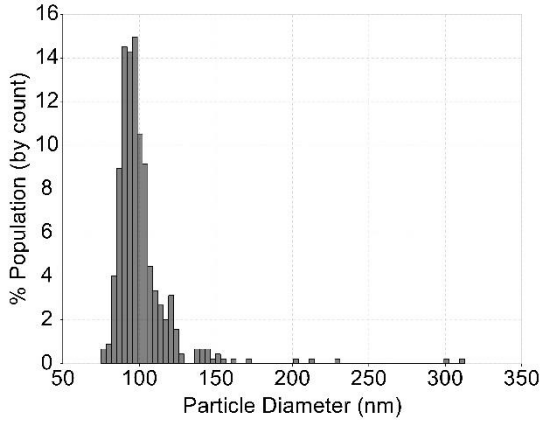

Figure A3.5: Size distribution histogram for the 4% sample at a shear rate of 686×10^3 s^{-1}. The particle count for this sample was 448.

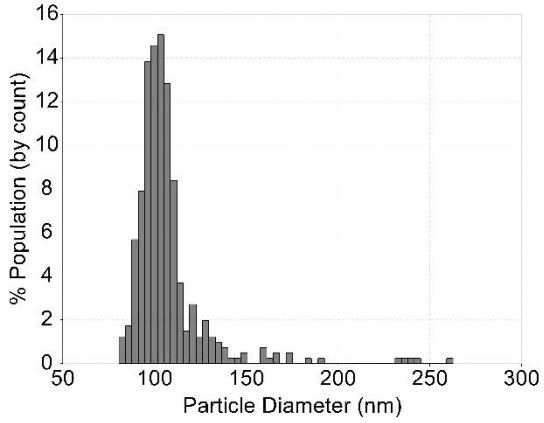

Figure A3.6: Size distribution histogram for the 8% sample at a shear rate of 121×10^3 s^{-1}. The particle count for this sample was 405.

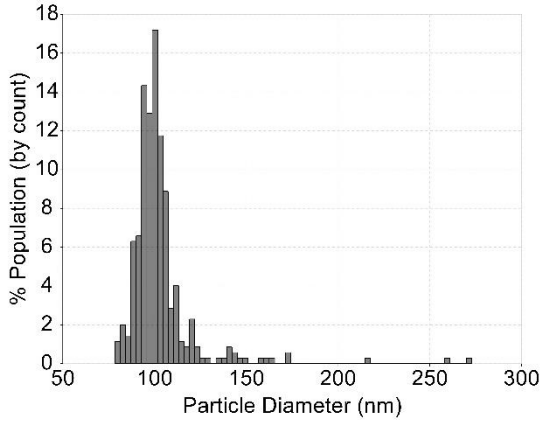

Figure A3.7: Size distribution histogram for the 8% sample at a shear rate of 258×10^3 s^{-1}. The particle count for this sample was 349.

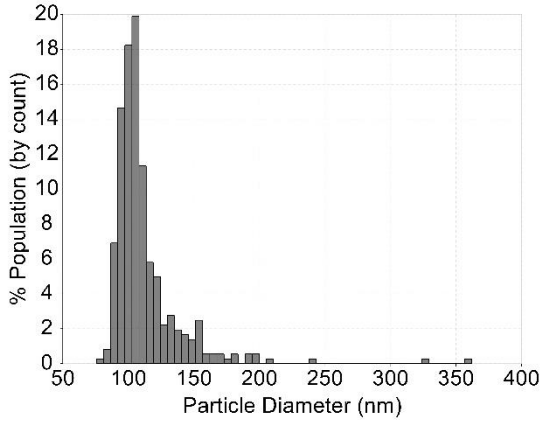

Figure A3.8: Size distribution histogram for the 8% sample at a shear rate of 686×10^3 s^{-1}. The particle count for this sample was 307.

Table A3.1: Mean particle size for all excipient solutions as measured using the qViro-X technique. The adenovirus control had a mean particle diameter of 99 ± 17 nm and the deactivated adenovirus sample had a mean particle diameter of 113 ± 28 nm.

Shear rate (x 10^3 s^{-1})	Mean particle diameter for 4% formulation (nm)	Mode particle diameter for 4% formulation (nm)	Mean particle diameter for 8% formulation (nm)	Mode particle diameter for 8% formulation (nm)
"no shear"	104 ± 27	93	103 ± 18	101
121	105 ± 26	94	107 ± 22	100
258	-	-	103 ± 19	103
391	101 ± 21	98	-	-
686	101 ± 21	97	106 ± 20	95

Chapter 4: Acoustic levitation as a screening method for excipient selection in the development of dry powder vaccines

Acoustic levitation is a promising technique to investigate the spray drying process as it extends the droplet drying time scale while maintaining the properties of spray dried powders. It can be used as a simplified single-droplet model for the heat and mass transfer that occur during spray drying and has the potential to screen stabilizing excipients or excipient blends without the use of large amounts of costly viral material. In this work, an acoustic levitator modified with a custom heating system was used to model the spray drying process to understand the effects of the environment on spray dried materials and assess its potential as a screening method. The acoustic levitator was found to produce materials with similar physical characteristics and viral activity trends to spray dried materials and was suggested as a suitable screening method. This work was the first report of acoustic levitation to study materials containing viral vectors in the literature, as well as one of the first comprehensive material comparisons between acoustic levitation and spray drying.

In this chapter, I was responsible for the design of experiments, preparation of all spray dried and acoustically levitated materials, and all characterization methods except for XRD analysis. XRD analysis was performed by Victoria Jarvis at McMaster University as described in the acknowledgements. The manuscript was drafted by myself, with editorial assistance from my supervisors Dr. Michael Thompson and Dr. Emily Cranston, as well as author Dr. Zhou Xing, and was approved by all authors before submission.

B. A. Morgan, Z. Xing, E. D. Cranston, M. R. Thompson, **2019**. "Acoustic levitation as a screening method for excipient selection in the development of dry powder vaccines", *International Journal of Pharmaceutics*, **563**, 71-78, DOI: 10.1016/j.ijpharm.2019.03.026.

Abstract

Spray drying is emerging as a promising technique to produce thermally stable powder vaccines containing viral vectors. One of the most important factors in developing dry powder vaccines is the selection of the excipient carrier, however this process is time intensive, and uses large amounts of costly viral material. In this work, an acoustic levitator modified with a hot air delivery system was evaluated for its ability to mimic spray drying and acts as a screening method for excipient selection. The ability of three binary excipient blends to stabilize a human type 5 adenovirus was evaluated through an *in vitro* activity assay based on the expression of green fluorescent protein. Dried particle size and shape, glass transition temperature, moisture content, and crystallinity of powders produced by levitation and spray drying were compared. The particles created in the acoustic levitator under moderate heat can be considered representative of the powders that would be produced via spray drying. Viral vector titre losses differ between the methods, however, the trends with respect to excipient performance remain the same. Key material characteristics such as particle morphology and thermal properties are conserved when using the levitator. The acoustic levitator is a good starting point for dry powder vaccine development, and can be used to identify promising excipients while consuming minimal amounts of the viral vector.

Keywords

Acoustic levitation, spray drying, screening method, vaccine, excipient, droplet drying

4.1 Introduction

One of the most commonly reported techniques for creating thermally stable vaccines is vitrification, where a biologic is encapsulated within the amorphous phase of a solid excipient.[1] Carbohydrates, amino acids, and proteins have all been reported in the literature as successful excipients to encapsulate and retain biologic potency at higher temperatures than current refrigeration conditions necessary for cold chain compliancy.[2–5] Freeze drying is the method traditionally used for vitrification in the pharmaceutical industry; however, spray drying is becoming more wide-spread and increasingly preferable due to its low cost, scalability, high throughput processing, and easy customization.[3,6,7]

Previous work has shown spray drying to be an effective method for preparing a thermally stable viral-vectored vaccine, with retained activity demonstrated even after storage at elevated temperatures as high as 55°C.[2,8] However, the selection of an excipient or blend of excipients that will successfully stabilize a viral vector is often done by trial and error, which can consume large amounts of expensive viral vectors, and even after selection must be optimized to reach its full potential as a stabilizer.[8,9] In order to avoid the pitfalls associated with excipient selection, an effective screening method is required that preserves key characteristics of spray dried powders while reducing either the time or the costs involved in successful development of the vaccine platform.

The literature does not contain any examples of screening methods used to select excipients for spray dried pharmaceutical products (of any type, not just limited to vaccines), although several single droplet analysis techniques have been reported as models for the spray drying process itself.[10,11] The main premise of any screening method is that it must match the trends seen in activity loss after spray drying. That is, one would conclude that the same excipient is ideal from both spray drying and the screening method, and additionally that the screening method would preserve certain key powder properties that have been identified as crucial for thermal stabilization, such as particle morphology and glass transition temperature.[2,8]

Acoustic levitation is one method suggested in the literature for evaluating single droplet drying kinetics, as well as modelling particles produced in a spray dryer.[12,13] In this method, a high amplitude standing wave is created using a reflector plate to reflect an ultrasonic acoustic wave. When a small object or droplet is placed in this standing wave, the upward pressure from the wave

counteracts the downward force of gravity and the droplet is suspended in place.[14,15] In order to avoid oscillations in position, the distance between the reflector plate and the wave generator can be adjusted until stable levitation is achieved.

The extended and motionless nature of droplet drying in an acoustic levitator, compared to a spray dryer, allows for *in situ* measurements to be made as droplets dry and particles form. Studies have been done using X-ray scattering to track crystallization of materials in the levitator as a function of time, and other contactless characterization techniques such as Raman spectroscopy have also been employed.[16,17] Mondragon et al. (2011) investigated the drying kinetics of multiphase droplets using a levitator modified to produce high-temperature conditions equivalent to those found in a spray dryer. They reported similar changes to drying behaviour with changing temperature, volume, and concentration, as those reported for spray drying.[8,18] Schiffter and Lee (2006a) noted that the Sherwood and Reynolds dimensionless numbers for levitated droplets were within the same range as those produced by spray drying, asserting that acoustic levitation followed an equivalent droplet drying mechanism. Additionally, they found that they could use the acoustic levitator to produce particles of mannitol, trehalose, and catalase that showed similar morphologies to spray dried powders.[19] Acoustic levitation has been considered as 'slow motion' spray drying, to determine the deactivation kinetics of an enzyme by removing droplets at various timepoints during the drying process.[20] We infer that particle morphology as a function of drying time could also be investigated using the slower drying process that occurs during levitation.

In our current work, we seek to confirm that important particle morphology characteristics are conserved between the screening method and the production method, and that importantly, when a viral vector is included in the formulation, that activity loss from both methods is consistent. Initially, our concerns with acoustic levitation as a screening method were the fact that the particles produced are much larger, there is no shear, and the drying time is much longer than in spray drying. Conversely, acoustic levitation provides a unique opportunity to separate the effects of processing conditions on the drying of materials since the droplet can be suspended indefinitely.

Herein we demonstrate the use of single-droplet drying via acoustic levitation as an excipient selection screening method for the spray drying of sugar-encapsulated viral vectors.

Specifically, a human type 5 adenovirus expressing green fluorescent protein (AdHu5GFP) was tested with mannitol/dextran, lactose/trehalose, and xylitol/dextran binary excipient blends. Although the viral activity losses from spray drying and levitation were not the same, the trends in activity loss with excipient blends were comparable. X-ray diffraction (XRD), scanning electron microscopy (SEM), differential scanning calorimetry (DSC), and thermogravimetric analysis (TGA) were used to characterize powder crystallinity, size and shape, thermal properties, and water content, respectively. Spray-dried and levitated particles were directly compared and powder property trends were correlated with activity losses to identify promising excipient blends. Acoustic levitation offers a less costly method than spray drying to select and optimize excipients. This study also identified the key powder properties that need to be matched to develop the best possible screening method for spray drying. To the best of our knowledge, this is the first report of acoustic levitation as a means of producing vaccine or virus-containing particles.

4.2 Materials and Methods

4.2.1 Chemicals and adenoviral vector

Excipients chosen for the study included anhydrous lactose, D-mannitol, D-(+)-trehalose dihydrate, dextran (M_r 40,000 kDa), and xylitol, all purchased as USP grades from Millipore-Sigma (Ontario, Canada). Cell media was prepared in-house using Life Technologies protocol from α-minimum essential medium (α-MEM) supplemented with 10% fetal bovine serum and 1% streptomycin/penicillin (Invitrogen, Ontario, Canada). A recombinant replication deficient human serotype 5 adenovirus expressing green fluorescent protein (AdHu5GFP) was produced in-house at the vector facility of the McMaster University Immunology Research Center as described previously.[21,22]

4.2.2 Spray drying, and acoustic levitation

Three excipient blend formulations were evaluated: (1) 90% lactose and 10% trehalose, (2) 75% mannitol and 25% dextran, and (3) 25% xylitol and 75% dextran (all compositions are based on percent by weight). Mannitol/dextran and xylitol/dextran formulations were dissolved into purified water to make a 4 wt.% solution, while lactose/trehalose was dissolved into purified water to give a 1 wt.% solution. All water was purified using a Barnstead GenPure Pro water purification system from ThermoFisher Scientific (Waltham, MA) and had a resistivity of 18.2 MΩ cm. For all

powders containing viral vector, 10 µL of viral vector stock solution was added to the dissolved excipient solution. The stock viral vector solution consists of phosphate buffered saline (PBS) with 10% by volume glycerol. Each milliliter of viral stock contains 2.35×10^{12} viral particles, and 3.8×10^{10} plaque forming units (pfu).

Spray dried powders were produced using a B-290 Mini Spray Dryer (Büchi, Switzerland) equipped with a 0.7 mm spray nozzle and a high performance cyclone following a protocol described previously.[2,8] All spray drying experiments were completed without optimization per formulation, using a constant nozzle temperature of 110°C, an outlet-measured air temperature of 55°C, a spray gas flow rate of 439.11 L/h, and a feed solution rate of 188.5 mL/h (corresponding to a pump setting of 13%). For all characterization techniques that did not require activity testing, AdHu5GFP was not included in the formulation due to biosafety requirements. Previous results from our group have found that powders spray dried both with and without viral vector are virtually indistinguishable by SEM due to the small amount of viral vector added to the solutions (less than 1/10,000th of the liquid volume).[2] All powder characterization was performed on the same day as the powders were produced to avoid any effects from aging.

Levitated particles, from the same excipient-virus solutions prepared for spray drying, were produced using a 13D10 ultrasonic levitator with a single-walled process chamber (tec5USA; Plainview, NY). A 10 µL glass syringe (Hamilton; Reno, NV) with a 26G needle (Becton Dickinson; Ontario, Canada) was used to deposit liquid droplets and collect dried particles from the acoustic levitator. A custom-made hot air delivery system was used to heat a suspended droplet. The relative humidity within the levitator corresponded to ambient room conditions (35-43% RH), considerably lower than in a spray dryer (near 100% RH). The system was monitored by a K-type thermocouple (Omega, Canada) and a USB microscope (AVEN; Ann Arbor, MI). MicroViewer 1.3M software (AVEN; Ann Arbor, MI) was used to record video and images of the droplet drying process and ImageJ (National Institute of Health) was used to measure the dimensions of the dried particles .[23] Spray drying yields were in the range of 20 – 100 mg, and levitation yields were in the range of 0.2 – 1.5 mg. The lactose/trehalose blend had lower yields than mannitol/dextran and xylitol/dextran due to the lower concentration of solute in solution. There were several nodes in the levitator available for multiple droplets to simultaneously dry; however, particles were produced one at a time in this study to avoid difficulties in retrieving one particle without

disrupting others. For comparison, a control experiment consisted of drying 3 mL of the same excipient-virus solutions in polystyrene petri dishes (35 x 10 mm, Corning; Corning, NY) for 2 hours at 55°C followed by activity testing.

4.2.3 Particle imaging

Particle size and shape were investigated using a JEOL JSM-7000 F scanning electron microscope (SEM) (JEOL Ltd., Japan). Particles were attached to aluminum stubs using double-sided tape and sputter-coated with a 5.0 nm layer of gold. Images were collected at working distances between 5.4 and 13.1 mm and electron accelerating voltages between 3.0 and 10.0 kV. Image analysis was done using ImageJ software.[23]

4.2.4 Differential scanning calorimetry (DSC)

A Q200 differential scanning calorimeter (TA Instruments; New Castle, DE) was used to measure the glass transition temperatures of powders (without viral vector). Powders were weighed into hermetically sealed aluminum pans and heated from 20°C to 300°C at a rate of 10°C per minute under a nitrogen purge gas flowing at 50 mL/min. A modulation period of 60 seconds and a modulation amplitude of 1°C was used. Thermal events were recorded from a single heating ramp to avoid dehydration of the powder and compare data between preparation methods.

4.2.5 Thermogravimetric analysis (TGA)

Spray dried and levitated powders without viral vector were heated in alumina crucibles at a rate of 5°C per minute up to 150°C under argon gas using a TGA/DSC 3+ instrument (Mettler Toledo; Columbus, OH). Star^e software (Mettler Toledo; Columbus, OH) was used to monitor the mass and determine the stable mass loss at 100°C.

4.2.6 Powder crystallinity

The powders produced from different excipient formulations (without viral vector) were characterized by powder X-ray diffraction (XRD) on a Bruker D8 Discover with DAVINCI.DESIGN diffractometer (Bruker; Billerica, MA) using a cobalt sealed tube source ($\lambda_{avg} = 1.79026$ Å$, 2\theta = 5 - 70°$). Powders were mounted on a silica base, and a blank silica signal was subtracted from the data using GADDS software (Bruker; Billerica, MA). The signal intensity was integrated into a crystallographic figure using DIFFRAC.EVA software (Bruker;

Billerica, MA) and crystalline content determined using TOPAS software (Bruker; Billerica, MA). We take the error in these measurements to be 1%.

4.2.7 Excipient solution viscosity

Dynamic viscosities of the three excipient blend solutions were measured using a Discovery Hybrid Rheometer (TA Instruments; New Castle, DE) with a Peltier plate. A 40 mm cone geometry was used. Experiments were done at a controlled temperature of 25°C, and a flow sweep was conducted from a shear rate of 0.1 s^{-1} to 5000 s^{-1} using approximately 0.5 mL of solution. All excipient solutions exhibited shear thickening behaviour beginning at a shear rate of 400 s^{-1}. At a shear rate of 100 s^{-1} and a temperature of 25°C, the lactose/trehalose blend had a viscosity of $2.4 \cdot 10^{-4}\ Pa \cdot s$, mannitol/dextran had a viscosity of $3.4 \cdot 10^{-4}\ Pa \cdot s$, and xylitol/dextran had a viscosity of $4.1 \cdot 10^{-4}\ Pa \cdot s$. As the shear rate was increased, the differences in solution viscosities diminished.

4.2.8 *In vitro* activity testing

A549 lung epithelial cells were cultured in T150 culture flasks with prepared α-MEM culture media and incubated in a humidified Forma Series II water jacketed CO_2 incubator (Thermo Scientific Corporation; Waltham, MA) at 37°C and 5.0% CO_2. At 80-90% confluency, cells were either split into a new T150 flask or plated into a 96-well plate for activity testing.

On the same day that they were produced, spray dried and levitated powders containing AdHu5GFP were reconstituted in 1 mL of culture media and eight-fold serial volume dilutions were created ranging from 10^0 to 10^{-7} of the reconstituted powder. A549 cells were then incubated with the dilutions for 24 hours, after which they were imaged for GFP fluorescence using an EVOS FL cell imaging system (ThermoFisher Scientific; Waltham, MA). The median tissue culture infectious dose ($TCID_{50}$) was calculated using the Reed-Muench method and then compared to the initial titre to determine titre loss incurred from spray drying/drying in the acoustic levitator.[24]

4.3 Results and Discussion

The viral vector candidate selected for the study, human type 5 adenovirus, is a promising vaccine platform for immunization against various mucosal pathogens, while a dry powder form of the vaccine is considered an ideal deliverable form for inhaled administration.[25,26] This viral

vector must be stored at -80°C in aqueous media in order to retain its activity, meaning it is susceptible to damage at any of the temperature conditions used in this study. A high viral potency in the stock solution of 10^{10} pfu was used and when added to the excipient solution resulted in a dilution to 10^{7} pfu in 10 mL. This high concentration of viral vector minimized the number of repeated levitated particle drying experiments needed (approximately 7 particles which takes 7 runs) to produce a strong detectable response by *in vitro* analysis. Each particle dried in the levitator takes approximately 15 min and as such, a starting titer lower than 10^{10} pfu would require more particles and considerably more time to obtain reproducible *in vitro* data. The three binary excipient blends selected as candidates in this work resulted from a preliminary study examining twenty different excipients (and excipients blends) and were chosen for their acceptability in the pharmaceutical industry. The blends were also deliberately chosen with the understanding that they would lead to a range of retained viral activity after drying: lactose-trehalose was expected to show poor stability in contrast to xylitol-dextran which was shown in preliminary studies to produce excellent thermal stability with AdHu5GFP.

A single set of operational parameters was used in the spray dryer, without optimization, to compare the excipients under comparable drying conditions. This allowed for meaningful comparisons between spray dried powders as well as between levitated and spray dried powders. Lack of optimization meant viral activity losses were higher than normally acceptable but for screening excipients, the trend in activity between formulations was the primary consideration. Our group has previously shown that the optimization of spray drying conditions plays an important role in minimizing viral activity losses caused by processing.[8]

4.3.1 Comparing viral vector activity between spray dried and levitated powders

4.3.1.1 Room-temperature acoustic levitation

Acoustic levitation offers a unique opportunity to decouple contributing physical parameters affecting droplet drying, specifically for their effect on the retained activity of the viral vector. The most notable feature of the acoustic levitator is the ability to prepare particles at any ambient temperature where the solvent exhibits a vapour pressure, whereas the constrained space in a spray dryer requires conditions closer to the solvent boiling point that may harm the activity of the virus. Studying droplet drying at room temperature, which cannot be accomplished in a spray dryer, minimizes thermal contributions to deactivation while allowing researchers to

investigate activity losses caused physically by drying phenomena, and chemically by associative effects as the excipients replace water surrounding the viral vector. Figure 4.1 shows viral vector activity loss with the three binary excipient blends and compares spray dried powders to particles dried in the levitator at room temperature.

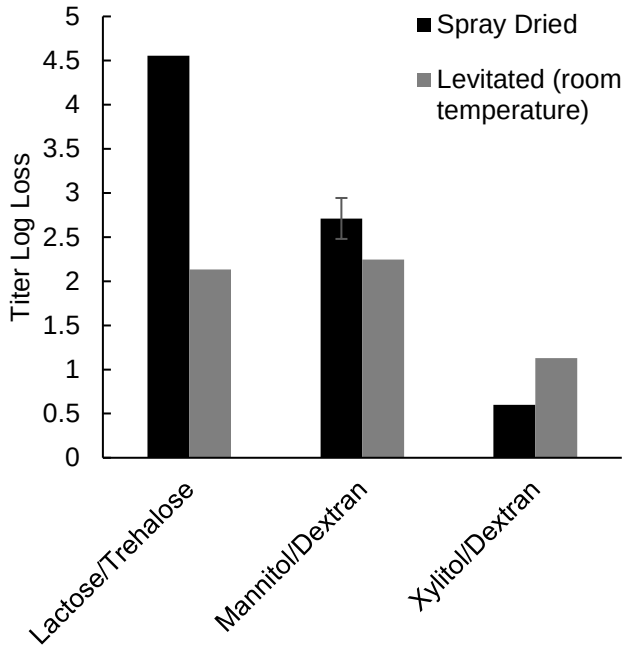

Figure 4.1. Titer log losses of AdHu5GFP activity with binary excipient blends dried by spray drying (black) and acoustic levitation (grey). Starting solution concentration was 4 wt.% solute for mannitol/dextran and xylitol/dextran, and 1 wt.% for lactose/trehalose. To evaluate process reproducibility, three separate samples of mannitol/dextran were spray dried and the result is shown as mean $\pm$SD.

Results in Figure 4.1 imply that drying through levitation at room temperature does not suitably mimic spray drying; both the activity loss values and trends in activity are different for the two methods. Drying through levitation showed less loss of the original viral titer (i.e., higher activity) compared to spray drying in two out of three cases. In general, the spray dried powders had large titer losses (4.6 log loss for lactose/trehalose and 2.7 log loss for mannitol/dextran). Xylitol/dextran showed excellent retention of activity with a low titer loss for both levitated (1.1 log) and spray dried (0.06 log) powders. A log loss of 1.1 is likely a realistic upper limit to continue testing/optimizing a given screened candidate for product development. Despite the lack of

agreement between the two methods, this set of experiments demonstrates that acoustic levitation can be used to produce dried particles that retain viral activity, which has not been shown previously, and which alleviated concerns about physical distortions under the acoustic wave possibly causing damage to the viral vector.

The difference in activity losses between the two methods provides insight into how drying time, temperature and shear forces may affect viral activity during drying. The lower activity losses seen in levitated particles imply that longer drying times did not adversely affect the viral vector despite prolonged exposure to temperatures above -80^{o}C (where the excipient and viral vector have high mobility). The greater losses seen in spray dried samples are attributed to the higher drying temperature and/or exposure of the viral vector to high shear in the nozzle, which have both been shown to negatively impact spray dried biologics.[8,27] The effects of drying temperature were subsequently further explored.

4.3.1.2 Acoustic levitation at elevated temperatures

To more closely mimic the surrounding air conditions in the spray dryer, as well as to investigate the effect of air drying temperature on particle formation, excipient blends containing AdHu5GFP were dried at 30°C, 40°C, 55°C, and 62°C within the acoustic levitation chamber. For reference, air temperature in the drying chamber and cyclone unit of the spray dryer was measured to be 55^{o}C. In the acoustic levitator a temperature of 62°C was selected as the uppermost limit that would not cause damage to the equipment. Figure 4.2 shows the activity losses for levitated particles dried with increasing air temperature for the three excipient blends (compared to spray drying data from Figure 4.1).

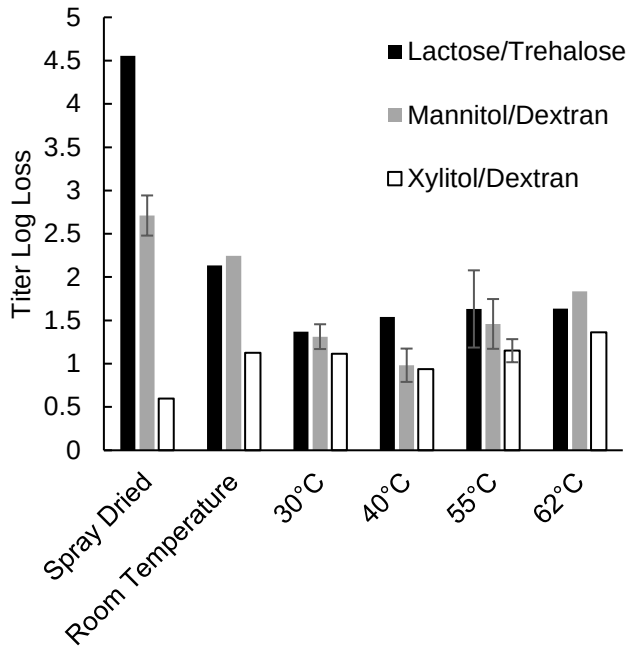

Figure 4.2. Titer log losses of AdHu5GFP activity with excipient blends dried by spray drying and acoustic levitation under varying temperature conditions. To evaluate process reproducibility, three separate samples of mannitol/dextran were spray dried or levitated, as well as all excipients in the levitator at 55°C, and the results shown are the mean ±SD.

Figure 4.2 shows that as the air temperature was increased in the acoustic levitator, all three formulations showed a decrease in titer loss going from room temperature up to 40°C. Above 40°C, titer losses for all three formulations increased once again but never exceeded the results at room temperature. Evaporative cooling as the droplet dried partially shielded the viral vector from thermal degradation but as the surrounding air temperature rose, this benefit was increasingly diminished. All temperatures tested for mannitol/dextran and lactose/trehalose blends indicated better viral stability than from the spray dryer; however, for xylitol/dextran the spray dryer remained the better performing drying method. From this we can infer that slightly higher air temperature does not necessarily infer more damage occurring to the viral vector, as it is partially protected from the heat by the evaporating liquid phase and benefits from a more rapid drying rate. With faster drying there will be less opportunity for the virus to migrate to the liquid-air interface. However, above a certain temperature, viral damage becomes the dominant outcome in spray drying encapsulated vaccine particles.[8]

Excipient solutions evaporated in a Petri dish at 55°C were found to have higher activity losses than either spray drying or levitation (i.e., 3.0 log loss for mannitol/dextran, 2.8 log loss for lactose/trehalose; no measurable activity was found for xylitol/dextran). This data suggests that the extended drying time necessary for basic evaporation is non-representative of the spray drying process. The acoustic levitator also avoids the air-water-solid interface present in more simplistic evaporation experiments. This air-water-solid interface has been shown to cause increased deactivation of bacteriophage, making removal of the solid phase during drying beneficial to mimicking spray drying.[28] Several studies have also been published on the effect of acoustic streaming on droplet drying kinetics, which would change how the particles dry compared to the spray dryer.[29] However, the disruption in air flow caused by the hot air in the levitator is likely greater than the acoustic streaming effect, and comparisons between the evaporated controls, levitation, and spray drying show that acoustic streaming is not detrimental to mimicking the spray drying process.

Variability in the test data was assessed with the mannitol/dextran formulation by running trials in true triplicate. The main source of error and variability in the results was found to come from the endpoint dilution *in vitro* assay for measuring viral activity, determined by testing control samples of the stock viral vector for activity as well; the control showed a standard deviation of 0.204 log for the three trials. The overall conclusion drawn from Figure 4.2 was that moderate heat (30-55°C) enabled acoustic levitation to produce similar trends in activity between the excipient blends when compared to spray drying, even though titer losses remained significantly lower.

4.3.1.3 Effect of particle size on activity loss

The major physical difference between acoustic levitation and spray drying is the size of the particles produced. Particles produced using the spray dryer have diameters in the range of 10 – 50 μm, whereas particles created via acoustic levitation have diameters approximately one order of magnitude larger, in the range of 300 – 800 μm.[2] In the acoustic levitator, particles are necessarily large since they need to be collected and manipulated manually by an operator, and it is desirable that individually they contain as much virus as possible so that only a few particles (approximately 7) are needed for a detectable response in *in vitro* (or *in vivo*) testing. To determine the effect that droplet size had on viral activity post drying, three different droplet sizes were placed at 40°C in the levitator without changing the mannitol/dextran concentration in solution. The

smallest particles were created by levitating 0.5 μL of solution, the smallest amount that was easily detachable from the needle tip, and produced particles with an average Feret diameter of 360 ± 30 μm. The largest particles that could be levitated in a stable manner used 2.8 μL of solution and gave particles with an average Feret diameter of 780 ± 60 μm. The average Feret diameter for the intermediate size was 510 ± 50 μm. Figure 4.3 reports the average particle sizes and resulting activity losses for mannitol/dextran levitated particles.

Activity testing shows that there is no significant difference in the titer loss of viral vector activity caused by changing the particle size; the variation in log loss data has already been attributed to the endpoint dilution method. All tested particle sizes show titer losses of 1.5 log or less, which indicate overall good performance, as expected for the mannitol/dextran formulation with AdHu5.[2] While particle size intuitively may be linked to activity loss (based on a higher interfacial area per unit volume at which viruses may be deactivated with smaller particles), the size range investigated here (360 – 777 μm) did not show this trend. Importantly, Figure 4.3 shows that the difference in particle size between the acoustic levitator and spray dryer does not invalidate the former as a screening method.

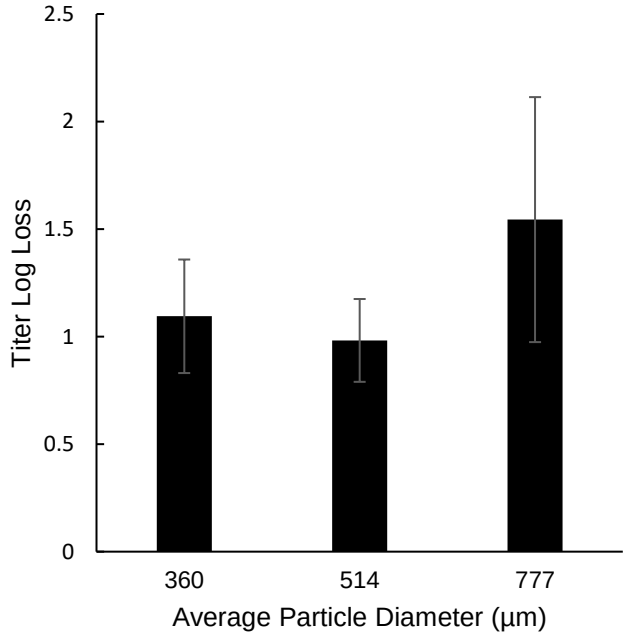

Figure 4.3. Effect of particle size on the measured AdHu5GFP titer log loss for mannitol/dextran particles levitated at 40°C.

4.3.2 Size and shape of spray dried and levitated powders

Particle size and shape of the dry powder vaccine is considered to impact its long term storage stability, where surface cracking/distortions and proximity of the virus to the surface influence the rate of declining activity. We have previously reported that spray dried particles showing surface nodules exhibited higher activity losses though the source of the nodules could not be conclusively identified as the virus.[2] Particles created using both the spray dryer and the acoustic levitator at 40°C, imaged using SEM, are compared side-by-side in Figure 4.4.

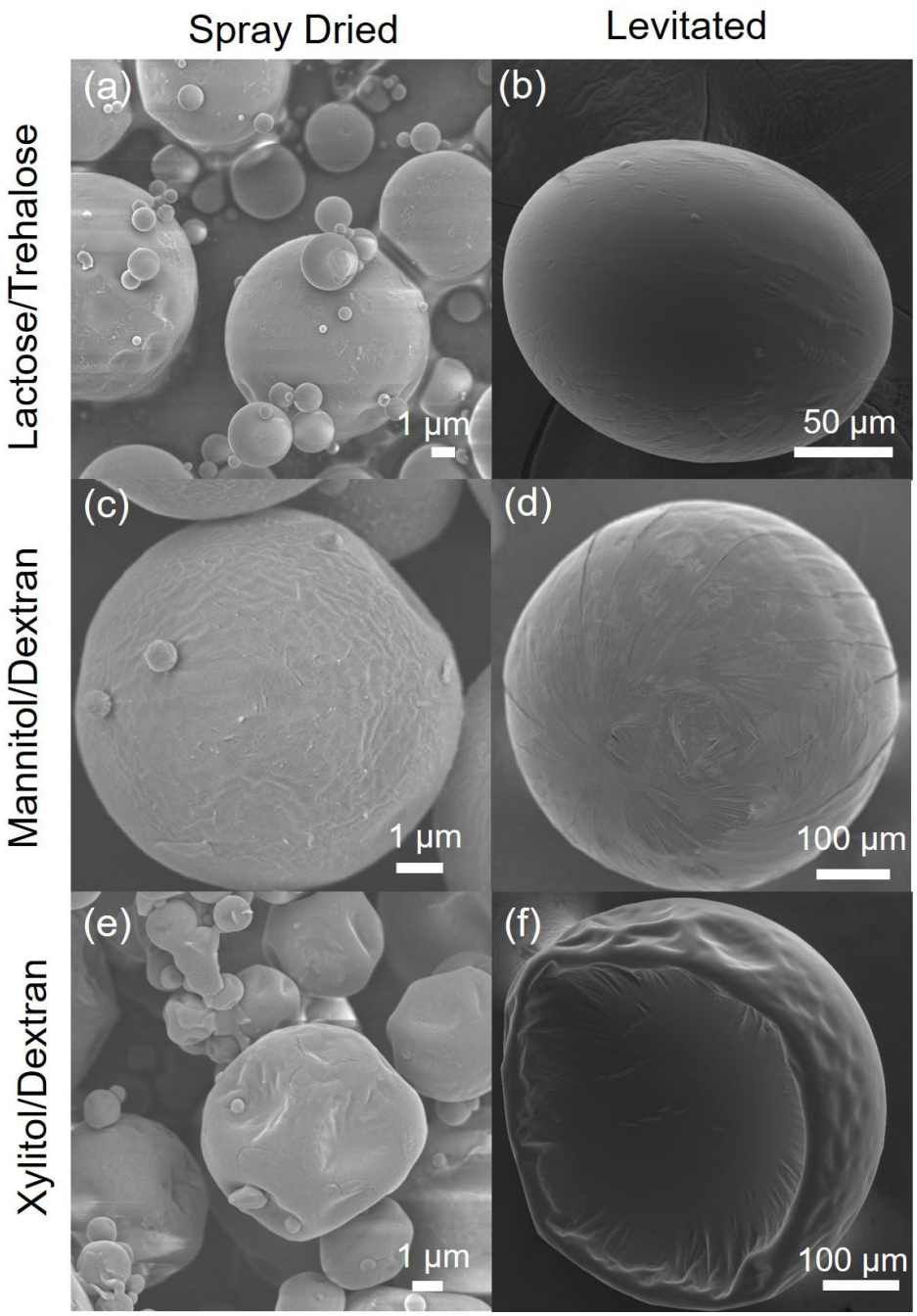

Figure 4.4. SEM images of particles dried by spray drying (a, c, e), and acoustic levitation at 40°C (b, d, f): lactose/trehalose (a, b), mannitol/dextran (c, d) and xylitol/dextran (e, f).

As shown in Figure 4.4, the shape and surface morphology of dried particles are consistent between acoustic levitation and spray drying. Both lactose/trehalose and mannitol/dextran show spherical particles, indicating a low Peclet number caused by high solubility and reduced surface activity.[30] Mannitol/dextran particles display a rougher, more wrinkled surface than the smooth

lactose/trehalose particles. Xylitol/dextran particles display a more dimpled and slightly collapsed shape, indicating a higher Peclet number which would cause the formation of hollow spheres that may collapse. This may be caused by the higher fraction of dextran present in these particles (75% vs. 25%), as the high molecular weight of dextran would hinder diffusion and lead to earlier precipitation at the droplet surface. The most notable difference between the methods is that acoustically levitated particles appear more oblong rather than spherical for all excipient blends due to the pressure exerted on the levitating droplet by the acoustic wave. The acoustic wave may also be the cause of small striations that are seen on the surface of some levitated particles (Figure 4.4d) but not on the spray dried particles.

4.3.3 Powder glass transition temperature, water content, and crystallinity

There are several factors present in spray drying that are not easily replicated in the acoustic levitator and that may cause differences in titer losses between particles created by the two methods, as highlighted in Figure 4.1 and Figure 4.2. One of these is the shear stress experienced by the liquid feed solution through the spray dryer nozzle, causing atomization. Previous work has demonstrated that increased shear can cause denaturation of proteins, and damage to the biologic may be even more pronounced when combined with the increase in air-water interface caused by atomization.[8,31–33] However, by using relatively low solute concentrations (1% and 4%) in the trials, viscosity is low (and differences between the three excipient blends are minimal; see values in Materials and Methods section 2.7) which suggests that shear was not a dominant cause for the differences in titer losses between formulations in spray drying specifically. Future studies may clarify the importance of shear on final activity losses.

Particle glass transition temperatures and moisture contents for all three excipient blends produced by both methods were analyzed to explain the differences in viral activity (Table 4.1). All acoustically levitated particles denoted in Table 4.1 were made at 40°C (i.e., the center point in the range of acceptable temperatures). Particles with the xylitol/dextran and mannitol/dextran blends displayed similar moisture contents between spray dried and levitated powders, with T_g values varying due to the slight differences in the amount of water present. Levitated lactose/trehalose had over five times the moisture content of the spray dried powder, depressing the blend T_g significantly to 91°C from 116°C; water is a known plasticizer of carbohydrates.[34] The results show that minor differences in moisture content can produce large differences in T_g.

Viewing this information in combination with the activity loss results in Figure 4.2, the implications of moisture content can be seen: powders with a higher T_g and hence lower moisture content generally experienced a lower titre loss (or higher T_g leads to higher viral activity in dried particles). The relevance of T_g on viral stability for thermally stable vaccines was previously reported by LeClair (2016a). The increased mobility of the viral vector in the encapsulating excipient opens it up to degradation mechanisms that are dependent on movement such as aggregation, and therefore a higher glass transition temperature is desirable because higher external temperatures are required to cause destabilization of the viral vector.[35–37] Several groups have published results linking moisture content of dried materials to enzyme and viral activity loss.[38,39]

Table 4.1. Glass transition temperatures measured by DSC, and moisture content measured by TGA for three binary excipient formulations, spray dried and acoustically levitated at 40°C.

Formulation	Glass Transition Temperature (°C)		Moisture Content	
	Spray Dried	Levitated	Spray Dried	Levitated
Lactose/Trehalose	116	91	4.4%	23.0%
Mannitol/Dextran	117	130	10.7%	7.0%
Xylitol/Dextran	142	118	8.4%	10.7%

Levitated particles were found to have similar or higher moisture content to spray dried powders of the same formulation. This was expected due to the higher temperatures found in the spray dryer that are not replicated in this case by the levitator, causing more water to evaporate from spray dried powders even though the residence time is much shorter than in the levitator. The differing moisture content can also be related to differences in the crystallinity of the dried particles between the two methods. XRD analysis was done to determine whether the powders were crystalline or amorphous, and to examine the extent of crystallization that was occurring during the different drying processes.

X-ray diffractograms for the three excipient blends are presented in Figure 4.5. All three formulations displayed similar XRD spectra between spray dried and levitated powders. Lactose/trehalose and xylitol/dextran displayed amorphous diffraction patterns with a single broad peak for both methods. Lactose and trehalose are known to inhibit crystallization in each other by interfering with crystal lattice growth, causing the amorphous peak seen here.[40,41] The amorphous peak of the xylitol/dextran blend is similar to the peak for amorphous xylitol reported using wide-angle X-ray scatterings (WAXS) by Palomäki, and dextran was not expected to show any crystalline peaks in XRD based on previous reports.[42,43] Mannitol/dextran displayed a crystalline spectrum that was similar to that published by us for spray dried mannitol/dextran.[2] Levitated mannitol/dextran was found to have 62% crystalline content, higher than the 40% crystalline content measured for spray dried mannitol/dextran. This is likely due to the extended drying time in the levitator, which prolongs the period available for the excipients to crystallize.[44] This may account for the lower moisture content seen in the levitated mannitol/dextran powder as well, as the higher crystallinity makes it less likely to uptake moisture.[45] Overall, these results show that the acoustic levitator can create either crystalline or amorphous particles that are representative of the powders produced through spray drying.

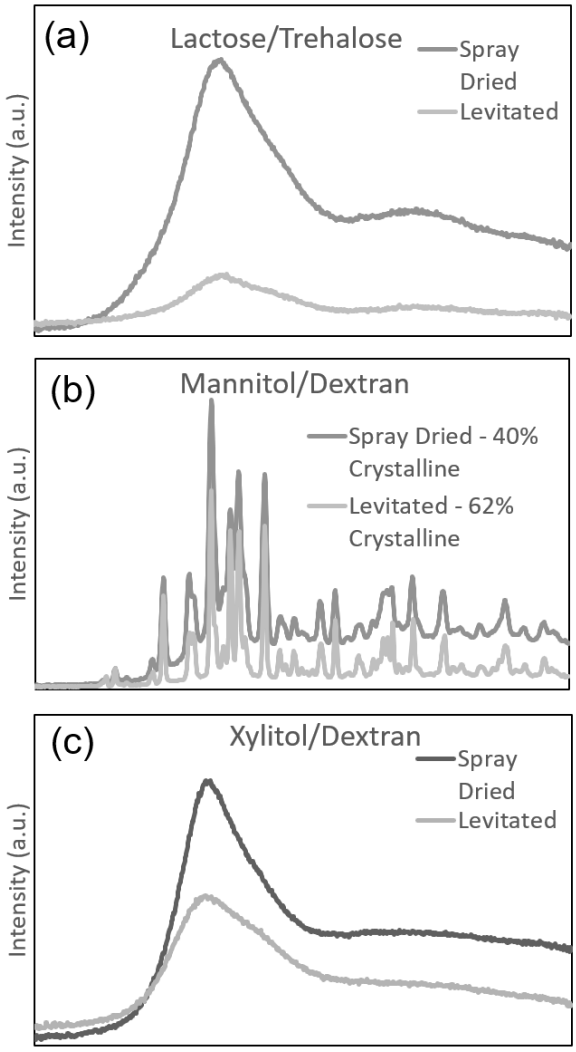

Figure 4.5. XRD spectra for xylitol/dextran (left), lactose/trehalose (middle), and mannitol/dextran blends created via spray drying or acoustic levitation at 40°C.

4.4 Conclusion

These results represent a library of new data comparing powder vaccines comprised of different excipient blends with AdHu5GFP and produced using spray drying and acoustic levitation (under similar conditions). The viral activity trends discussed here are all based on non-optimized spray drying conditions, and fairly large variances seen in the *in vitro* assay employed may add increased uncertainty to the results. However, after thorough characterization of viral activity and physical properties of dried powders, we believe that the acoustic levitator can act as a screening method to narrow down potential excipients to the most promising options based on

activity testing, T_g values, and moisture content. More specifically, ideal formulations should lead to particles with moderate water content (ca. 10%) and T_g values over 100°C, which can easily be assessed on particles created by acoustic levitation. Heating the acoustic levitator chamber in the 30-55°C range was the key to obtaining similar trends in viral activity between the two drying methods and the larger size of particles produced by acoustic levitation was not a decisive factor in predicting viral activity. The downside to using the acoustic levitator is the large amount of time necessary to produce enough mass for activity testing and characterization (approximately three hours to generate a milligram of powder), however, the microlitre amounts of liquid sample needed means that this method does not use large amounts of potentially costly viral vector.

4.5 Acknowledgements

The authors thank Prof. A. Adronov and Prof. M. Miller for equipment use; Victoria Jarvis for XRD analysis; Sam Afkhami, Xueya Feng and Anna Zganiacz for cell culture training and assistance; and Dan LeClair, Heera Marway, and Steven Toniolo for equipment training and troubleshooting help. The authors gratefully acknowledge facilities in the Canadian Center for Electron Microscopy. This study is supported by funds from the Canadian Institutes of Health Research, the Natural Sciences and Engineering Research Council of Canada, the Quebec Consortium for Drug Discovery (CQDM), and Ontario Centres of Excellence (OCE).

4.6 References

1. Crowe, J. H., Oliver, A. E., Hoekstra, F. A. & Crowe, L. M. Stabilization of Dry Membranes by Mixtures of Hydroxyethyl Starch and Glucose: The Role of Vitrification. *Cryobiology* **35**, 20–30 (1997).

2. LeClair, D. A., Cranston, E. D., Xing, Z. & Thompson, M. R. Evaluation of excipients for enhanced thermal stabilization of a human type 5 adenoviral vector through spray drying. *Int. J. Pharm.* **506**, 289–301 (2016).

3. Amorij, J. P., Huckriede, A., Wilschut, J., Frijlink, H. W. & Hinrichs, W. L. J. Development of stable influenza vaccine powder formulations: Challenges and possibilities. *Pharm. Res.* **25**, 1256–1273 (2008).

4. Ohtake, S. *et al.* Heat-stable measles vaccine produced by spray drying. *Vaccine* **28**,

1275–1284 (2010).

5. Alcock, R. *et al.* Long-Term Thermostabilization of Live Poxviral and Adenoviral Vaccine Vectors at Supraphysiological Temperatures in Carbohydrate Glass. **2**, 1–9 (2010).

6. Ré, M. I. Microencapsulation By Spray Drying. *Drying Technol.* **16**, 1195–1236 (1998).

7. Langford, A., Bhatnagar, B., Walters, R., Tchessalov, S. & Ohtake, S. Drying technologies for biopharmaceutical applications: Recent developments and future direction. *Drying Technol.* **36**, 677–684 (2018).

8. LeClair, D. A., Cranston, E. D., Xing, Z. & Thompson, M. R. Optimization of Spray Drying Conditions for Yield, Particle Size and Biological Activity of Thermally Stable Viral Vectors. *Pharm. Res.* **33**, 2763–2776 (2016).

9. Kristensen, D. & Chen, D. Stabilization of vaccines: Lessons learned. *Hum. Vaccin.* **6**, 227–231 (2010).

10. Vehring, R., Foss, W. R. & Lechuga-Ballesteros, D. Particle formation in spray drying. *J. Aerosol Sci.* **38**, 728–746 (2007).

11. Schutyser, M. A. I., Perdana, J. & Boom, R. M. Single droplet drying for optimal spray drying of enzymes and probiotics. *Trends Food Sci. Technol.* **27**, 73–82 (2012).

12. Sadek, C. *et al.* Drying of a single droplet to investigate process–structure–function relationships: a review. *Dairy Sci. Technol.* **95**, 771–794 (2015).

13. Sloth, J. *et al.* Model based analysis of the drying of a single solution droplet in an ultrasonic levitator. *Chem. Eng. Sci.* **61**, 2701–2709 (2006).

14. Yarin, A. L., Pfaffenlehner, M. & Tropea, C. On the acoustic levitation of droplets. *J. Fluid Mech.* **356**, 65–91 (1998).

15. Yarin, A. L., Brenn, G., Kastner, O., Rensink, D. & Tropea, C. Evaporation of acoustically levitated droplets. **399**, 151–204 (1999).

16. Leiterer, J., Delißen, F. & Emmerling, F. Structure analysis using acoustically levitated droplets. *Anal. Bioanal. Chem.* **391**, 1221–1228 (2008).

17. Klimakow, M. *et al.* Combined Synchrotron XRD / Raman Measurements : In Situ Identification of Polymorphic Transitions during Crystallization Processes. *Langmuir* **26**, 11233–11237 (2010).

18. Mondragon, R. *et al.* Study of the drying behavior of high load multiphase droplets in an acoustic levitator at high temperature conditions. *Chem. Eng. Sci.* **66**, 2734–2744 (2011).

19. Schiffter, H. & Lee, G. Single-droplet evaporation kinetics and particle formation in an acoustic levitator. Part 2: Drying kinetics and particle formation from microdroplets of aqueous mannitol, trehalose, or catalase. *J. Pharm. Sci.* **96**, 2284–2295 (2006).

20. Lorenzen, E. & Lee, G. Slow motion picture of protein inactivation during single-droplet drying: a study of inactivation kinetics of L-glutamate dehydrogenase dried in an acoustic levitator. *J. Pharm. Sci.* **101**, 2239–2249 (2012).

21. Wang, J. *et al.* Single Mucosal, but Not Parenteral, Immunization with Recombinant Adenoviral-Based Vaccine Provides Potent Protection from Pulmonary Tuberculosis. *J. Immunol.* **173**, 6357–6365 (2004).

22. Roediger, E. K., Kugathasan, K., Zhang, X. Z., Lichty, B. D. & Xing, Z. Heterologous boosting of recombinant adenoviral prime immunization with a novel vesicular stomatitis virus-vectored tuberculosis vaccine. *Mol. Ther.* **16**, 1161–1169 (2008).

23. Abràmoff, M. D., Magalhães, P. J. & Ram, S. J. Image processing with imageJ. *Biophotonics Int.* **11**, 36–41 (2004).

24. Reed, L. J. & Muench, H. A simple method of estimating fifty per cent endpoints. *Am. J. Hyg.* **27**, 493–497 (1938).

25. Zhu, F. C. *et al.* Safety and immunogenicity of a novel recombinant adenovirus type-5 vector-based Ebola vaccine in healthy adults in China: Preliminary report of a randomised, double-blind, placebo-controlled, phase 1 trial. *Lancet* **385**, 2272–2279 (2015).

26. Afkhami, S., Yao, Y. & Xing, Z. Methods and clinical development of adenovirus-vectored vaccines against mucosal pathogens. *Mol. Ther. - Methods Clin. Dev.* **3**, 16030 (2016).

27. Grasmeijer, N. Improving protein stabilization by spray drying: formulation and process development. (University of Groningen, 2016).

28. Thompson, S. S. & Yates, M. V. Bacteriophage Inactivation at the Air-Water-Solid Interface in Dynamic Batch Systems. *Appl. Environ. Microbiol.* **65**, 1186–1190 (1999).

29. Bänsch, E. & Götz, M. Numerical study of droplet evaporation in an acoustic levitator. *Phys. Fluids* **30**, (2018).

30. Elversson, J. & Millqvist-Fureby, A. Particle size and density in spray drying - Effects of carbohydrate properties. *J. Pharm. Sci.* **94**, 2049–2060 (2005).

31. Maa, Y.-F. & Hsu, C. C. Effect of high shear on proteins. *Biotechnol. Bioeng.* **51**, 458–465 (1996).

32. Maa, Y. F. & Hsu, C. C. Protein denaturation by combined effect of shear and air-liquid interface. *Biotechnol. Bioeng.* **54**, 503–512 (1997).

33. Ghandi, A., Powell, I. B., Howes, T., Chen, X. D. & Adhikari, B. Effect of shear rate and oxygen stresses on the survival of Lactococcus lactis during the atomization and drying stages of spray drying: A laboratory and pilot scale study. *J. Food Eng.* **113**, 194–200 (2012).

34. Hancock, B. C. & Zografi, G. The Relationship Between the Glass Transition Temperature and the Water Content of Amorphous Pharmaceutical Solids. *Pharmaceutical Research* **11**, 471–477 (1994).

35. Duddu, S. & Dal Monte, P. Effect of glass transition temperature on the stability of lyophilized formulations containing a chimeric therapeutic monoclonal antibody. *Pharm. Res.* **14**, 591–595 (1997).

36. Hancock, B. C., Shamblin, S. L. & Zografi, G. Molecular Mobility of Amorphous Pharmaceutical Solids Below Their Glass Transition Temperatures. *Pharmaceutical Research* **12**, 799–806 (1995).

37. Bhandari, B. R. & Howes, T. Implication of glass transition for the drying and stability of dried foods. *J. Food Eng.* **40**, 71–79 (1999).

38. Savage, M., Torres, J., Franks, L., Masecar, B. & Hotta, J. A. Determination of adequate moisture content for efficient dry-heat viral inactivation in lyophilized factor VIII by loss on drying and by near infrared spectroscopy. *Biologicals* **26**, 119–124 (1998).

39. Perdana, J., Fox, M. B., Schutyser, M. A. I. & Boom, R. M. Enzyme inactivation kinetics: Coupled effects of temperature and moisture content. *Food Chem.* **133**, 116–123 (2012).

40. Miao, S. & Roos, Y. H. Crystallization Kinetics and X-ray Diffraction of Crystals Formed in Amorphous Lactose , Trehalose , and Lactose/Trehalose Mixtures. *J. Food Sci.* **70**, 350–358 (2005).

41. Mazzobre, F., Soto, G. & Aguilera, José M.Buera, M. P. Crystallization kinetics of lactose in sytems co-lyofilized with trehalose . Analysis by differential scanning calorimetry. *Food Res. Int.* **34**, 903–911 (2001).

42. Palomäki, E., Ahvenainen, P., Ehlers, H., Svedström, K. & Huotari, S. Monitoring the recrystallisation of amorphous xylitol using Raman spectroscopy and wide-angle X-ray scattering. *Int. J. Pharm.* **508**, 71–82 (2016).

43. Taylor, B. N. W., Zobel, H. F. & Hellman, N. N. Effect of structure and crystallinity on water sorption of dextrans. *J. Phys. Chem.* **617**, 1955–1959 (1959).

44. Hoe, S. *et al.* Use of a Fundamental Approach to Spray-Drying Formulation Design to Facilitate the Development of Multi-Component Dry Powder Aerosols for Respiratory Drug Delivery. *Pharm. Res.* 449–465 (2014). doi:10.1007/s11095-013-1174-5

45. Ahlneck, C. & Zografi, G. The molecular basis of moisture effects on the physical and chemical stability of drugs in the solid state. *Int. J. Pharm.* **62**, 87–95 (1990).

46. Corbanie, E. A. *et al.* Spray drying of an attenuated live Newcastle disease vaccine virus intended for respiratory mass vaccination of poultry. *Vaccine* **25**, 8306–8317 (2007).

47. LeClair, D. A., Li, L., Rahman, N., Cranston, E. D. & Thompson, M. R. Stabilization of HSV-2 viral vaccine candidate by spray drying. *Int. J. Pharm.* **569**, 118615 (2019).

48. Saluja, V. *et al.* A comparison between spray drying and spray freeze drying to produce an influenza subunit vaccine powder for inhalation. *J. Controlled Release* **144**, 127–133

(2010).

49. Morgan, B. A., Xing, Z., Cranston, E. D. & Thompson, M. R. Acoustic levitation as a screening method for excipient selection in the development of dry powder vaccines. *Int. J. Pharm.* **563**, 71–78 (2019).

50. He, P., Davis, S. S. & Illum, L. Chitosan microspheres prepared by spray drying. *Int. J. Pharm.* **187**, 53–65 (1999).

51. Gong, P. *et al.* Injury Mechanisms of Lactic Acid Bacteria Starter Cultures During Spray Drying : A Review. *Drying Technol.* **32**, 793–800 (2014).

52. To, B. C. S. & Etzel, M. R. Survival of Brevibacterium linens (ATCC 9174) after Spray Drying , Freeze Drying , or Freezing. *J. Food Sci.* **62**, 167–170 (1997).

53. Shiu, C., Zhang, Z. & Thomas, C. A comparison of the mechanical properties of different bacterial species. in *Focus on Biotechnology, vol. 2* 155–162 (Springer, Dordrecht, 2001). doi:10.1007/0-306-46888-3_11

54. Snijder, J. *et al.* Integrin and Defensin Modulate the Mechanical Properties of Adenovirus. *J. Virol.* **87**, 2756–2766 (2013).

55. Levy, M. S. *et al.* Effect of shear on plasmid DNA in solution. *Bioprocess Eng.* **20**, 7–13 (1999).

56. Michalsky, R., Pfromm, P. H., Czermak, P., Sorensen, C. M. & Passarelli, A. L. Effects of temperature and shear force on infectivity of the baculovirus Autographa californica M nucleopolyhedrovirus. *J. Virol. Methods* **153**, 90–96 (2008).

57. D'Souza, D. H., Su, X., Roach, A. & Harte, F. High-Pressure Homogenization for the Inactivation of Human Enteric Virus Surrogates. *J. Food Prot.* **72**, 2418–2422 (2009).

58. Toniolo, S. P. *et al.* Excipient selection for thermally stable enveloped and non-enveloped viral vaccine platforms in dry powders. *Int. J. Pharm.* **561**, 66–73 (2019).

59. Thompson, M. R., Xing, Z., LeClair, D. A. & Cranston, E. D. Enhanced thermal stability for adenoviral vectors through spray drying. (2019).

60. Hede, P. D., Bach, P. & Jensen, A. D. Two-fluid spray atomisation and pneumatic nozzles

for fluid bed coating / agglomeration purposes : A review. *Chem. Eng. Sci.* **63**, 3821–3842 (2008).

61. Rumpf, H. The strength of granules and agglomerates. *Agglom. First Int. Symp. Agglom. Philadelphia, 1962* 379–418 (1962).

62. Zaiontz, C. Real Statistics Resource Pack (Release 6.2). (2019).

63. Appaiahgari, M. B. & Vrati, S. Adenoviruses as gene/vaccine delivery vectors: promises and pitfalls. *Expert Opin. Biol. Ther.* **15**, 337–351 (2015).

64. Lasaro, M. O. & Ertl, H. C. J. New insights on adenovirus as vaccine vectors. *Mol. Ther.* **17**, 1333–1339 (2009).

65. Eischeid, A. C., Meyer, J. N. & Linden, K. G. UV disinfection of adenoviruses: Molecular indications of DNA damage efficiency. *Appl. Environ. Microbiol.* **75**, 23–28 (2009).

66. Beck, S. E., Hull, N. M., Poepping, C. & Linden, K. G. Wavelength-dependent damage to adenoviral proteins across the germicidal UV spectrum. *Environ. Sci. Technol.* **52**, 223–229 (2018).

67. Vogel, R. *et al.* Quantitative Sizing of Nano/Microparticles with a Tunable Elastomeric Pore Sensor. *Anal. Chem.* **83**, 3499–3506 (2011).

68. Kennedy, M. A. & Parks, R. J. Adenovirus virion stability and the viral genome: Size matters. *Mol. Ther.* **17**, 1664–1666 (2009).

69. Bondoc Jr., L. L. & Fitzpatrick, S. Size distribution analysis of recombinant adenovirus using disc centrifugation. *J. Ind. Microbiol. Biotechnol.* **20**, 317–322 (1998).

70. Berkowitz, S. A. & Philo, J. S. Monitoring the homogeneity of adenovirus preparations (a gene therapy delivery system) using analytical ultracentrifugation. *Anal. Biochem.* **362**, 16–37 (2007).

71. McEvoy, M. *et al.* Improved Particle Counting and Size Distribution Determination of Aggregated Virus Populations by Asymmetric Flow Field-Flow Fractionation and Multiangle Light Scattering Techniques. *Biotechnol. Prog.* **27**, 547–554 (2011).

72. Ortega-Esteban, A. *et al.* Minimizing tip-sample forces in jumping mode atomic force

microscopy in liquid. *Ultramicroscopy* **114**, 56–61 (2012).

73. Rexroad, J., Evans, R. K. & Middaugh, C. R. Effect of pH and ionic strength on the physical stability of adenovirus type 5. *J. Pharm. Sci.* **95**, 237–247 (2006).

74. Flesch, J. C., Spicer, P. T. & Pratsinis, S. E. Laminar and turbulent shear-induced flocculation of fractal aggregates. *AIChE J.* **45**, 1114–1124 (1999).

75. Meakin, P. Fractal aggregates. *Adv. Colloid Interface Sci.* **28**, 249–331 (1987).

76. Carrasco, F., Chornet, E., Overend, R. P. & Costa, J. A generalized correlation for the viscosity of dextrans in aqueous solutions as a function of temperature, concentration, and molecular weight at low shear rates. *J. Appl. Polym. Sci.* **37**, 2087–2098 (1989).

77. Dobrowsky, T. M. *et al.* Adhesion and fusion efficiencies of human immunodeficiency virus type 1 (HIV-1) surface proteins. *Sci. Rep.* **3**, 1–9 (2013).

Chapter 5: Validation of a diffusion-based single droplet drying model for encapsulation of a viral-vectored vaccine using an acoustic levitator

Numerical modelling of the spray drying process is a useful tool that can predict spray dried powder properties without the need for experimentation, however many of the models presented in the literature do not provide any experimental validation of their computed results, and there are no models in the literature that are linked to viral vector activity. For this work, a diffusion-based model was developed for a single-droplet drying process using inputs that are readily available in literature and from chemical suppliers. The computed results were verified using an acoustic levitator, with silica nanoparticles used as viral vector analogues. The experimental results were found to closely match the model predictions, and the ability to predict distribution of adenovirus within a dry particle was linked to trends in viral activity. The developed model will reduce time and costs associated with formulation development by identifying promising excipients before beginning experiments. This is the first report that spatially locates adenovirus within a dry particle with experimental validation, and is also the first report linking a spray drying model to viral vector activity.

In this chapter, all modelling work was done by myself, as well as all acoustic levitation experiments and sample preparation. I was also responsible for preparing and characterizing pSiNPs for use in drying experiments (FTIR, zeta potential measurements, DLS measurements). All AFM was performed by author Elina Niinivaara, and confocal microscopy was performed at the University of British Columbia's bioimaging facility by Kevin Hodgson and Eun Kyoung Lee as described in the acknowledgements. All XRD data was collected by Anita Lam at the University of British Columbia, also as described in the acknowledgements. The manuscript was drafted by myself, with editorial assistance from supervisors Dr. Michael Thompson and Dr. Emily Cranston, as well as author Dr. Zhou Xing, and was approved by all authors before submission.

B. A. Morgan, E. Niinivaara, Z. Xing, M. R. Thompson, E. D. Cranston, **2021**. "Validation of a diffusion-based single droplet drying model for encapsulation of a viral-vectored vaccine using an acoustic levitator", Manuscript submitted to *International Journal of Pharmaceutics*.

Abstract

Development of thermally stable spray dried vaccine powders is dependent on the selection of a proper excipient or excipient blend for encapsulation, which can be a time and resource intensive process. In this work, a diffusion-based droplet drying model was developed to compute droplet drying time, size, and component distribution. The model predictions were validated using an acoustic levitator to dry droplets containing protein-coated or fluorescently labelled silica nanoparticles (as adenovirus analogues) and a range of excipient blends. Surface morphology of the dried particles was characterized by atomic force microscopy and the distribution of silica nanoparticles was quantified by confocal microscopy. The modelled distributions of adenovirus agreed with the microscopy results for three mannitol/dextran excipient blends with varying molecular weight dextrans, verifying the equations and assumptions of the model. Viral vector activity data for adenovirus in a range of (poly)saccharide/sugar alcohol formulations were also compared to the model outputs, suggesting that viral activity decreases when the model predicts increasing adenovirus concentration near the air-solid interface. Using a validated model with excipient property inputs that are readily available in the literature can facilitate the development of viral-vectored vaccines by identifying promising excipients without the need for experimentation.

Keywords

Acoustic levitation, modelling, spray drying, droplet drying, excipient, vaccine development

5.1 Introduction

Spray drying has the potential to play a major role in the production of thermally stable vaccine powders and next generation pharmaceutics with high temperature storage capacity and particle characteristics suitable for pulmonary delivery. Compared to other popular drying technologies such as freeze drying or vacuum drying, spray drying allows for more control over the final product, is more cost effective, and can more easily process large amounts of product.[1,2] By controlling the input parameters during spray drying, dry powder characteristics such as particle size, morphology, and moisture content can be controlled.[3] For these reasons, there are many examples in the literature of droplet and spray drying models that can be used to assist in particle engineering by predicting powder properties without experiments.[4–6] However, when formulations containing biologic materials, such as proteins or viral vectors, are spray dried, the ability to retain the effectiveness of the biologic is the most vital characteristic. Component distribution (the weight fraction variance of each chemical species with respect to the radius of a droplet or solid particle) is known to have a significant impact on the performance of a final dry powder, particularly in pharmaceutical products where exposure of biologic materials to the air-solid interface can lead to a decrease in activity.[7–9] Despite this, there is a lack of predictive models in the literature that are intended to guide the encapsulation strategies for stabilizing biologics.

In addition to the lack of models describing the effectiveness of biologics after spray drying, experimental methods to link biologic material distribution/location within a powder to activity loss are limited. Standard characterization techniques such as microscopy and surface elemental analysis are inadequate for powders containing viral vectors because of the relatively small volume of virus particles compared to the total volume of the powder, and the low probability of finding a viral particle at the surface. The sensitivity and spatial coverage and resolution of these techniques is often insufficient and, in some cases, working with biologically active/infectious agents is prohibited in instruments and facilities due to biosafety concerns. Employing an inactive "analogue" in the formulation to represent the biologic material can facilitate powder characterization and, as shown here, model validation. In the present study, we aim to develop an appropriate theoretical model to give formulators added insight into the location and activity of a viral vector in the encapsulating matrix of a drying droplet – this is beyond the apparent chemical interactions and makes for a cost-saving resource in an otherwise expensive development process.

The spray drying process in its entirety is complex, involving mass and heat transport within a droplet along with progressive phase transitions, all of which occur on a time scale of milliseconds. To best approximate the process, it is desirable to simplify the system to an individual droplet containing dissolved or suspended solids that is drying in a controlled environment.[10] This simplified system can be broken down into two drying stages: the first stage of drying occurs as solvent begins to evaporate from the droplet surface at a constant rate, dependent on the surrounding temperature and humidity, known as the *constant rate period*.[11] The radius of the droplet begins to shrink, and as more solvent evaporates, the concentration of the dissolved solutes will eventually reach saturation at the surface and precipitation will occur. This causes the formation of a solid shell around a liquid core. During the second stage, the evaporation rate slows significantly as water must now diffuse through the solid shell to reach the air-solid interface and evaporate, known as the *falling-rate period*.[12] Over time, the shell thickness will increase as water is removed from the droplet until a dry particle is formed. Depending on the rate of diffusion, the evaporation rate, and the mechanical strength of the shell, the particle may either remain the same size, or buckle and fold into a smaller particle during the falling rate period.[13] Two-stage models are the most common in the literature, as they make simulating the system less complex.

There are several models available in the literature that are specific to droplet drying, including semi-empirical models, deterministic models, and reaction engineering approach models.[6] Many of these models have been developed with spray drying in mind, and all can predict droplet or particle bulk characteristics such as size, drying time, and temperature, while several models can also predict the component distribution.[14–17] However, most of these models present computed results without experimental validation, or provide validation for basic predictions such as droplet size and drying time but do not verify their more complex predictions such as component distribution.[18] This detailed level of particle engineering has critical importance to new dry powder vaccines (our focus), making it necessary to create a comprehensive model of droplet drying where the component distribution is reasonably predicted and its results are experimentally verified. As such, the goal of this work was to explain the diminished activity of a human type-5 adenovirus (AdHu5) seen in our previous spray drying studies where the loss of effectiveness in this dry powder vaccine was hypothesized to be related to the virus proximity to the particle surface.[7]

Herein, predictions were made using a continuous, diffusion-based droplet drying model based on the deterministic model of Grasmeijer et al.[18] and compared to observations of experimentally produced particles using an acoustic levitator. The distribution of components and their relationship to viral activity loss were studied using an adenoviral analogue, specifically, protein coated silica nanoparticles (pSiNPs) to mimic AdHu5.[19] To the best of our knowledge, this is the first work that spatially locates adenovirus or adenoviral analogues within a dried particle, which is an important step towards understanding viral deactivation routes and excipient performance in thermally stable vaccine powders, leading to products with improved viral stability and effectiveness.

5.2 Materials and Methods

5.2.1 Preparation of protein coated silica nanoparticles (pSiNPs)

The particle size and coating were chosen to mimic AdHu5 without the associate biohazard. Carboxylated silica nanoparticles (SiNPs; 100 nm diameter) were purchased from Creative Diagnostics (New York, NY), at concentrations of 25 mg/mL. The SiNPs were covalently coupled to α_1-acid-glycoprotein (Millipore-Sigma; Oakville, Canada) using a two-step 1-ethyl-3-(3-dimethylaminopropyl) carbodiimide hydrochloride (EDC) reaction based on Pang et al. and a protocol from Bangs Laboratories.[19,20] Two rounds of centrifugation were used to wash 1 mL of SiNPs. In each round, 10 mL of 2-ethanesulfonic acid (MES) buffer (Millipore-Sigma; Oakville, Canada; pH 6.0) was added to the SiNPs, followed by centrifugation at 10,000 G for 15 minutes and removal of the supernatant. After the second round of centrifugation, the SiNP pellet was re-suspended in 2.5 mL MES buffer (pH 6.0) using 15 minutes of bath sonication. After re-suspension, 100 mg of EDC was added while stirring the SiNP suspension continuously for 15 minutes at room temperature to allow the reaction to occur. The SiNPs were then washed again with two rounds of centrifugation in MES buffer (pH 7.2) and the pellet was re-suspended in 5 mL of MES buffer (pH 7.2) using bath sonication. The α_1-acid-glycoprotein (1 mg, Millipore-Sigma; Oakville, Canada) was dissolved in 5 mL of MES buffer (pH 7.2) was added to the SiNP suspension, and this mixture was agitated for 4 hours at room temperature to allow the coupling reaction to occur. In the final steps, the pSiNP suspension was washed in 10 mL of purified water while being centrifuged at 10,000 G for 15 minutes, and the pellet re-suspended in 10 mL of purified water using bath sonication for 15 minutes. The final pSiNP suspension was stored at 4°C

until use. All purified water used had a resistivity of 18.2 MΩ cm. Dynamic light scattering, zeta potential measurements, atomic force microscopy (AFM), and Fourier-transform infrared (FTIR) spectroscopy were all used to confirm that the coupling reaction was successful (Appendix 5, Table A5.1 and Figures A5.1 and A5.2).

5.2.2 Droplet drying by acoustic levitation

Excipients for the experiments included D-mannitol and dextran of three different molecular weights (M_r 10 kDa, 40 kDa, and 500 kDa), all purchased as USP grades from Millipore-Sigma (Oakville, Canada) and used as received. Mannitol was dissolved into purified water with a dextran of chosen molecular weight at a ratio of 75:25 by mass, respectively, at a total solids concentration of 4 wt%. Two different concentrations of pSiNPs were examined with this excipient solution, either at the so-called 'normal' loading, and a 'high' loading (50 times normal, which was more easily detected in dry particles). For the normal loading concentration, 16 µL of pSiNP suspension at a concentration of 1.51×10^{12} pSiNPs/mL was added to 10 mL of the excipient solution to give an equivalent loading of particles to the viral vector in dry powder vaccines.[21,22] For the 'high' loading concentration, 800 µL of pSiNP suspension at a concentration of 1.51×10^{12} pSiNPs/mL was added to 10 mL of excipient solution.

In some cases, fluorescent carboxylated SiNPs (fSiNPs; 100 nm diameter) purchased from Creative Diagnostics (New York, NY) were used instead of pSiNPs, for visualization in confocal microscopy. The received fSiNPs (10 mL at 25 mg/mL concentration) were diluted to a concentration of 2.35×10^{12} fSiNPs/mL in purified water and combined with mannitol/dextran equivalent to the 'high' loading (500 µL of fSiNP suspension for 10 mL of excipient solution) for pSiNPs, i.e., 50-fold the normal AdHu5 loading.

A model 13D10 ultrasonic levitator with single-walled process chamber (tec5USA; Plainview, NY) was used to prepare particles; levitated particles are about 50 times larger than spray dried particles but have been shown to exhibit similar viral activity trends when drying conditions are replicated and are much easier to characterize for their surface morphology.[21] A 10 µL glass syringe (Hamilton; Reno, NV) with a 26G needle (Becton Dickinson; Mississauga, Canada) was used to place liquid droplets of approximately 2.5 µL in the standing acoustic wave of the levitator as well as to collect dried particles. The levitator was operated in a custom-made

glove box with a programmable heat gun (Steinel; Bloomington, MN) to control the surrounding temperature of the droplet. Temperature and relative humidity (RH) measurements were measured continuously throughout the drying process using a USB sensor (Dracal; Brossard, Canada). The RH in the glove box was not controlled, varying with temperature, from approximately 30% RH at room temperature, to approximately 4% RH at the set temperature between 55°C and 60°C. A Celestron MicroDirect USB microscope and accompanying software (Celestron; Torrance, CA) was used to take a series of time-lapsed images during the drying process. In order to increase the sharpness of the droplet edge during imaging, droplets were backlit using an LED ring light passed through a light diffusing sheet. Custom-made Python software was used to measure both major and minor droplet axis lengths in pixels from the time-lapse images, as pressure from the acoustic wave flattens the droplet so that the cross-sectional area is elliptical in shape. These values were converted into micrometers using a calibration.

5.2.3 Particle microscopy

Samples mounted on a magnetic metal specimen support disc with double sided tape were imaged by AFM using tapping mode on a Bruker Multimode 8 AFM (Bruker; Santa Barbara, CA) at a scan rate of 0.25 Hz. Al coated silicon probes were used (NCHR probes from Asylum Research, Oxford Instruments, Santa Barbara, CA) with a nominal 42 N/m spring constant and 30 kHz resonance frequency. All images were processed with a standard third-order polynomial flattening technique in the NanoScope analysis software v.8.10 (Bruker; Santa Barbara, CA).

Confocal laser scanning microscopy was done using an Olympus FV1000 laser scanning/two-photon confocal microscope (Waltham, MA) with an excitation wavelength of 559 nm. 75 scans spaced 2 µm apart were taken for a total depth of 150 µm for each levitated particle (dried in the acoustic levitator at 60°C and 4% RH; one particle for each mannitol/dextran blend was imaged) using the Olympus 20x NA 0.75 air objective. Particles were held in place using double sided tape. The images were captured using Fluoview FV100 software (Olympus; Waltham, MA) and image analysis was done using the Fiji package for ImageJ software (National Institutes of Health; Bethesda, MD) according to a previously published method.[23]

5.3 Numerical modelling – droplet drying

The droplet drying model used in this work was developed in Matlab (Mathworks Inc.; Natick, MA), adapted from a published model.[18] In this model, the droplet was comprised of 40 concentric spherical shells of progressively increasing diameter but equal volume, each composed of a uniform composition that changed as a function of time. For every iteration in the modelled droplet drying process, as the solvent evaporated from the outer surface of the droplet, the diameter of each shell was recalculated to keep the volume of each of the 40 subshells equal.

The original model was modified to improve its accuracy for the current set of results, and to improve the ease of use when modelling new materials. Due to 'acoustic streaming' caused by the ultrasonic wave used for droplet levitation, the mass transfer from droplet to surroundings is higher than drying in stagnant air.[24] To account for this, a temperature-dependant dimensionless Sherwood number was added to the term calculating evaporative mass transfer rate of water from the droplet to its surroundings. At each temperature, a constant Sherwood number was assumed for the duration of drying, using reported Sherwood numbers at 25°C and 60°C in the literature.[25] The evaporative mass transfer rate from the outermost subshell to the air was calculated using the following equation, derived from Fick's law:[26]

$$\dot{M}_w = 4\pi \frac{D_{w,air} \cdot \Delta P \cdot MW_w \cdot r}{R \cdot T_{gas}} \tag{5.1}$$

where $D_{\mathrm{w,air}}$ is the diffusion coefficient of water vapour in air (m^2/s), ΔP is the difference in vapour pressure at the surface of the droplet and the surrounding atmosphere (Pa), MW_w is the molecular weight of water (kg/mol), r is the radius of the gas layer (m), R is the universal gas constant ($\frac{\mathrm{J}}{\mathrm{mol}*\mathrm{K}}$), and T_{gas} is the temperature of the surrounding atmosphere (K).

Diffusion coefficients for the original model's various dissolved components came from fitting data.[18,27] To reduce reliance of the model on experimental diffusion data, subsequent coefficients D_i of all solutes were calculated using the Stokes-Einstein equation:

$$D_i = \frac{k_B T}{6\pi\eta R_{Hi}} \tag{5.2}$$

where k_B is the Boltzmann constant (J/K), T is the droplet temperature (K), η is the viscosity of the solvent (Pa*s), and R_{Hi} is the hydrodynamic radius of component i (m). The diffusion coefficient of water was also adjusted using a correlation from Mendoza and Schmalko, who measured the diffusion coefficient of water for the osmotic dehydration of papaya:[28]

$$D_w = 9.3 \times 10^{-10}(1 + 0.29x_w) \tag{5.3}$$

where x_w is the mass fraction of water. This correlation was selected to increase the robustness of the model at predicting the drying behaviour of carbohydrate-based formulations, as this equation was used to model the diffusion of water in a variety of carbohydrates. Diffusion coefficients for all components vary radially, based on the size of the 40 subshells. Movement of the droplet components are considering the basis of Fick's first law of diffusion; to simplify the model, negligible internal circulation and flow within the droplet are assumed based on the model of Sloth et al., although this assumption could be removed in future iterations of the model to increase accuracy.[12]

To calculate the viscosity of systems containing dextran, an equation from Carrasco et al. was used to correlate the viscosity to temperature, concentration of dextran, and the molecular weight of dextran:[29]

$$\eta = (\eta_0 + \alpha_v c) \cdot \exp\left(\frac{(E_0 + \delta_v c)}{RT}\right) \tag{5.4}$$

where η_0 is a pre-exponential factor at infinite dilution (Pa*s), α_v and δ_v are constants for a given molecular weight, c is the concentration of dextran (%), and E_0 is the activation energy of viscous flow at infinite dilution (J/mol). The predicted viscosities for a 4% mannitol/dextran solution (1.6 mPa*s) and an 8% mannitol/dextran solution (1.9 mPa*s) were comparatively similar to measured viscosities at 25°C for the same solutions (1.1 mPa*s for a 4% solution and 1.3 mPa*s for an 8% solution).[22] This correlation was chosen as dextran was the largest excipient molecule modelled in this study and was considered to be the dominant cause for changes in viscosity, whereas the mannitol was assumed to have a relatively negligible influence on the modelled system viscosity.

Additionally, the model was modified to significantly decrease the diffusion of solutes once the radius of the droplet stopped shrinking (i.e., once a solid shell had formed). This was to prevent the unrealistically rapid self diffusion of excipients in the highly concentrated media. The diffusion

of water was allowed to continue as predicted by equation (5.3), since it reportedly accounts for the mobility of water through carbohydrates.

In order to run the model, measured values for surrounding air temperature, RH, and initial cross-sectional area of the droplet were required as inputs. Several other material properties were required as inputs for each excipient being modelled, namely density, molecular weight, hydrodynamic radius, and solubility in water. These properties can be readily found in the literature or in material data sheets provided by suppliers for most common excipients, including those used for these experiments. The model inputs for hydrodynamic radius, density, and molecular weight used in this work for the three dextrans, mannitol, and AdHu5 are provided in Table 5.1. We note that the density and radii of pSiNPs and fSiNPs are similar to AdHu5.[19] Code for the model is available upon request by emailing the authors.

Table 5.1: Model input values for hydrodynamic radius, density, and molecular weight for dextrans, mannitol, and AdHu5.

Component	Hydrodynamic Radius (m)	Density (kg/m^3)	Molecular Weight (kg/mol)	References
10 kDa Dextran	1.9×10^{-9}	1050	10	29, 30
40 kDa Dextran	4.8×10^{-9}	1050	40	
500 kDa Dextran	15.9×10^{-9}	1050	500	
Mannitol	4×10^{-10}	1490	0.182	31-33
AdHu5	5×10^{-8}	1335	157×10^{3}	34-36

5.4. Result and Discussion

5.4.1 Droplet drying time, droplet size, and evaporation rate

To ensure that the model could accurately predict drying time, final particle size, and solvent evaporation rate, experimental drying results for pure mannitol, pure dextran, and a 3:1 blend by mass of mannitol/dextran (40 kDa) were compared to drying model predictions at both 23°C (room temperature) and 60°C. For comparisons to spray drying, 60°C was the more important temperature to consider, as it matches the outlet temperature of the spray dryer when drying

powders containing AdHu5.[30] The 2D projected droplet areas seen by the USB microscope for these formulations were compared to their predicted areas by the model with respect to drying time, shown in Figure 5.1. Cross-sectional areas of the droplets rather than droplet diameters were examined to account for the slightly oblong shape of the droplets caused by the acoustic field in the experiments. Discontinuous gaps in the experimental data were caused by fluctuations of the droplet position within the acoustic field, leading to blurry images that could not be measured by the Python software and were removed from the drying curves.

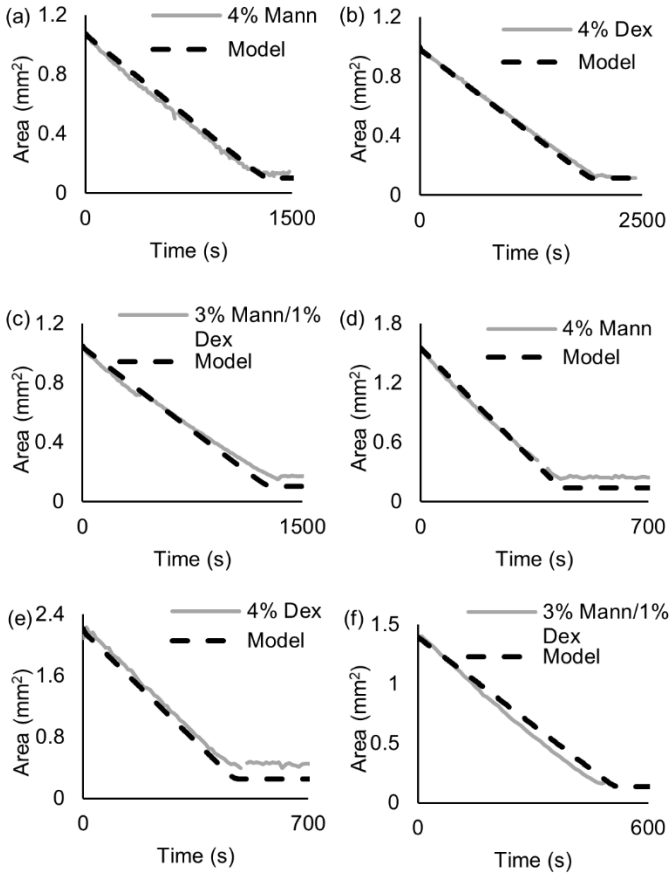

Figure 5.1: Comparisons of experimental data collected from an acoustic levitator to predictions made by the model for (a) 4% mannitol at 23°C and 26% RH; (b) 4% 40 kDa dextran at 23°C and 32% RH; (c) 4% mannitol and 40 kDa dextran at a 3:1 ratio at 23°C and 28% RH; (d) 4% mannitol at 60°C and 3% RH; (e) 4% 40 kDa dextran at 60°C and 3% RH; and (f) 4% mannitol and 40 kDa dextran at a 3:1 ratio at 60°C and 3% RH. Levitator images were collected every 10

seconds during drying. Irregularities in the experimental data plots are caused by fluctuations of the droplet position in the acoustic levitator while drying.

In all 12 drying curves (Figure 5.1), the constant and falling rate stages can be identified by the two sloped lines in each plot. These comparisons show that the model accurately predicted the time to dry, indicated by the matching inflection point on each curve, for all excipients at both temperatures studied. The model also accurately matched the evaporation rate of water from the droplets, as the slope of the constant rate stage (region with the highest negative slope) is the same for both experimental and modelled results in all 6 samples. The model under-predicted the final particle size when experiments were performed at 60°C, possibly due to early precipitation of excipients experimentally at the increased evaporation rate. Since the droplet is shrinking faster than the diffusion of excipients away from the surface, there is an increase in excipient concentration at the surface, leading to faster shell formation.[31] This would cause the formation of particles with interior voids which are not accounted for in the model, leading to a bigger experimental particle than predicted by the model. Although drying time, particle size, and evaporation rate are not novel predictions for modelling a droplet drying process, it was important to validate the accuracy of the model before moving forward with more complex predictions. We also note that this is one of only a few examples in the literature where such a model has been matched to drying curves of acoustically levitated droplets containing dissolved solids.

5.4.2 Model validation of the component distribution

One of the most important and novel aspects of this modelling effort was the ability to predict the distribution of up to four different components, plus water, throughout a final dry particle. Although there are models in the literature that can predict component distribution, they are limited to single component systems or surface composition only, and few of these models have been validated with experimental results, such as those published by Ordoubadi et al. for leucine-trehalose particles and multi-component systems.[14,18,32–35] There are also no examples of models in the literature that predict the distribution of viral vectors suspended in solution, nor any that link model predictions to viral activity. The ability of an excipient or blend of excipients to encapsulate a viral vector, avoiding its exposure to a solid-air interface, is a critical factor to consider in formulation and process development. Biologics that are at or near the solid-air interface are more exposed to degradation stresses, such as heat, and more likely to undergo

damaging chemical reactions or aggregation.[36] There are several examples in the literature of the link between increased biologics at the air-solid interface and their decreased activity and stability, and the amount of protein at the air-solid interface has been reported to be the dominant factor that determined protein degradation in freeze-dried samples.[8,9] LeClair et al. compared three different excipients or excipient blends for their ability to stabilize AdHu5, and found that the worst-performing excipient was the only formulation to have visible surface nodules, which were hypothesized based on their size to be viral particles.[7]

To explore the capability of the model to accurately reflect component distribution, three excipient formulations based on the 3:1 mannitol/dextran formulation containing AdHu5 were studied with the different molecular weight dextrans (10 kDa, 40 kDa, and 500 kDa). The dextrans were chosen to significantly vary the AdHu5 distribution in a particle, making for easier experimental validation. Figure 5.2 shows the component distributions in final dry particles of the three formulations, modelled at 60°C and 4% RH, for the same initial droplet diameter. These results are presented as mass fractions normalized for each component *i* (i.e., mass of component *i* in shell *x*/total mass of component *i*) so that all excipient distributions can be viewed on the same scale, as the AdHu5 makes up a very small portion of the overall mass in a particle and would be indistinguishable otherwise.

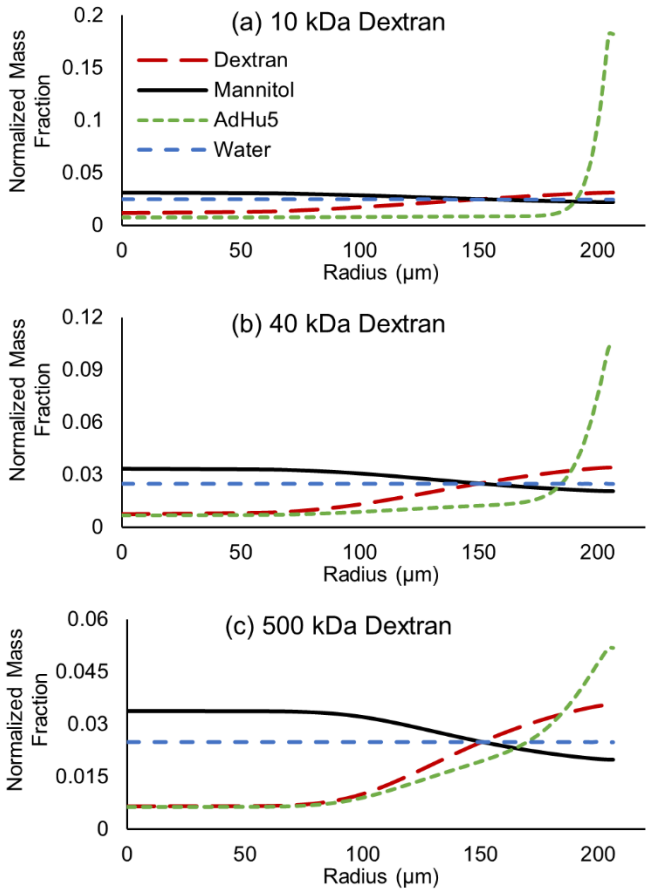

Figure 5.2: Predicted component distributions for a 3:1 mannitol/dextran excipient blend containing AdHu5 dried at 60°C and 4% RH in the acoustic levitator for three different molecular weight dextrans: (a) 10 kDa, (b) 40 kDa, and (c) 500 kDa.

Among these three formulations, the greatest component change was the distribution of AdHu5 in each particle. Going from 10 kDa to 40 kDa to 500 kDa dextran caused a decline in AdHu5 particle concentration at the surface of a final dry particle, changing from 18% (10 kDa dextran) to 10% (40 kDa dextran) to 5% (500 kDa dextran). This is caused by a nearly ten-fold increase in hydrodynamic radius of dextran as its molecular weight increased from 10 to 500 kDa. As reported by Armstrong et al., the corresponding hydrodynamic radii for 10 kDa, 40 kDa, and 500 kDa dextrans are 1.9 nm, 4.8 nm, and 15.9 nm, respectively.[37] This increase in hydrodynamic radius caused slower diffusion, and thus the larger dextran became concentrated at the air-liquid interface as the particle dried. The increase in dextran at the interface excluded the more freely mobile mannitol molecules and AdHu5 particles from concentrating at the same location. A similar segregation of the two excipients, mannitol and dextran, was also expected based on the differences

in diffusion coefficients for mannitol and dextran in water reported in the literature.[32] This segregation can be seen in the component distributions shown in Figure 5.2, caused by the differences in diffusion rate discussed previously.

Computed drying histories showing the distribution of components in the droplet as a function of time for the three cases depicted in Figure 5.2 can be found as time-lapse videos in Appendix 5, Videos A5.1, A5.2, and A5.3. In all three videos, the composition changes rapidly until a shell forms at approximately 400 seconds, at which point water is the only component that diffuses at a noticeable rate. The videos also demonstrate that AdHu5 is initially driven to the interface, then begins to diffuse throughout the droplet and becomes more evenly distributed as the droplet nears shell formation. The change in the composition profiles over time for the three molecular weight dextrans are fairly similar making the component distributions of the final dried particle the most relevant for the discussion here.

To experimentally validate these modelling results, the three different formulations with increasing dextran molecular weights and containing the ‘high’ loading of pSiNPs were tested in the levitator at 60°C and 4% RH, and the corresponding particle surfaces were imaged using AFM. Particles with ‘normal’ pSiNP loading proved ineffective in highlighting the component distribution differences, as no particles were detected at the surface likely due to the low probability of finding pSiNPs in the scanned region by AFM (data not shown). A control sample of 3:1 mannitol/dextran (10 kDa) containing no pSiNPs was imaged for comparison to establish a baseline for surface morphology. Figure 5.3 shows a side-by-side comparison of the surface of four samples: the control and three different formulations containing pSiNPs. Insets in Figure 5.3 highlight visible pSiNPs or clusters of pSiNPs as inferred from their spherical shape and dimensions.

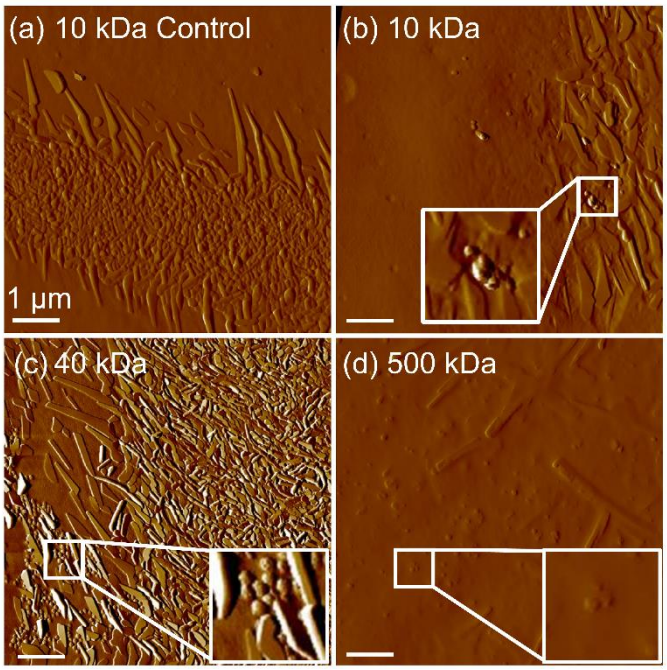

Figure 5.3: Surface images captured using AFM (amplitude images in tapping mode) of levitated particles at 60°C and 4% RH. All particles were composed of 3:1 mannitol/dextran, with various molecular weight dextrans: (a) 10 kDa dextran with no pSiNPs; (b) 10 kDa dextran with 'high' pSiNP loading; (c) 40 kDa dextran with 'high' pSiNP loading; and (d) 500 kDa dextran with 'high' pSiNP loading. Insets indicate examples of individual or clusters of pSiNPs. All scale bars are 1 µm. AFM height images with their color scales indicated are provided in Appendix 5, Figure A5.3, and all features measured are from height images, not the amplitude images shown here.

The pSiNPs were seen on the levitated particle surfaces for all formulations except for the control, although the limited area probed by AFM (7 µm × 7 µm) made it impossible to quantify differences in their surface content as a function of dextran molecular weight. Image analysis confirmed the diameter of these spherical surface features was between 115 – 125 nm, matching the size of pSiNPs dried from suspensions without excipients (also determined by AFM, Appendix 5, Figure A5.1). Long shard-like crystalline regions of mannitol with well-defined edges could be seen as well as smoother regions corresponding to the amorphous dextran, indicating the heterogeneity of the particle surface; x-ray diffraction (XRD) analysis of levitated mannitol/dextran particles in a previous study showed that mannitol is the only crystalline component in this formulation.[21] It should be noted that after mannitol crystallizes, the calculated diffusion coefficient no longer applies as the crystals continue to grow and diffusion is hindered

by the increased size. We note that AFM does not allow for quantification of the mannitol and dextran surface composition and differences in the visible amount of crystalline mannitol in Figure 5.3 are an artefact of the specific regions selected and should not be overinterpreted. XRD patterns of the three formulations were indistinguishable supporting that changing the molecular weight of dextran does not influence mannitol crystallinity or the overall particle crystallinity (Appendix 5, Figure A5.4).

Importantly, the detected pSiNPs were only present in the dextran regions and were excluded from the mannitol crystals (Figure 5.3); we believe the pSiNPs mimic the surface chemistry and mobility of adenoviral particles in an evaporating droplet sufficiently well to compare to experiments with AdHu5 and the model developed here. Although this experimental result appears to support the hypotheses of others that crystalline materials are less likely to encapsulate and stabilize biologic materials, the importance of amorphous phases for stabilization of AdHu5 requires further research quantifying the long term (thermal) stabilization capabilities of crystalline and semicrystalline excipients .[7,38]

In attempts to experimentally quantify the distribution of components at the air-solid interface for the three formulations, we focused on the AdHu5 component, whose location is likely the most crucial for viral stability and vaccine effectiveness. Fluorescently tagged fSiNPs were substituted into the samples at the same ‘high’ loading and imaged by confocal laser scanning microscopy, shown in Figure 5.4. The samples were imaged in air to limit the amount of fluorescent signal from inside the particle, although some signal penetration into the particle interior was still evident. The large images in Figure 5.4 were generated by creating a z-stack of average pixel intensity of 75 slices for each particle, representing the 2D flattened surface density of fSiNPs for an entire sphere. The small images at the bottom of Figure 5.4 are slices taken 0 µm, 50 µm, 100 µm and 150 µm from the outer top surface of the particle (left to right). Control samples of each formulation without fSiNPs confirmed that the levitated particles did not display any intrinsic fluorescence (data not shown).

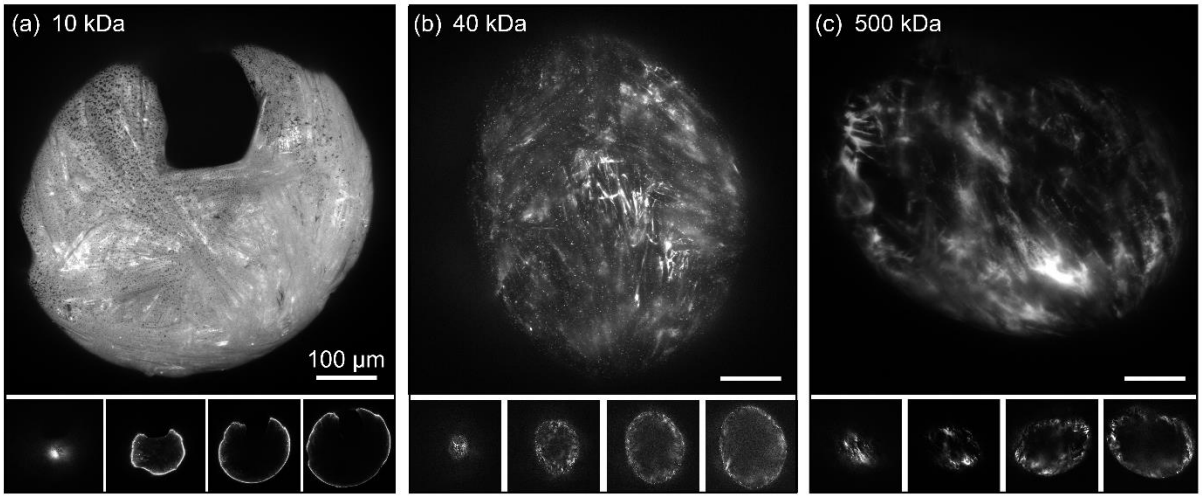

Figure 5.4: Confocal laser scanning microscopy images of mannitol/dextran particles levitated at 60°C and 4% RH with various molecular weight dextrans, all containing a 'high' loading of fSiNPs: (a) 10 kDa dextran; (b) 40 kDa dextran; (c) 500 kDa dextran. Large images are z-stacks created from average pixel intensities of 75 images taken 2 µm apart; smaller bottom images are (left to right) 0 µm, 50 µm, 100 µm, and 150 µm from the top of the particle. All scale bars are 100 µm.

This distribution of fSiNPs in Figure 5.4 is in agreement with the predicted AdHu5 distributions in Figure 5.2. The fSiNPs were highly concentrated at the surface of the sample with the 10 kDa dextran particles showing much more fluorescence (Figure 5.4a) than the other two formulations (Figure 5.4b and 5.4c). Despite the weak fluorescent signal from the interiors, there appeared to be many more fSiNPs distributed deeper in the dried particle as the molecular weight of dextran increased. To quantify this representation of the AdHu5 distribution, the overall emitted fluorescent signal was calculated from the average pixel intensity in each large image in Figure 5.4. The 10 kDa sample had the highest average pixel intensity of 20441, the 40 kDa sample had an average intensity of 9812, and the 500 kDa sample had the lowest average intensity of 6214. The ratios of fluorescent intensity are very similar to the model: for the 40 kDa sample the fluorescent intensity was 48% of the 10 kDa sample and the modelled surface mass fraction was 56% of the 10 kDa model; similarly, the 500 kDa sample had ratios of 30% and 28% for fluorescent intensity and modelled surface mass fraction, respectively. We note that fSiNPs and pSiNPs were equally representative of AdHu5 in this model since the assumed motion is calculated based solely on diffusion and does not account for chemical interactions between excipients and AdHu5/SiNPs.

5.4.3. Viral activity of different formulations interpreted based on model predictions

Previously published AdHu5 viral activity data for three types of acoustically levitated particles with different excipients were compared with the model to see if their component distributions correlated with activity.[21] Levitated particles were composed of 9:1 lactose/trehalose, 3:1 mannitol/dextran (40 kDa), or 1:3 xylitol/dextran (40 kDa), where the ratios quoted are weight fractions. Figure 5.5 shows the activity results for these three excipient blends and the component distributions as predicted by the model (with drying conditions of 55°C, 6% RH, and the same starting droplet size). According to our hypothesis, we expect activity losses to be proportionally higher when the virus is concentrated near the surface of the dried particles – the model was able to predict the trend in performance of different excipient formulations based on the modelled component distribution reasonably well.

The lactose/trehalose formulation with the highest reported viral activity losses (1.6 log loss) was predicted to have 17% of all AdHu5 virus at or near the surface (calculated from the outer 2 μm), while the xylitol/dextran had only 5% of the virus at or near the surface and the lowest reported loss (1.0 log loss). Mannitol/dextran, which is predicted to have moderate activity loss between the other two blends (1.4 log loss), was predicted to have 10% of AdHu5 at or near the surface. These findings appear to support our hypothesis, originating from research done linking degradation of various proteins to the amount of protein at the air-solid interface and observations of LeClair et al. that found virus-sized nodules on the surfaces of spray dried leucine and lactose/trehalose AdHu5 vaccines which demonstrated high activity losses.[7–9] While this work does not speculate on the precise mechanism of deactivation of AdHu5 at air-solid interfaces, it does indirectly support that activity is linked to viral location within a dried particle.

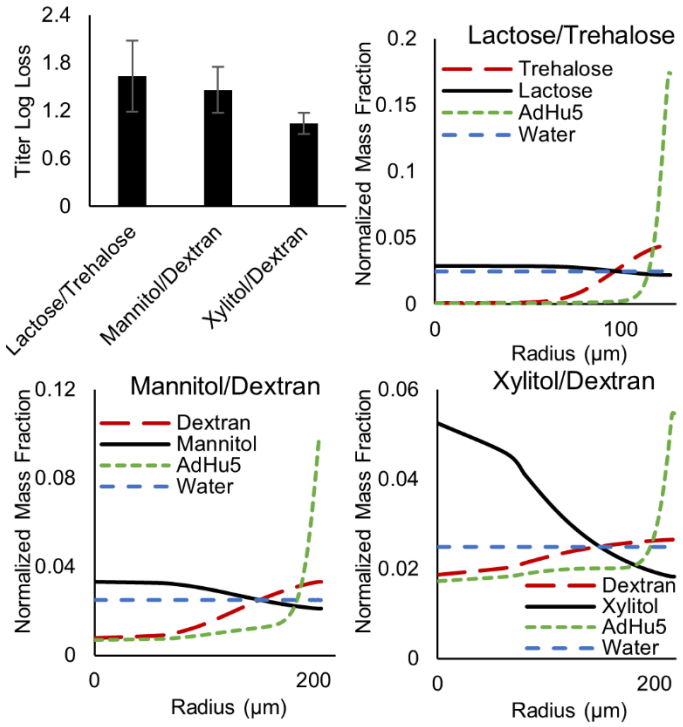

Figure 5.5: A comparison of experimentally determined viral activity data (top left, from reference 21) to component distribution predictions made by the model for lactose/trehalose (top right), mannitol/40 kDa dextran (bottom left), and xylitol/40 kDa dextran (bottom right).

5.4.4 Particle engineering using modelling

In order to make recommendations on formulation and drying conditions, the input parameters to the model were adjusted with the aim of creating a more 'ideal' adenovirus distribution where the AdHu5 would be less concentrated at the surface of the final dried particle. The impacts of RH, drying temperature, and the addition of a fourth component to a base formula of 3:1 mannitol/dextran (40 kDa) was examined with all other parameters remaining the same. Temperature was modelled at 10°C, 23°C, 50°C, and 80°C with a constant RH of 4%; RH was modelled at 0%, 25%, 50%, and 75% with a constant temperature of 60°C; and the addition of SiNPs with diameters of 500 nm as the fourth component was modelled at concentrations of 0, 10, 100, and 1000 times the concentration of AdHu5 at a constant temperature of 60°C and a constant RH of 4%. Figure 5.6 shows the modelled distributions under these various conditions where only the distribution of AdHu5 at each condition is shown for clarity. The complete component distributions for all 12 conditions explored are provided in Appendix 5, Figures A5.5– A5.7.

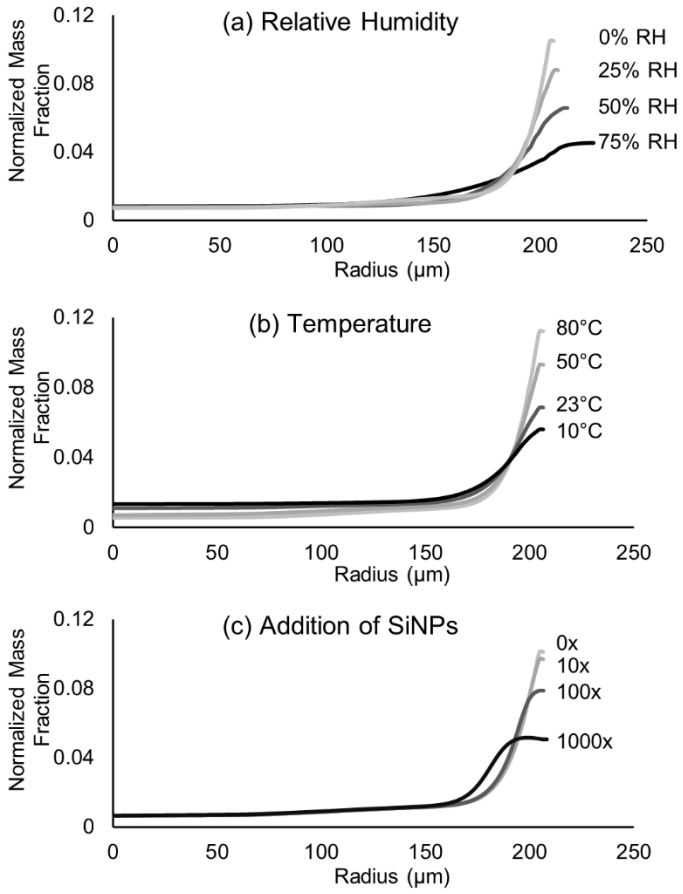

Figure 5.6: The impact of increasing (a) relative humidity, (b) temperature, and (c) addition of SiNPs on the distribution of AdHu5 within the final dried particle. All modelling was done using a 3:1 mannitol/dextran (40 kDa) formulation.

Figure 5.6a and Figure 5.6b show that a decrease in temperature or increase in RH during drying have the same effect of reducing the amount of AdHu5 at the surface, making it more evenly distributed. Both a lower temperature and a higher RH would lengthen the droplet drying time, allowing time for the components to diffuse throughout the droplet more evenly. Given slow enough drying, the distribution of components would tend toward a more uniform composition throughout the particle. However, this allows more time for AdHu5 to aggregate, which also leads to deactivation.[39] Lower drying temperatures and higher RH would also lead to a final product with a higher moisture content which can lower the stability of the powder as water is a plasticizing agent that can depress the glass transition temperature.[40] Storage at or above the glass transition temperature can greatly increase the mobility of AdHu5 in the matrix and increase the chance of degradation; both the chemical and physical stability of the material are dependant on the glass

transition temperature as well.[40,41] An increase in RH would also produce a larger particle as seen in Figure 5.6a (i.e., the modelled line ends at a larger radius for higher RH values), because the droplet does not completely dry out.

Figure 5.6c shows that the addition of 500 nm SiNPs can also reduce the tendency of AdHu5 to partition at the surface of the final dry particle. In this case, the larger size of the SiNPs compared to AdHu5 would cause the SiNPs to diffuse slower and concentrate near the particle surface, forcing AdHu5 towards the center.[42] This is similar to the effect seen using formulation additives such as surfactants like Tween 20, which competes to partition at the air-solid interface and can limit aggregation of proteins.[43] However, selection of these additive components must be done carefully to ensure that they are approved for human consumption and non-toxic. Overall, these modelling results show that there are many different ways to approach particle engineering with an end goal of creating an even distribution of AdHu5, although the route towards "ideal" particles needs to be carefully considered to maintain biologic activity, thermal/storage stability and safety of the final product.

5.5 Conclusions

These results show that the proposed diffusion-based droplet drying model can make accurate predictions for time to dry, final particle size, and component distribution within an individual drying droplet under various environmental conditions. The model also suggested trends in viral vector activity by demonstrating that activity decreases when the model predicts large amounts of AdHu5 at the particle surface, although future work should further investigate the predictive power of the model related to activity. We believe that the use of this model for particle engineering (with inputs of excipient properties easily available in the literature) is an ideal first step in formulation development and can reduce time and costs by identifying good encapsulating excipients and excipient blends without the need for experimental work. Overall, combining modelling predictions with experimental results from the acoustic levitator can substantially facilitate dry powder vaccines development without requiring large amounts of the active biologic; once a promising composition is identified, the activity of the final product can be optimized through spray drying.

5.6 Acknowledgements

The authors wish to thank Kevin Hodgson and Eun Kyoung Lee for the confocal laser scanning microscopy data, as well as facilities in the University of British Columbia Bioimaging Facility. The authors gratefully acknowledge Dr. Xing's lab in the McMaster Immunology Research Center, and Muzaffer Karaaslan in Dr. Scott Renneckar's lab at the University of British Columbia for FTIR training. The authors would also like to thank Anita Lam for collecting XRD data and Yoen-Ju Son from Merck for her suggestions and advice. This study is supported by funds from the Canadian Institutes of Health Research, the Natural Sciences and Engineering Research Council of Canada (Collaborative Health Research Program CHRP523837-18), Ontario Centres of Excellence (OCE), and the Academy of Finland (grant no. 321801).

5.7 Supporting Information

The supporting information contains: dynamic light scattering, zeta potential, FTIR, and AFM data for control SiNPs and pSiNPs, as well as the associated method information; XRD methods and spectra for three mannitol/dextran blends containing SiNPs; complete modelled component distributions for the 12 drying conditions in Figure 5.6; and videos showing the complete modelled drying histories of the mannitol/dextran blends in Figure 5.2. Code for the droplet drying model is available upon request by emailing the authors.

5.8 References

1. Amorij, J. P., Huckriede, A., Wilschut, J., Frijlink, H. W. & Hinrichs, W. L. J. Development of stable influenza vaccine powder formulations: Challenges and possibilities. *Pharm. Res.* **25**, 1256–1273 (2008).

2. Ré, M. I. Microencapsulation By Spray Drying. *Drying Technol.* **16**, 1195–1236 (1998).

3. Mondragon, R. *et al.* Study of the drying behavior of high load multiphase droplets in an acoustic levitator at high temperature conditions. *Chem. Eng. Sci.* **66**, 2734–2744 (2011).

4. Schutyser, M. A. I., Perdana, J. & Boom, R. M. Single droplet drying for optimal spray drying of enzymes and probiotics. *Trends Food Sci. Technol.* **27**, 73–82 (2012).

5. Langrish, T. A. G. Multi-scale mathematical modelling of spray dryers. *J. Food Eng.* **93**, 218–228 (2009).

6. Mezhericher, M., Levy, A. & Borde, I. Theoretical models of single droplet drying kinetics: A review. *Drying Technol.* **28**, 278–293 (2010).

7. LeClair, D. A., Cranston, E. D., Xing, Z. & Thompson, M. R. Evaluation of excipients for enhanced thermal stabilization of a human type 5 adenoviral vector through spray drying. *Int. J. Pharm.* **506**, 289–301 (2016).

8. Xu, Y. *et al.* Protein quantity on the air-solid interface determines degradation rates of human growth hormone in lyophilized samples. *J. Pharm. Sci.* **103**, 1356–1366 (2014).

9. Devineni, D. *et al.* Storage stability of keratinocyte growth factor-2 in lyophilized formulations: Effects of formulation physical properties and protein fraction at the solid-air interface. *Eur. J. Pharm. Biopharm.* **88**, 332–341 (2014).

10. Sadek, C. *et al.* Drying of a single droplet to investigate process–structure–function relationships: a review. *Dairy Sci. Technol.* **95**, 771–794 (2015).

11. Mezhericher, M., Levy, A. & Borde, I. Modelling the morphological evolution of nanosuspension droplet in constant-rate drying stage. *Chem. Eng. Sci.* **66**, 884–896 (2011).

12. Sloth, J. *et al.* Model based analysis of the drying of a single solution droplet in an

ultrasonic levitator. *Chem. Eng. Sci.* **61**, 2701–2709 (2006).

13. Vehring, R. Pharmaceutical particle engineering via spray drying. *Pharm. Res.* **25**, 999–1022 (2008).

14. Porowska, A. *et al.* Predicting the surface composition of a spray-dried particle by modelling component reorganization in a drying droplet. *Chem. Eng. Res. Des.* **110**, 131–140 (2016).

15. Farid, M. A new approach to modelling of single droplet drying. *Chem. Eng. Sci.* **58**, 2985–2993 (2003).

16. Huang, D. Modeling of Particle Formation during Spray Drying. *Eur. Dry. Conf. - EuroDrying'2011* 26–28 (2011).

17. Sazhin, S. S., Rybdylova, O., Pannala, A. S., Somavarapu, S. & Zaripov, S. K. A new model for a drying droplet. *Int. J. Heat Mass Transf.* **122**, 451–458 (2018).

18. Grasmeijer, N., Frijlink, H. W. & Hinrichs, W. L. J. Model to predict inhomogeneous protein–sugar distribution in powders prepared by spray drying. *J. Aerosol Sci.* **101**, 22–33 (2016).

19. Pang, L. *et al.* Mimicking filtration and transport of rotavirus and adenovirus in sand media using DNA-labeled, protein-coated silica nanoparticles. *Water Res.* **62**, 167–179 (2014).

20. Laboratories, B. Microsphere coupling protocols. (2013).

21. Morgan, B. A., Xing, Z., Cranston, E. D. & Thompson, M. R. Acoustic levitation as a screening method for excipient selection in the development of dry powder vaccines. *Int. J. Pharm.* **563**, 71–78 (2019).

22. Morgan, B. A. *et al.* Effect of Shear Stresses on Adenovirus Activity and Aggregation during Atomization To Produce Thermally Stable Vaccines by Spray Drying. *ACS Biomater. Sci. Eng.* **6**, 4304–4313 (2020).

23. Schindelin, J. *et al.* Fiji: An open-source platform for biological-image analysis. *Nat. Methods* **9**, 676–682 (2012).

24. Kawahara, N., Yarin, A. L., Brenn, G., Kastner, O. & Durst, F. Effect of acoustic streaming on the mass transfer from a sublimating sphere. *Phys. Fluids* **12**, 912–923 (2000).

25. Schiffter, H. & Lee, G. Single-droplet evaporation kinetics and particle formation in an acoustic levitator. Part 1: Evaporation of water microdroplets assessed using boundary-layer and acoustic levitation theories. *J. Pharm. Sci.* **96**, 2274–2283 (2006).

26. Grasmeijer, N., Frijlink, H. W. & Hinrichs, W. L. J. An adaptable model for growth and/or shrinkage of droplets in the respiratory tract during inhalation of aqueous particles. *J. Aerosol Sci.* **93**, 21–34 (2016).

27. Ekdawi-Sever, N., De Pablo, J. J., Feick, E. & Von Meerwall, E. Diffusion of sucrose and α,α-trehalose in aqueous solutions. *J. Phys. Chem. A* **107**, 936–943 (2003).

28. Mendoza, R. & Schmalko, M. E. Diffusion coefficients of water and sucrose in osmotic dehydration of papaya. *Int. J. Food Prop.* **5**, 537–546 (2002).

29. Carrasco, F., Chornet, E., Overend, R. P. & Costa, J. A generalized correlation for the viscosity of dextrans in aqueous solutions as a function of temperature, concentration, and molecular weight at low shear rates. *J. Appl. Polym. Sci.* **37**, 2087–2098 (1989).

30. LeClair, D. A., Cranston, E. D., Xing, Z. & Thompson, M. R. Optimization of Spray Drying Conditions for Yield, Particle Size and Biological Activity of Thermally Stable Viral Vectors. *Pharm. Res.* **33**, 2763–2776 (2016).

31. Vehring, R., Foss, W. R. & Lechuga-Ballesteros, D. Particle formation in spray drying. *J. Aerosol Sci.* **38**, 728–746 (2007).

32. Meerdink, G. & van't Riet, K. Modeling segregation of solute material during drying of liquid foods. *AIChE J.* **41**, 732–736 (1995).

33. Grosshans, H. *et al.* Numerical and experimental study of the drying of bi-component droplets under various drying conditions. *Int. J. Heat Mass Transf.* **96**, 97–109 (2016).

34. Ordoubadi, M. *et al.* On the particle formation of leucine in spray drying of inhalable microparticles. *Int. J. Pharm.* **592**, 120102 (2021).

35. Ordoubadi, M. *et al.* Multi-Solvent Microdroplet Evaporation: Modeling and Measurement of Spray-Drying Kinetics with Inhalable Pharmaceutics. *Pharm. Res.* **36**, (2019).

36. Crowe, J. H., Carpenter, J. F. & Crowe, L. M. The Role of Vitrification in Anhydrobiosis. *Annu. Rev. Physiol.* **60**, 73–103 (1998).

37. Armstrong, J. K., Wenby, R. B., Meiselman, H. J. & Fisher, T. C. The hydrodynamic radii of macromolecules and their effect on red blood cell aggregation. *Biophys. J.* **87**, 4259–4270 (2004).

38. Weers, J. G., Tarara, T. E. & Clark, A. R. Design of fine particles for pulmonary drug delivery. *Expert Opin. Drug Deliv.* **4**, 297–313 (2007).

39. Evans, R. K. *et al.* Development of Stable Liquid Formulations for Adenovirus-Based Vaccines. *J. Pharm. Sci.* **93**, 2458–2475 (2004).

40. Ameri, M. & Maa, Y. F. Spray drying of biopharmaceuticals: Stability and process considerations. *Drying Technol.* **24**, 763–768 (2006).

41. Hancock, B. C. & Zografi, G. The Relationship Between the Glass Transition Temperature and the Water Content of Amorphous Pharmaceutical Solids. *Pharmaceutical Research* **11**, 471–477 (1994).

42. Walters, R. H. *et al.* Next generation drying technologies for pharmaceutical applications. *J. Pharm. Sci.* **103**, 2673–2695 (2014).

43. Kreilgaard, L., Frokjaer, S., Flink, J. M., Randolph, T. W. & Carpenter, J. F. Effects of additives on the stability of recombinant human factor XIII during freeze-drying and storage in the dried solid. *Arch. Biochem. Biophys.* **360**, 121–134 (1998).

44. Colilla, M. *et al.* Synthesis and characterization of zwitterionic SBA-15 nanostructured materials. *Chem. Mater.* **22**, 6459–6466 (2010).

Appendix 5: Chapter 5 Supporting Information

A5.1. MATERIALS AND METHODS

A5.1.1 Dynamic Light Scattering (DLS) and Zeta Potential Measurements

Light-scattering based size (hydrodynamic diameter) and zeta potential measurements were performed with a Zetasizer Nano ZS (Malvern; Malvern, United Kingdom). DLS measurements were performed on 0.025 wt% suspensions of SiNPs and pSiNPs. Electrophoretic mobility measurements were performed on 0.1 wt% suspensions of SiNPs and pSiNPs with 5 mM NaCl and converted to a zeta potential measurement using Smoluchowski theory. For both DLS and zeta potential measurements, the sample average from three measurements is reported. Zeta potential was also measured for both SiNPs and pSiNPs after adjusting the pH of the suspensions to 2.5 with HCl. The isoelectric point of α_1-acid-glycoprotein is at a pH of 2.7, and the isoelectric point of SiNPs is at a pH of 2.0 supporting the use of these nanoparticles as AdHu5 analogues.[19,44]

A5.1.2 Fourier-Transform Infrared (FTIR) Spectroscopy Measurements

Samples were prepared for FTIR by combing SiNPs or pSiNPs with KBr at a ratio of 1:100 SiNPs:KBr. IR spectra were recorded using a Bruker INVENIO-S spectrometer (Billerica, MA) by averaging 32 scans per sample from 4000 to 400 cm^{-1} with a 4 cm^{-1} spectral resolution.

A5.1.3 X-Ray Diffraction (XRD)

Levitated particles of mannitol blended with dextran of 10 kDa, 40 kDa, and 500 kDa (3:1 by mass) with a 'normal' loading of SiNPs produced at 60°C and 4% RH were characterized by powder XRD on a Bruker APEX DUO (Billerica, MA) using a copper source (λ_{avg} = 1.54184 Å, 2θ = 5-60°). Particles were mounted on a cryoloop using oil. Data processing was done using the Bruker Apex3 v2017.3-0 software (Billerica, MA).

Table A5.1: DLS size and zeta potential measurements for control SiNPs and pSiNPs. Measurements were taken the same day the EDC coupling reaction was done (Day 0). DLS size measurements for pSiNPs were also taken six and twelve days post-reaction to ensure that the coating was stable. Reported error is the standard deviation of three measurements.

	Control SiNPs (Day 0)	pSiNPs (Day 0)	pSiNPs (Day 6)	pSiNPs (Day 12)	Control SiNPs (pH 2.5)	pSiNPs (pH 2.5)
Size (nm)	116.8±1.2	168.6*	109.5±1.1	107.4±0.7	-	-
Zeta potential (mV)	-29.4±0.4	-35.9±0.7	-	-	-4.10±0.3	12.7±0.9

*The pSiNP Day 0 sample DLS measurement had a secondary peak at approximately 4800 nm that did not appear in any other measurements.

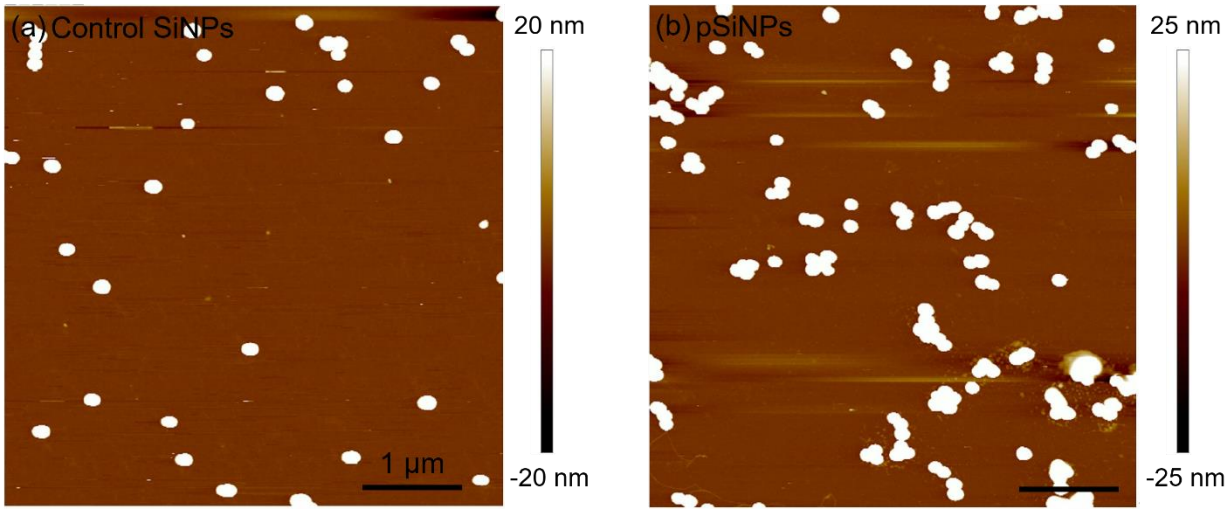

Figure A5.1: Surface images captured using AFM (height images in tapping mode) of: (a) control SiNPs and (b) pSiNPs showing their spherical shape and dimensions of approximately 100 nm in diameter.

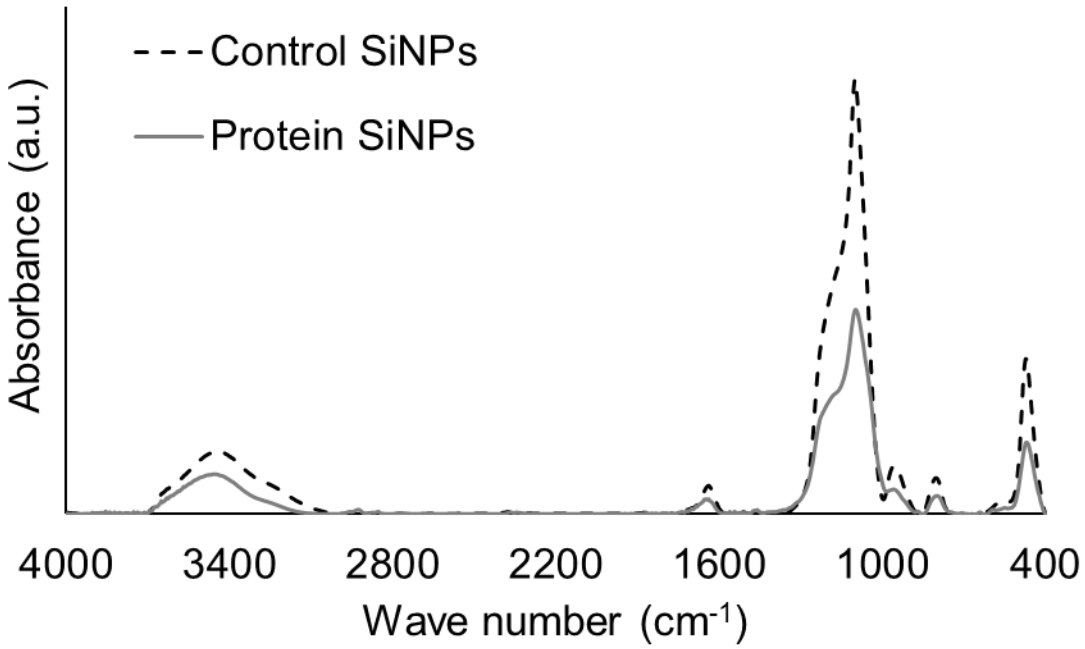

Figure A5.2: FTIR spectra comparing control SiNPs to pSiNPs.

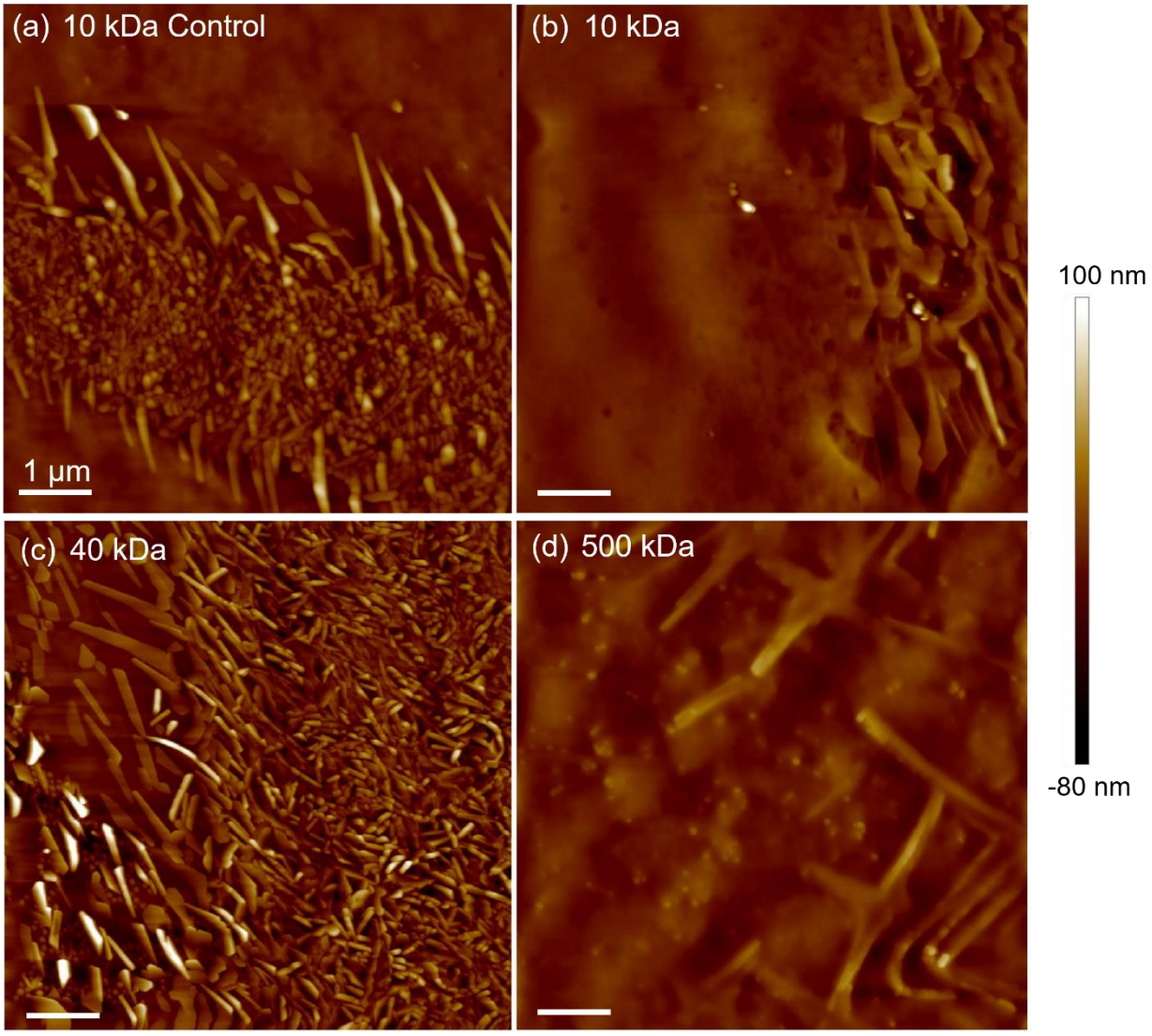

Figure A5.3: Surface images captured using AFM (height images in tapping mode) of levitated particles at 60°C and 4% RH. All particles were composed of 3:1 mannitol/dextran, with various molecular weight dextrans: (a) 10 kDa dextran with no pSiNPs; (b) 10 kDa dextran with 'high' pSiNP loading; (c) 40 kDa dextran with 'high' pSiNP loading; and (d) 500 kDa dextran with 'high' pSiNP loading. All scale bars are 1 µm and the height color scale is shown on the right and is the same for all panels.

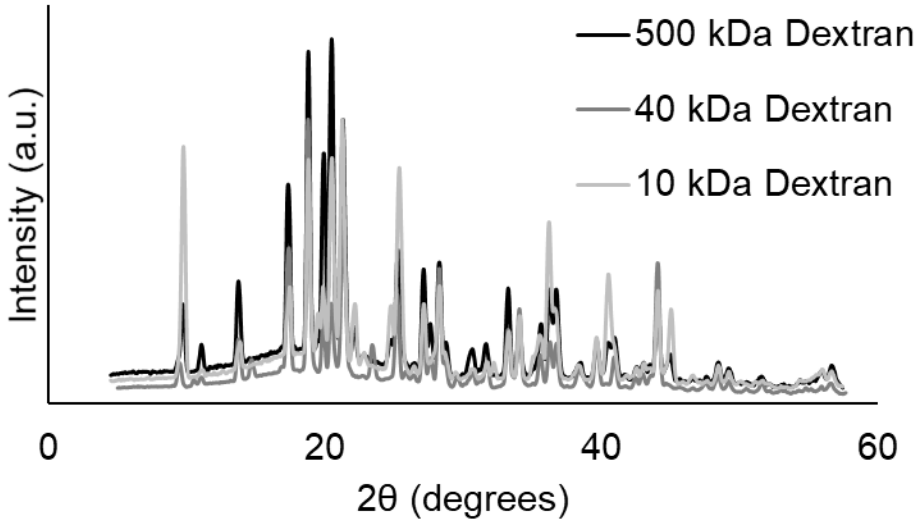

Figure A5.4: XRD spectra for the three different mannitol/dextran blends overlaid to show the similarities in crystal structure and degree of crystallinity. The only differences between the spectra are the intensity of the crystalline peaks.

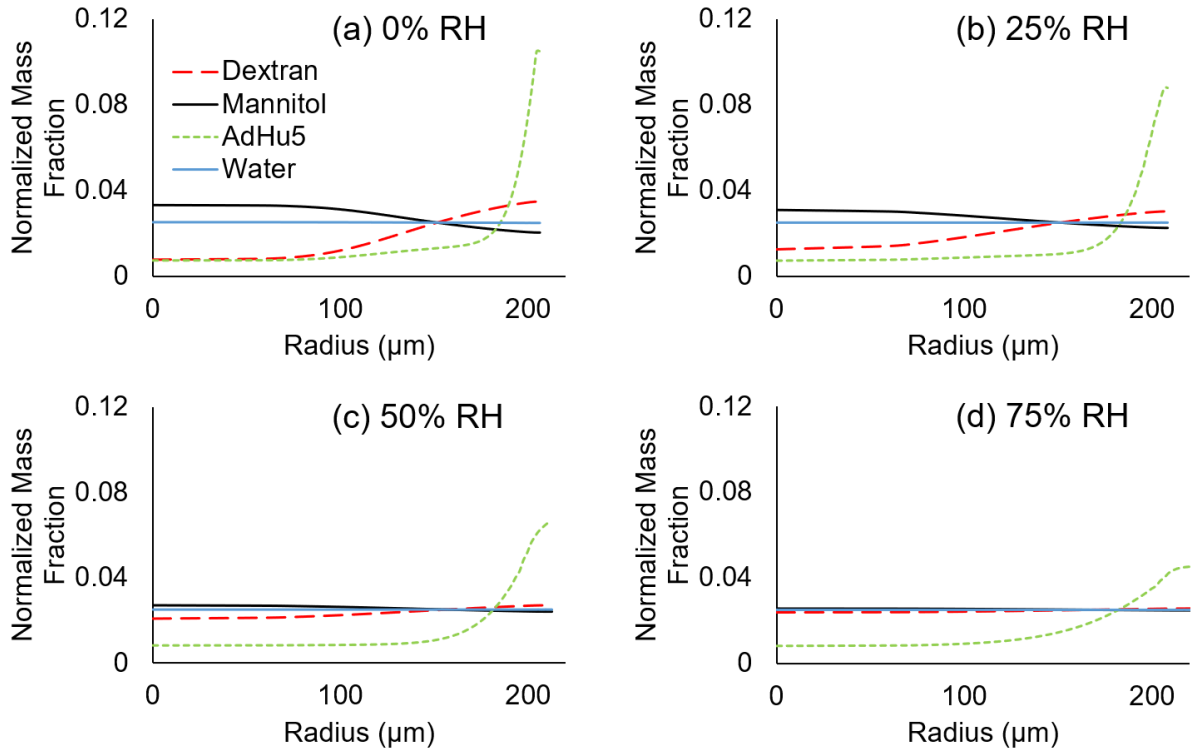

Figure A5.5: Modelled component distributions for a 3:1 mannitol/dextran (40 kDa) blend with AdHu5 dried at 60°C and varying RH: (a) 0% RH, (b) 25% RH, (c) 50% RH, and (d) 75% RH.

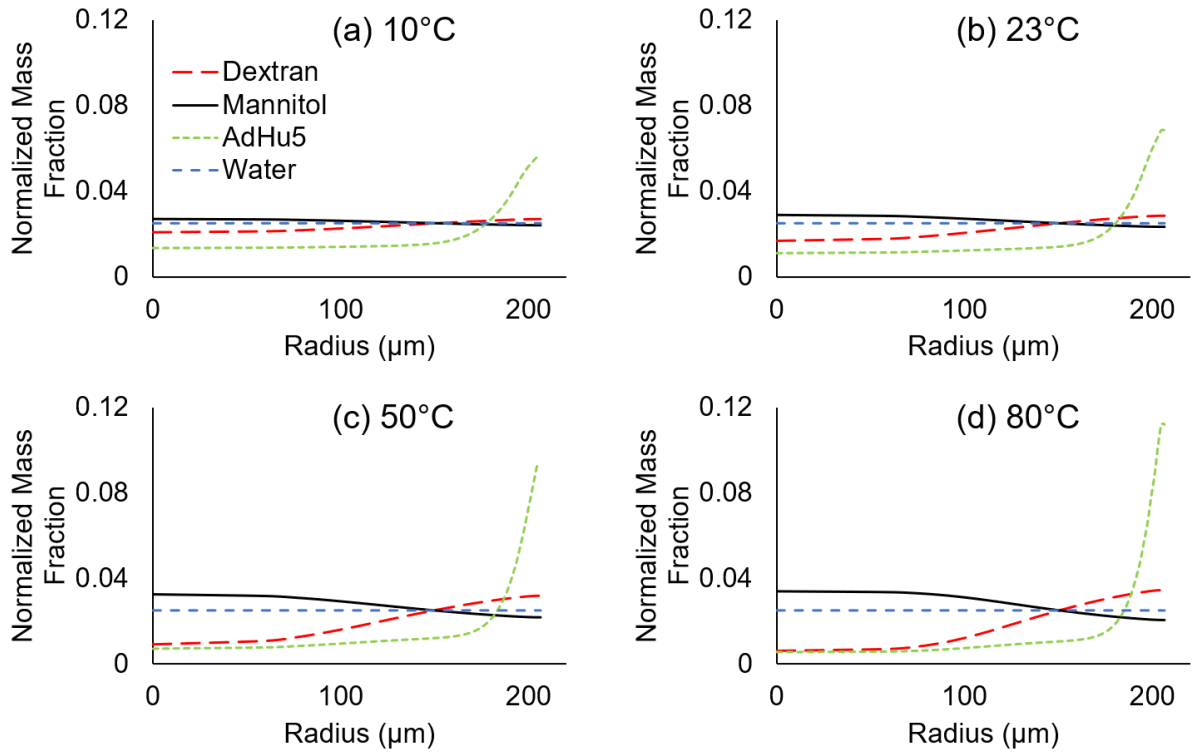

Figure A5.6: Modelled component distributions for a 3:1 mannitol/dextran (40 kDa) blend with AdHu5 dried at 4% RH and varying temperature: (a) 10°C, (b) 23°C, (c) 50°C, and (d) 80°C.

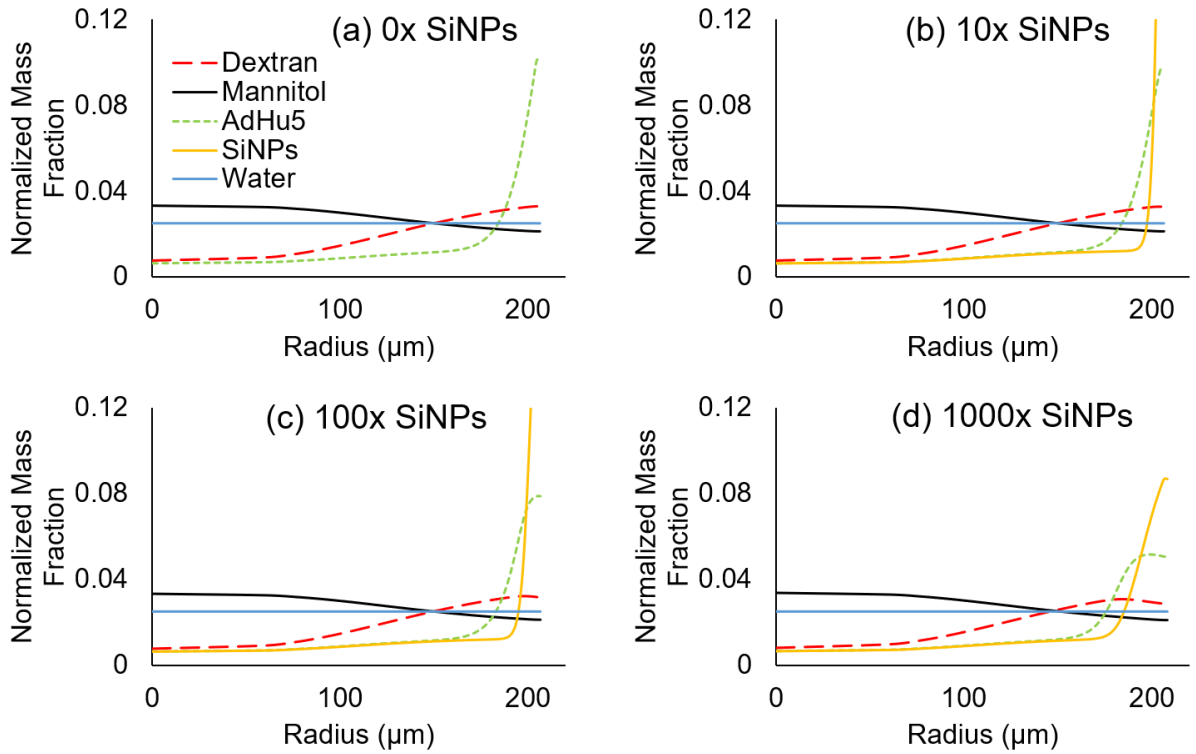

Figure A5.7: Modelled component distributions for a 3:1 mannitol/dextran (40 kDa) blend with AdHu5 dried at 60°C and 4% RH with varying amounts of 500 nm SiNPs included in the formulation: (a) 0x the AdHu5 concentration, (b) 10x the AdHu5 concentration, (c) 100x the AdHu5 concentration, (d) 1000x the AdHu5 concentration.

Chapter 6: Concluding Remarks and Future Outlook

The work done in this thesis provides several steps towards making a marketable, thermostable dry powder vaccine a reality, which will reduce vaccine wastage and distribution costs, as well as provide the ability to stockpile vaccines for future pandemics and outbreaks. This work demonstrates both experimental (acoustic levitation) and theoretical (droplet drying model) tools that can be used to reduce the time and cost of formulation development by reducing the amount of spray drying experimentation. Overall, the main objectives outlined in Chapter 1 were achieved:

1. **Investigate the effect of shear stresses on a human type 5 adenovirus (AdHu5).** Chapter 3 used the two-fluid atomizing nozzle from a spray dryer to isolate the effect of atomizing shear stresses on AdHu5. A range of specific shear stresses were applied to two concentrations of a liquid mannitol/dextran formulation containing AdHu5. The viral activity assays found that there were shear rates that minimized the amount of viral activity loss, having a positive effect in some cases. Quantification of AdHu5 aggregation before and after applying shear stresses found that reductions in activity loss, when occurring, were caused by shear breakup of AdHu5 aggregates that had formed when adding the AdHu5 suspension to a liquid solution of mannitol and dextran. However, at very high shear rates, this slight benefit was offset by structural damage to the virus. Overall, even the highest activity losses found due to shearing were significantly less than losses measured across the entire spray drying process, suggesting that shear does not need to be a major consideration. The unexpected finding by the study was that the mixing of the viral vector with a solution of carbohydrates could induce aggregation. This was the first reported study on the effect of shear stresses on viral vectors in the literature.
2. **Develop a screening method and a mathematical model that can accurately mimic or model spray drying.** Chapter 4 examined the use of an acoustic levitator as an experimental screening method to identify potentially stabilizing excipients for AdHu5. An acoustic levitator modified with a custom heating system was used to model the spray drying process to understand the effects of the environment on spray dried materials. Three different excipient blends were used to stabilize AdHu5 and materials made through both spray drying and levitation were characterized for morphology, glass transition

temperature, crystallinity, moisture content, and most importantly, viral activity loss. Adding heat to the acoustic levitation system (at temperatures between 40°C and 55°C, matching the spray dryer) was found to produce materials with the same trends in viral activity loss between formulations seen in spray drying. This comparison found that acoustic levitation is a promising screening technique for spray drying thermally stable dry powder vaccines, and can be used for suitable excipient selection before moving forward with more costly spray drying experiments. This was the first published report in the literature on the use of acoustic levitation with viral vectors.

Chapter 5 proposed a diffusion-based single droplet drying model that can be used to understand the spray drying process and predict excipient performance based on the distribution of AdHu5 within the final dried product. The model was validated by comparing modelled prediction for evaporation rate, time to dry, and final dry particle size to experimental results from the levitator. Component distribution predictions were validated by imaging levitated particles containing silica nanoparticles as viral analogues. Confocal microscopy and AFM confirmed that the modelled predictions for the amount of AdHu5 at the particle surface for three different blends of mannitol/dextran were reasonable, and modelled predictions for AdHu5 at the surface were also linked to trends in activity data for the three different excipient blends. The use of this model will allow for excipient identification with less experimental work, and the model can also be used to engineer dry particles that limit the amount of AdHu5 at the surface. This was the first report in the literature attempting to spatially locate viral vectors or viral vectors analogues within a dry particle. In combination, the diffusion-based model and the acoustic levitator can provide large amounts of information on excipients or excipient blends without the need to spray dry and with minimal viral vector use, and can be used to narrow down a list of potential excipients to those most likely to perform exceptionally.

Taken together, the components of this thesis will assist in reducing the time and monetary resources necessary for spray dried vaccine formulation development and will make it easier to select formulation excipients based on end targets and applications. This work will also be applicable to scaling up the spray drying process to industrial scales since transport phenomena like heat and shear stresses do not change to the same degree going from the lab to production.

Moving forward, we will continue this work with ongoing research into the distribution of AdHu5 in porous particles with internal air-solid interfaces and how the presence of these internal voids is related to activity loss and particle shape and crystallinity. Focused ion beam SEM imaging revealed that the internal structure of mannitol/dextran particles was not completely solid as previously thought but had internal voids, formed in between large mannitol crystals that spanned the center of the particle. Preliminary imaging of xylitol/dextran particles (having less activity loss compared to mannitol/dextran) suggest that they are completely solid, leading us to believe that there is a link between activity loss and porosity of the particle. This may also be linked to crystallinity, as mannitol/dextran particles are semicrystalline with visible crystal structures while xylitol/dextran particles are completely amorphous. Future work should also investigate the differences in AdHu5 stabilization between amorphous, semicrystalline, and crystalline materials and the impact of crystal morphology on both short and long-term thermal stability. Once the impact of porosity and crystallinity on AdHu5 encapsulation are better understood, the mathematical model can be improved to take into account these details.